Electronic Supplementary Material (ESI) for Catalysis Science & Technology.
This journal is © The Royal Society of Chemistry 2020

Supporting Information

Electro- and Photoelectro- Catalysts Derived from Bimetallic Amorphous Metal-Organic Frameworks

Javier Fonseca, and Sunho Choi**

Nanomaterial Laboratory for Catalysis and Advanced Separations, Department of Chemical Engineering, Northeastern University, 313 Snell Engineering Center, 360 Huntington Avenue, Boston, Massachusetts 02115-5000, United States

* Corresponding Author.
E-mail: fonsecagarcia.j@northeastern.edu

Table of Contents

1. Supplementary Figures

Figure S1. ^{1}H NMR (500 MHz, $CDCl_3$) spectra of 4’-(2-furyl)-2,2’:6’,2’’-terpyridine: δ = 8.74 (d, J = 4.6 Hz, 2H), 8.72 (s, 2H), 8.64 (d, J = 7.9 Hz, 2H), 7.90–7.84 (m, 2H), 7.59 (s, 1H), 7.35 (dd, J = 6.7, 5.4 Hz, 2H), 7.12 (d, J = 3.3 Hz, 1H), 6.57 (d, J = 1.5 Hz, 1H) ppm. 4’-(2-furyl)-2,2’:6’,2’’-terpyridine structure is confirmed by ^{1}H NMR.

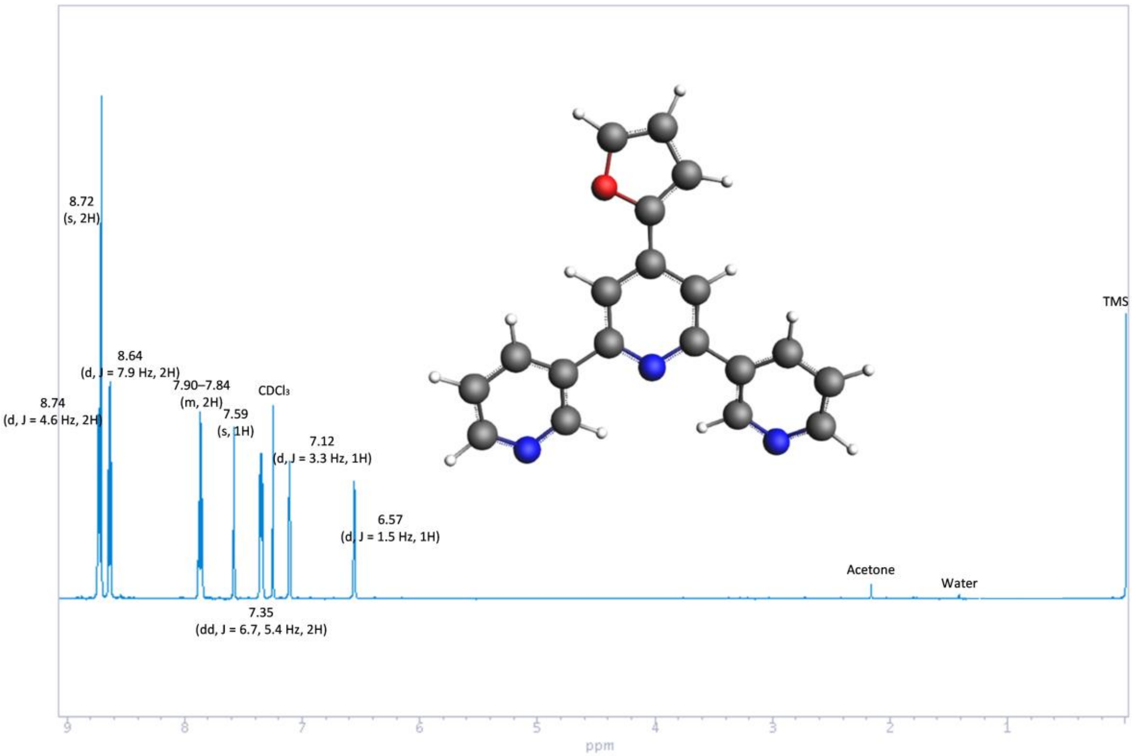

Figure S2. DSC of 4'-(2-furyl)-2,2':6',2''-terpyridine. The analysis shows the heat of boiling as well as the boiling temperature of 4'-(2-furyl)-2,2':6',2''-terpyridine. The boiling point depression due to impurities in the sample is zero.

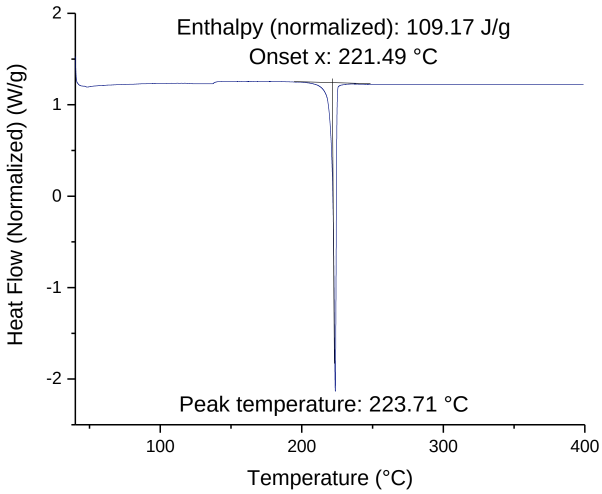

Figure S3. ^{1}H NMR (500 MHz, CD_3CN) spectra of (FeTpyCOOH)$(PF_6)_2$: δ = 9.40 (s, 4 H), 8.68 (d, J = 8.1 Hz, 4 H), 7.90 (dt, J = 8.1, 4.6 Hz, 4 H), 7.08 (2 x d, J = 4.6 Hz, 8 H) ppm. (FeTpyCOOH)$(PF_6)_2$ structure is confirmed by ^{1}H NMR.

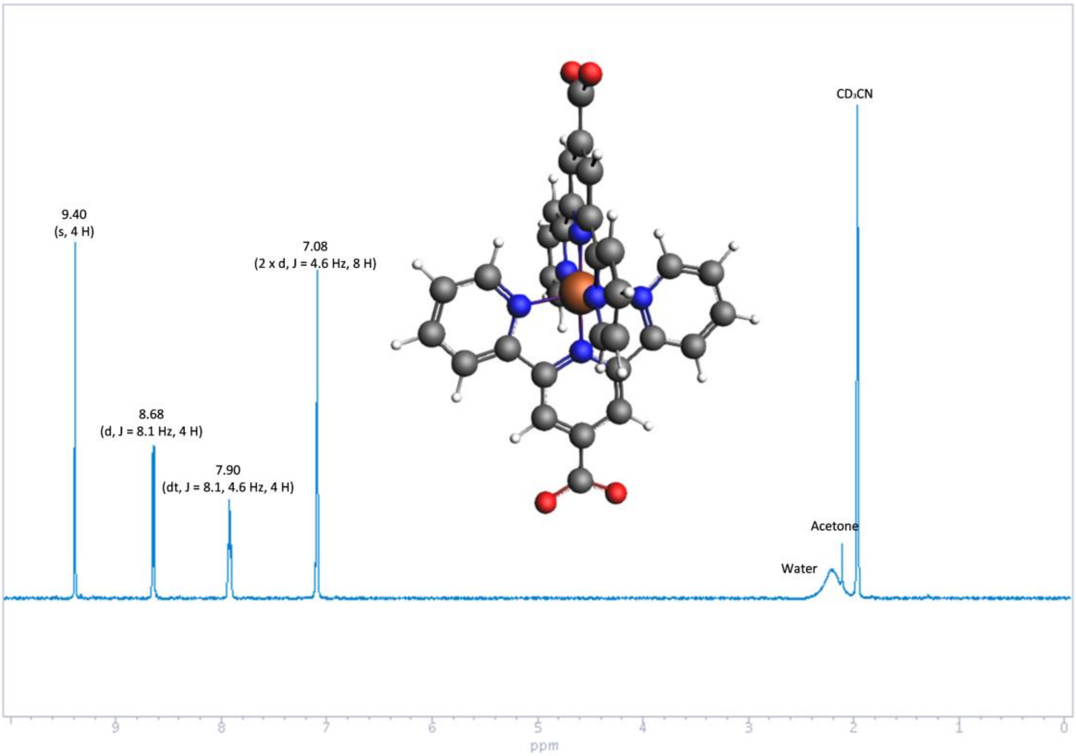

Figure S4. DSC of $(FeTpyCOOH)(PF_6)_2$. The analysis shows the heat of boiling as well as the boiling temperature of $(FeTpyCOOH)(PF_6)_2$. The boiling point depression due to impurities in the sample is zero.

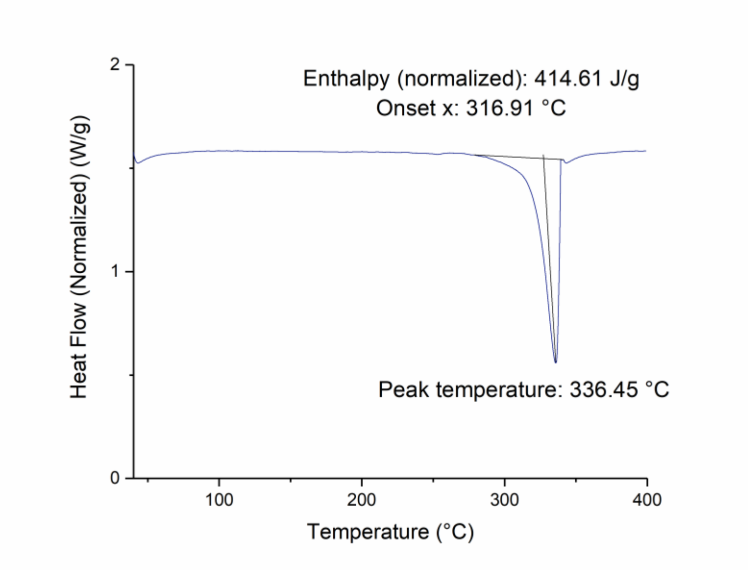

Figure S5. ^{1}H NMR (500 MHz, DMSO-d_6) spectra of [2,2':6',2''-terpyridine]-4'-carboxylic acid: δ = 8.85 (s, 2H), 8.75 (d, 2H), 8.64 (d, 2H), 8.03 (td, 2H), 7.53 (dd, 2H) ppm. [2,2':6',2''-terpyridine]-4'-carboxylic acid structure is confirmed by ^{1}H NMR.

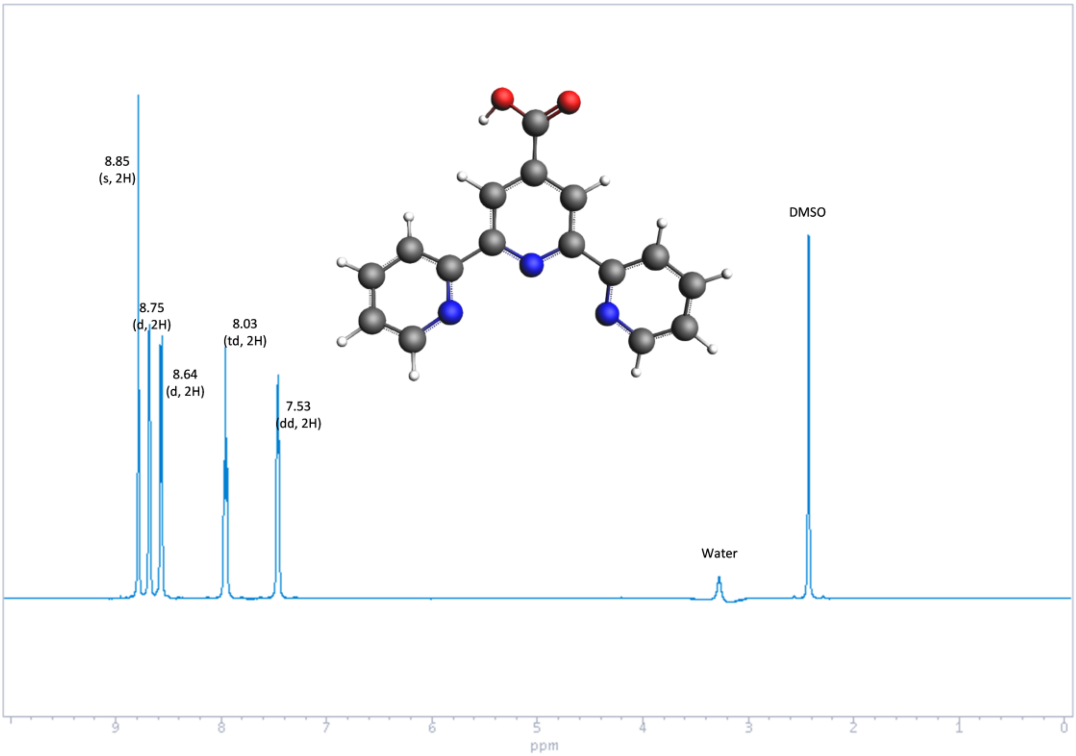

Figure S6. DSC of [2,2’:6’,2’’-terpyridine]-4’-carboxylic acid. The analysis shows the heat of boiling as well as the boiling temperature of [2,2’:6’,2’’-terpyridine]-4’-carboxylic acid. The boiling point depression due to impurities in the sample is zero.

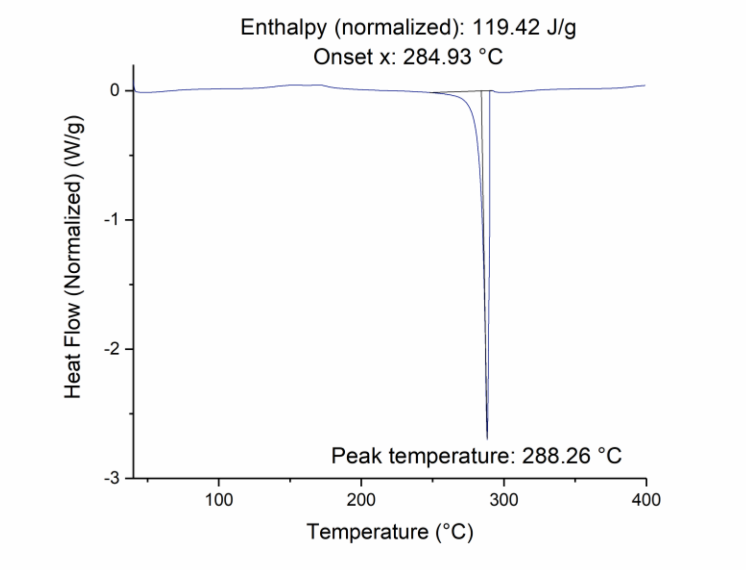

Figure S7. ^{1}H NMR (500 MHz, DMSO-d_6) spectra of $(Ru(terpy^*)_2)(PF_6)_2$: δ 9.45 (s, 2H), 9.09 (d, 2H), 8.02 (t, 2H), 7.53 (d, 2H), 7.26 (t, 2H) ppm. $(Ru(terpy^*)_2)(PF_6)_2$ structure is confirmed by ^{1}H NMR.

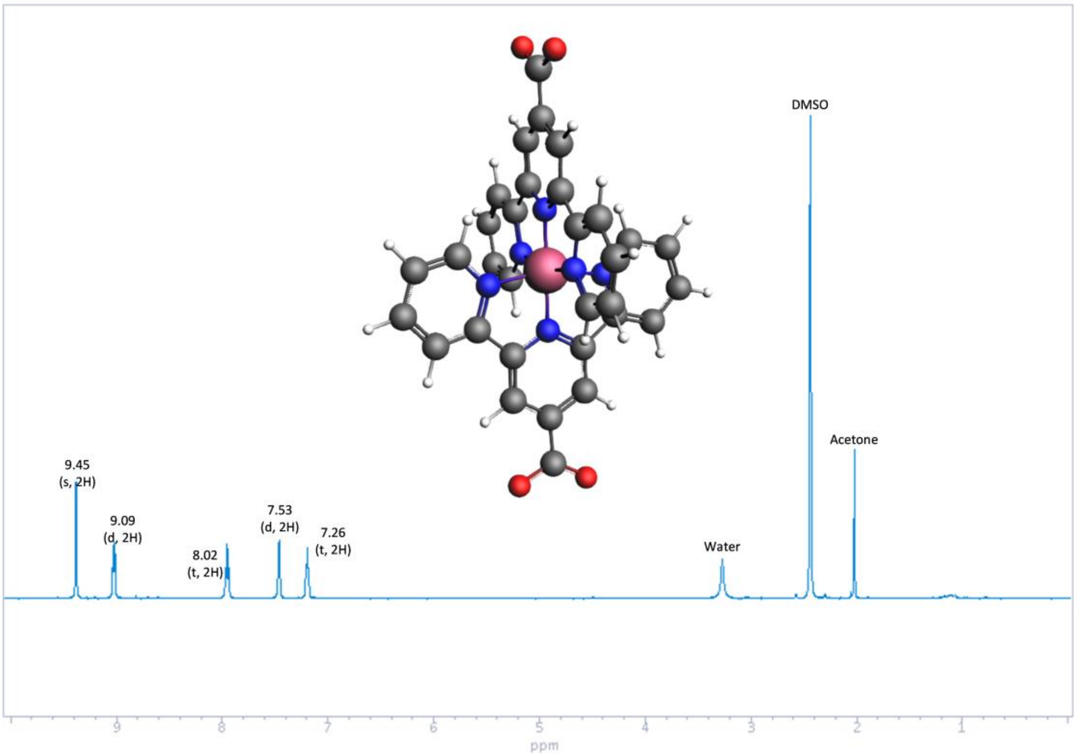

Figure S8. DSC of $(Ru(terpy^*)_2)(PF_6)_2$. The analysis shows the heat of boiling as well as the boiling temperature of $(Ru(terpy^*)_2)(PF_6)_2$. The boiling point depression due to impurities in the sample is zero.

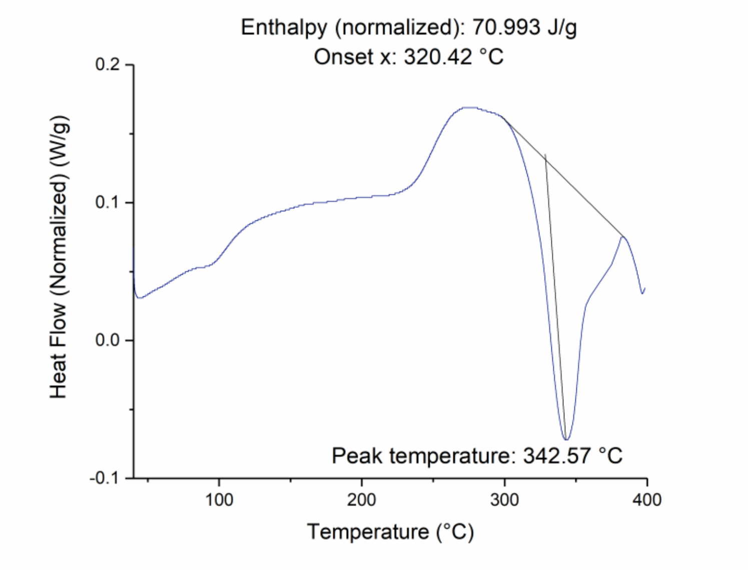

Figure S9. Coordinates of each atom in the local molecular structure of zinc within NEU-5. Atom labelling scheme: C = black; O = red; N = blue; Zn = grey; H = pink.

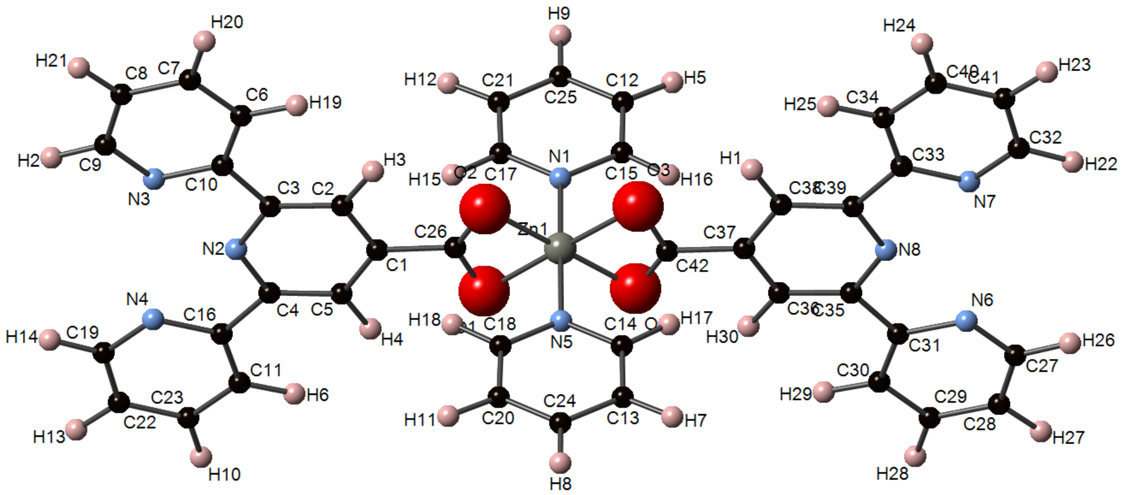

Label	Elmt	Fractional Coordinates x	y	z	Orthogonal Coordinates xor[Å]	yor[Å]	zor[Å]
1. C1	C	0.4995	0.6194	0.4990	8.492	-18.239	-8.683
2. C2	C	0.4286	0.6427	0.4989	7.287	-18.925	-8.682
3. C3	C	0.4297	0.6895	0.4991	7.305	-20.303	-8.685
4. C4	C	0.5681	0.6898	0.4993	9.658	-20.312	-8.689
5. C5	C	0.5702	0.6429	0.4992	9.694	-18.931	-8.687
6. C6	C	0.2855	0.7080	0.4990	4.854	-20.848	-8.683
7. C7	C	0.2284	0.7414	0.4989	3.883	-21.831	-8.682
8. C8	C	0.2514	0.7864	0.4986	4.274	-23.156	-8.676
9. C9	C	0.3305	0.7969	0.4983	5.619	-23.466	-8.671
10. C10	C	0.3638	0.7205	0.4988	6.185	-21.216	-8.680
11. C11	C	0.7120	0.7093	0.4995	12.105	-20.886	-8.692
12. C12	C	0.5029	0.4597	0.7332	8.550	-13.536	-12.759
13. C13	C	0.5020	0.4597	0.2719	8.534	-13.536	-4.732
14. C14	C	0.5019	0.4603	0.3513	8.533	-13.554	-6.113
15. C15	C	0.5030	0.4603	0.6538	8.551	-13.554	-11.377
16. C16	C	0.6335	0.7212	0.4995	10.770	-21.237	-8.692
17. C17	C	0.5023	0.5391	0.6527	8.540	-15.874	-11.358
18. C18	C	0.5026	0.5391	0.3524	8.545	-15.874	-6.132
19. C19	C	0.6654	0.7979	0.5002	11.312	-23.495	-8.704
20. C20	C	0.5028	0.5405	0.2731	8.548	-15.916	-4.752
21. C21	C	0.5021	0.5405	0.7320	8.536	-15.916	-12.738
22. C22	C	0.7447	0.7879	0.5003	12.660	-23.201	-8.706
23. C23	C	0.7685	0.7430	0.4999	13.065	-21.878	-8.699
24. C24	C	0.5024	0.5003	0.2322	8.541	-14.732	-4.041
25. C25	C	0.5025	0.5003	0.7730	8.543	-14.732	-13.452
26. C26	C	0.4951	0.5691	0.4988	8.417	-16.758	-8.680
27. C27	C	0.6689	0.2036	0.4999	11.372	-5.995	-8.699
28. C28	C	0.7479	0.2144	0.5011	12.715	-6.313	-8.720
29. C29	C	0.7703	0.2596	0.5018	13.096	-7.644	-8.732
30. C30	C	0.7129	0.2927	0.5013	12.120	-8.619	-8.723
31. C31	C	0.6347	0.2799	0.5001	10.790	-8.242	-8.703
32. C32	C	0.3340	0.2014	0.4964	5.678	-5.930	-8.638
33. C33	C	0.3651	0.2782	0.4977	6.207	-8.192	-8.661
34. C34	C	0.2864	0.2898	0.4974	4.869	-8.533	-8.656
35. C35	C	0.5685	0.3107	0.4996	9.665	-9.149	-8.694
36. C36	C	0.5691	0.3575	0.5000	9.675	-10.527	-8.701
37. C37	C	0.4979	0.3805	0.4997	8.465	-11.204	-8.696
38. C38	C	0.4275	0.3567	0.4989	7.268	-10.503	-8.682
39. C39	C	0.4301	0.3098	0.4985	7.312	-9.122	-8.675
40. C40	C	0.2303	0.2559	0.4965	3.915	-7.535	-8.640
41. C41	C	0.2545	0.2111	0.4959	4.327	-6.216	-8.630
42. C42	C	0.5016	0.4307	0.5001	8.528	-12.682	-8.703
43. H1	H	0.3717	0.3753	0.4987	6.319	-11.051	-8.678
44. H2	H	0.3509	0.8322	0.4980	5.966	-24.505	-8.666
45. H3	H	0.3742	0.6226	0.4986	6.362	-18.333	-8.676
46. H4	H	0.6257	0.6241	0.4993	10.637	-18.377	-8.689
47. H5	H	0.5032	0.4273	0.7640	8.555	-12.582	-13.295
48. H6	H	0.7290	0.6734	0.4993	12.394	-19.829	-8.689
49. H7	H	0.5017	0.4273	0.2411	8.529	-12.582	-4.196
50. H8	H	0.5025	0.5005	0.1692	8.543	-14.738	-2.944
51. H9	H	0.5024	0.5005	0.8359	8.541	-14.738	-14.546

52. H10	H	0.8311	0.7342	0.5000	14.129	-21.619	-8.701
53. H11	H	0.5033	0.5734	0.2438	8.557	-16.884	-4.243
54. H12	H	0.5016	0.5734	0.7614	8.528	-16.884	-13.250
55. H13	H	0.7877	0.8156	0.5008	13.392	-24.016	-8.715
56. H14	H	0.6443	0.8330	0.5004	10.954	-24.529	-8.708
57. H15	H	0.5020	0.5703	0.6184	8.534	-16.793	-10.761
58. H16	H	0.5020	0.4298	0.6184	8.534	-12.656	-10.761
59. H17	H	0.5029	0.4298	0.3867	8.550	-12.656	-6.729
60. H18	H	0.5029	0.5703	0.3867	8.550	-16.793	-6.729
61. H19	H	0.2693	0.6720	0.4992	4.578	-19.788	-8.687
62. H20	H	0.1660	0.7322	0.4990	2.822	-21.560	-8.683
63. H21	H	0.2079	0.8139	0.4985	3.534	-23.966	-8.675
64. H22	H	0.3554	0.1663	0.4960	6.042	-4.897	-8.631
65. H23	H	0.2119	0.1832	0.4951	3.602	-5.395	-8.616
66. H24	H	0.1676	0.2645	0.4962	2.849	-7.788	-8.635
67. H25	H	0.2690	0.3256	0.4979	4.573	-9.588	-8.664
68. H26	H	0.6488	0.1683	0.4994	11.030	-4.956	-8.690
69. H27	H	0.7916	0.1871	0.5015	13.458	-5.509	-8.727
70. H28	H	0.8327	0.2689	0.5028	14.157	-7.918	-8.750
71. H29	H	0.7287	0.3288	0.5018	12.388	-9.682	-8.732
72. H30	H	0.6232	0.3778	0.5007	10.595	-11.125	-8.713
73. N1	N	0.4991	0.5004	0.6104	8.485	-14.735	-10.622
74. N2	N	0.4988	0.7118	0.4993	8.480	-20.960	-8.689
75. N3	N	0.3857	0.7648	0.4983	6.557	-22.520	-8.671
76. N4	N	0.6108	0.7654	0.4996	10.384	-22.538	-8.694
77. N5	N	0.5020	0.5000	0.3909	8.534	-14.723	-6.802
78. N6	N	0.6133	0.2356	0.4994	10.427	-6.938	-8.690
79. N7	N	0.3883	0.2341	0.4973	6.601	-6.893	-8.654
80. N8	N	0.4997	0.2881	0.4988	8.495	-8.483	-8.680
81. O1	O	0.5660	0.5502	0.4995	9.622	-16.201	-8.692
82. O2	O	0.4333	0.5492	0.4982	7.366	-16.172	-8.670
83. O3	O	0.4304	0.4494	0.4995	7.317	-13.233	-8.692
84. O4	O	0.5631	0.4510	0.5008	9.573	-13.280	-8.715
85. Zn1	Zn	0.4993	0.5004	0.5012	8.488	-14.735	-8.722

Figure S10. X-ray absorption spectrum at the Zn K-edge of the NEU-5 before (a) and after normalization (b).

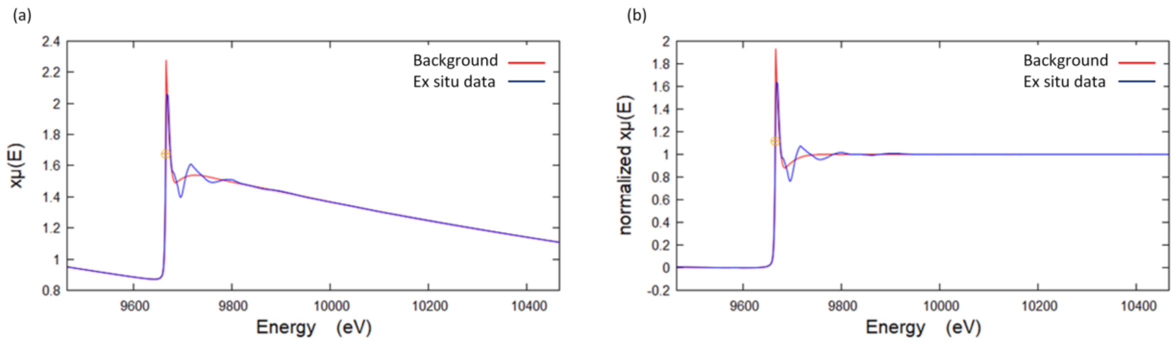

Figure S11. Coordinates of each atom in the local molecular structure of iron within NEU-5. Atom labelling scheme: C = black; O = red; N = blue; Fe = brown; H = pink.

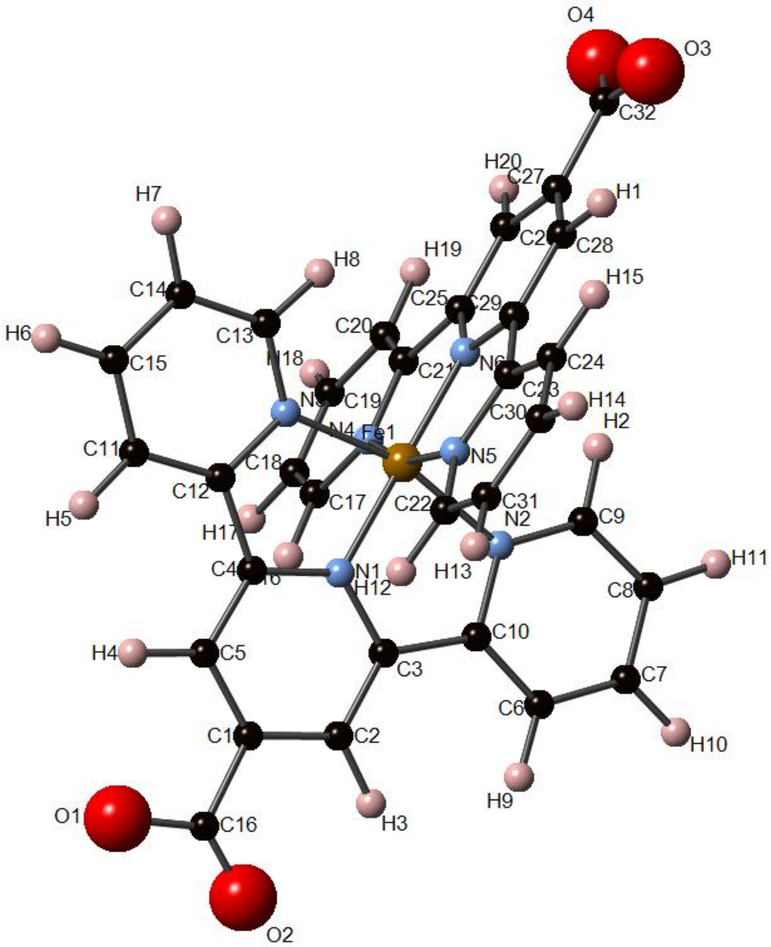

Label	Elmt	Fractional Coordinates x	y	z	Orthogonal Coordinates xor[Å]	yor[Å]	zor[Å]
1. C1	C	0.5007	0.7007	0.4983	-11.609	-9.889	12.876
2. C2	C	0.4296	0.6707	0.4984	-10.307	-9.900	12.400
3. C3	C	0.4307	0.6102	0.4983	-9.661	-8.697	12.208
4. C4	C	0.5695	0.6097	0.4980	-11.557	-7.512	12.944
5. C5	C	0.5715	0.6704	0.4981	-12.248	-8.692	13.153
6. C6	C	0.2862	0.5862	0.4984	-7.420	-9.447	11.360
7. C7	C	0.2290	0.5431	0.4985	-6.165	-9.082	10.916
8. C8	C	0.2520	0.4848	0.4988	-5.841	-7.737	10.855
9. C9	C	0.3313	0.4713	0.4991	-6.777	-6.800	11.240
10. C10	C	0.3647	0.5701	0.4986	-8.317	-8.465	11.731
11. C11	C	0.7137	0.5846	0.4978	-13.258	-5.796	13.631
12. C12	C	0.6350	0.5691	0.4979	-12.011	-6.157	13.162
13. C13	C	0.6670	0.4701	0.4972	-11.371	-3.933	13.001
14. C14	C	0.7465	0.4829	0.4970	-12.600	-3.512	13.464
15. C15	C	0.7703	0.5410	0.4974	-13.559	-4.457	13.786
16. C16	C	0.4963	0.7657	0.4985	-12.258	-11.209	13.066
17. C17	C	0.4975	0.5279	0.3305	-10.654	-6.404	9.629
18. C18	C	0.4963	0.5140	0.2513	-10.948	-6.091	8.317
19. C19	C	0.4956	0.4556	0.2288	-10.431	-4.931	7.766
20. C20	C	0.4961	0.4127	0.2864	-9.633	-4.117	8.547
21. C21	C	0.4974	0.4292	0.3647	-9.375	-4.480	9.853
22. C22	C	0.5012	0.5307	0.6662	-8.778	-6.636	15.000
23. C23	C	0.4998	0.4315	0.6350	-7.856	-4.673	14.175
24. C24	C	0.5001	0.4164	0.7139	-7.235	-4.421	15.383
25. C25	C	0.4978	0.3895	0.4311	-8.559	-3.735	10.783
26. C26	C	0.4974	0.3290	0.4305	-7.895	-2.544	10.576
27. C27	C	0.4978	0.2993	0.5019	-7.160	-2.000	11.618
28. C28	C	0.4986	0.3300	0.5725	-7.095	-2.642	12.845
29. C29	C	0.4989	0.3906	0.5699	-7.776	-3.833	13.002
30. C30	C	0.5011	0.4603	0.7701	-7.401	-5.313	16.425

31. C31	C	0.5016	0.5182	0.7458	-8.182	-6.436	16.228
32. C32	C	0.4974	0.2343	0.4982	-6.465	-0.719	11.347
33. Fe1	Fe	0.4994	0.5000	0.4987	-9.394	-5.942	12.225
34. H1	H	0.4988	0.3060	0.6284	-6.509	-2.202	13.658
35. H2	H	0.3517	0.4257	0.4994	-6.556	-5.728	11.206
36. H3	H	0.3751	0.6966	0.4987	-9.842	-10.872	12.197
37. H4	H	0.6272	0.6947	0.4980	-13.277	-8.700	13.528
38. H5	H	0.7307	0.6309	0.4981	-13.995	-6.565	13.877
39. H6	H	0.8331	0.5524	0.4973	-14.544	-4.150	14.157
40. H7	H	0.7895	0.4471	0.4965	-12.800	-2.442	13.570
41. H8	H	0.6458	0.4246	0.4969	-10.585	-3.215	12.736
42. H9	H	0.2699	0.6327	0.4981	-7.707	-10.502	11.418
43. H10	H	0.1664	0.5549	0.4983	-5.438	-9.844	10.616
44. H11	H	0.2084	0.4494	0.4988	-4.857	-7.408	10.507
45. H12	H	0.5015	0.5761	0.6447	-9.404	-7.516	14.806
46. H13	H	0.5024	0.5542	0.7886	-8.337	-7.166	17.030
47. H14	H	0.5014	0.4492	0.8330	-6.917	-5.131	17.392
48. H15	H	0.4996	0.3702	0.7313	-6.622	-3.525	15.508
49. H16	H	0.4981	0.5736	0.3506	-11.045	-7.313	10.100
50. H17	H	0.4959	0.5492	0.2074	-11.583	-6.762	7.730
51. H18	H	0.4946	0.4435	0.1663	-10.650	-4.662	6.727
52. H19	H	0.4956	0.3661	0.2705	-9.209	-3.192	8.140
53. H20	H	0.4967	0.3027	0.3763	-7.914	-1.998	9.624
54. N1	N	0.5000	0.5813	0.4980	-10.295	-7.540	12.481
55. N2	N	0.3866	0.5128	0.4991	-7.988	-7.150	11.670
56. N3	N	0.6122	0.5120	0.4977	-11.076	-5.223	12.852
57. N4	N	0.4981	0.4866	0.3862	-9.886	-5.619	10.385
58. N5	N	0.5002	0.4885	0.6118	-8.620	-5.779	13.992
59. N6	N	0.4987	0.4187	0.5001	-8.488	-4.346	11.981
60. O1	O	0.5674	0.7902	0.4978	-13.503	-11.089	13.514
61. O2	O	0.4343	0.7915	0.4992	-11.687	-12.243	12.829
62. O3	O	0.4980	0.2103	0.5696	-5.795	-0.285	12.408
63. O4	O	0.4966	0.2082	0.4365	-6.529	-0.173	10.276

Figure S12. X-ray absorption spectrum at the Fe K-edge of the NEU-5 before (a) and after normalization (b).

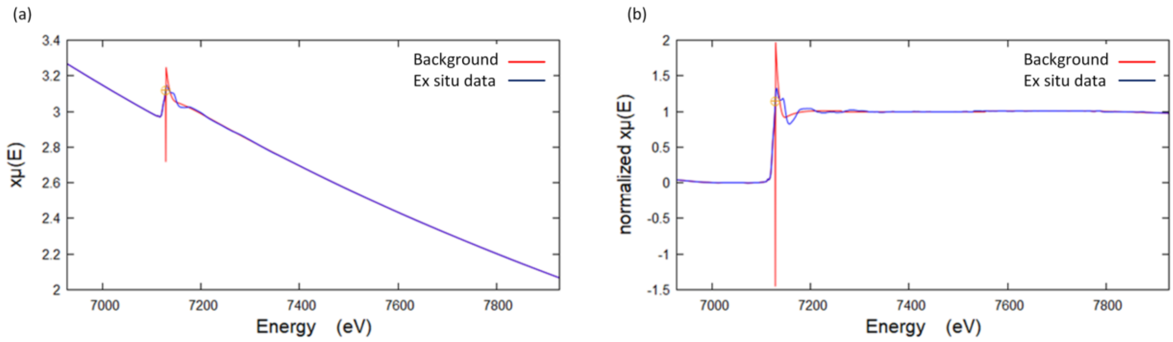

Figure S13. EDX characterization of NEU-5. It shows the presence of zinc (~5 %w) and iron (~3 %w) within the sample, as well as that of carbon (~47 %w), nitrogen (~4 %w), oxygen (~12 %w), fluorine (~21 %w), and phosphorus (~8 %w). Weight content was determined in different zones and the average was calculated.

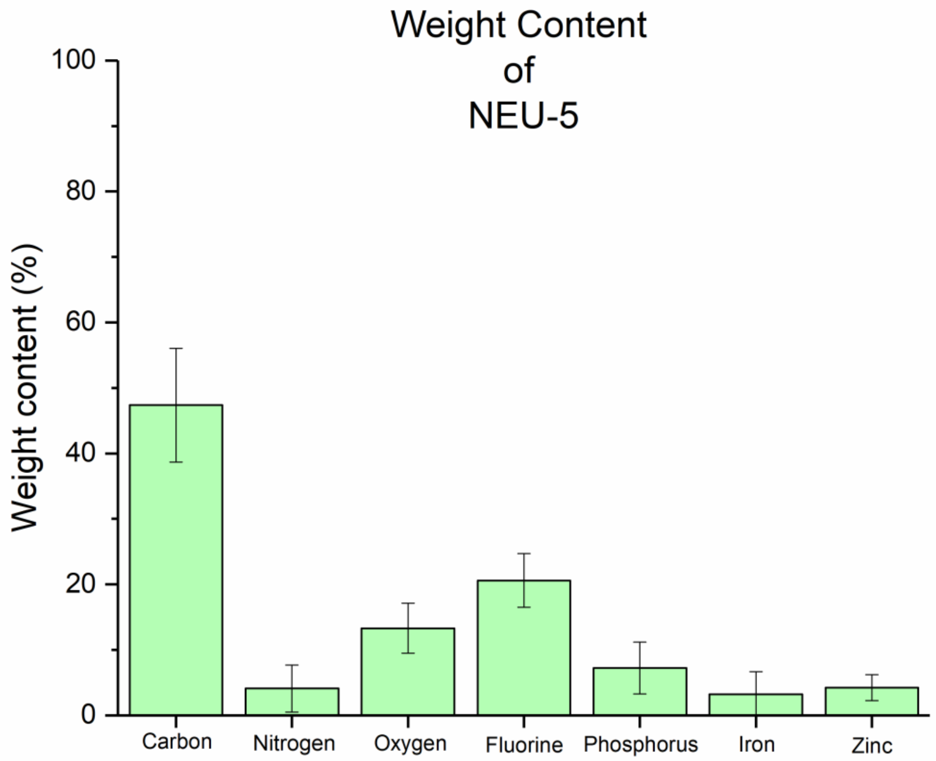

Figure S14. EDX characterization of NEU-5. It shows the presence of zinc (~2 %m) and iron (~2 %m) within the sample, as well as that of carbon (~60 %m), nitrogen (~4 %m), oxygen (~13 %m), fluorine (~16 %m), and phosphorus (~3 %m). Atomic content was determined in different zones and the average was calculated.

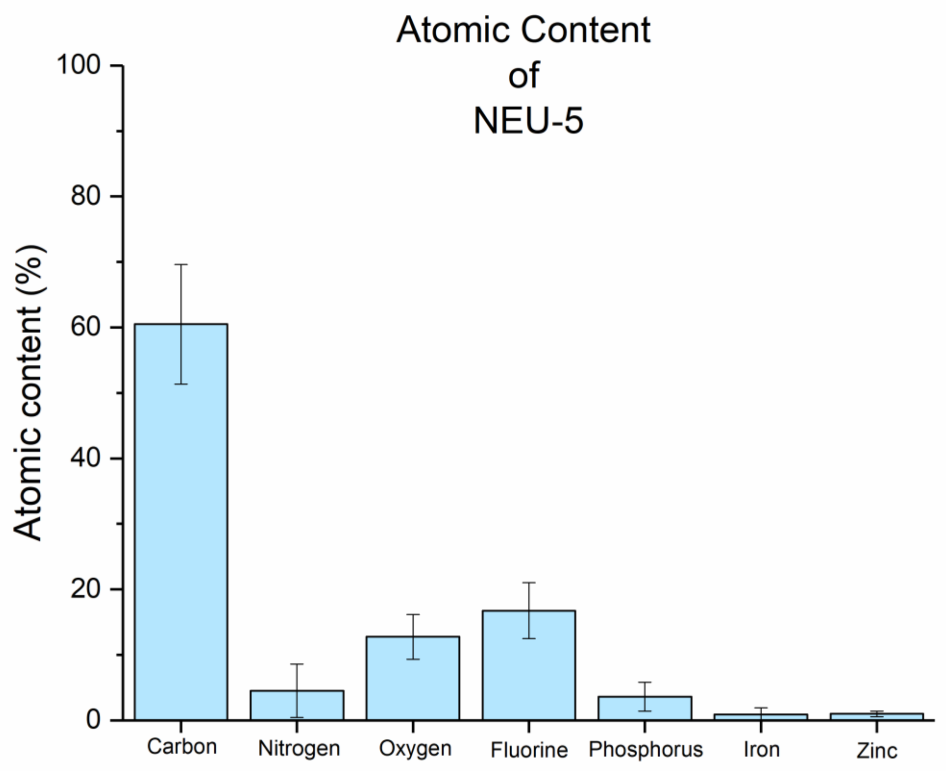

Figure S15. EDX characterization of NEU-6. It shows the presence of zinc (~9 %w) and ruthenium (~8 %w) within the sample, as well as that of carbon (~49 %w), nitrogen (~4 %w), oxygen (~8 %w), fluorine (~11 %w), and phosphorus (~11 %w). Weight content was determined in different zones and the average was calculated.

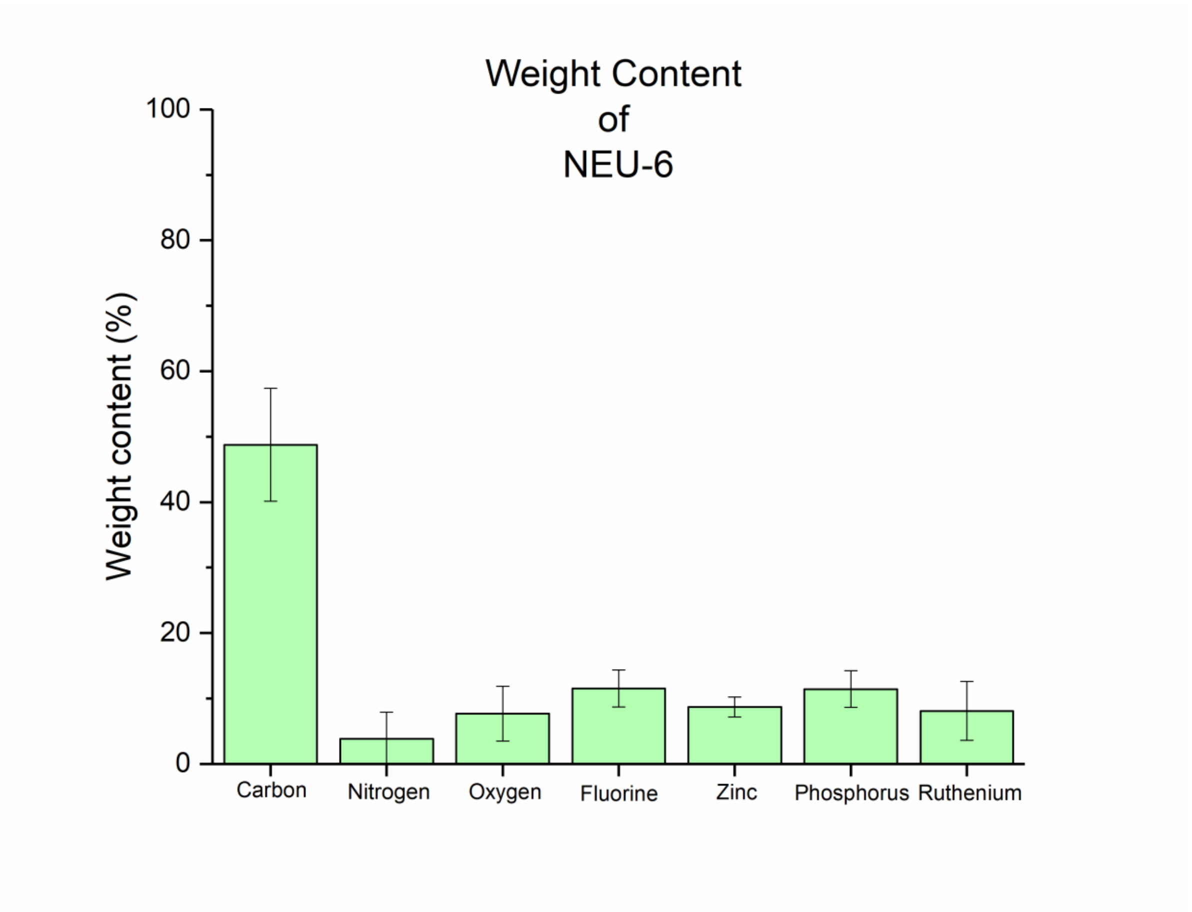

Figure S16. EDX characterization of NEU-6. It shows the presence of zinc (~2 %m) and ruthenium (~2 %m) within the sample, as well as that of carbon (~68 %m), nitrogen (~4 %m), oxygen (~8 %m), fluorine (~10 %m), and phosphorus (~6 %m). Atomic content was determined in different zones and the average was calculated.

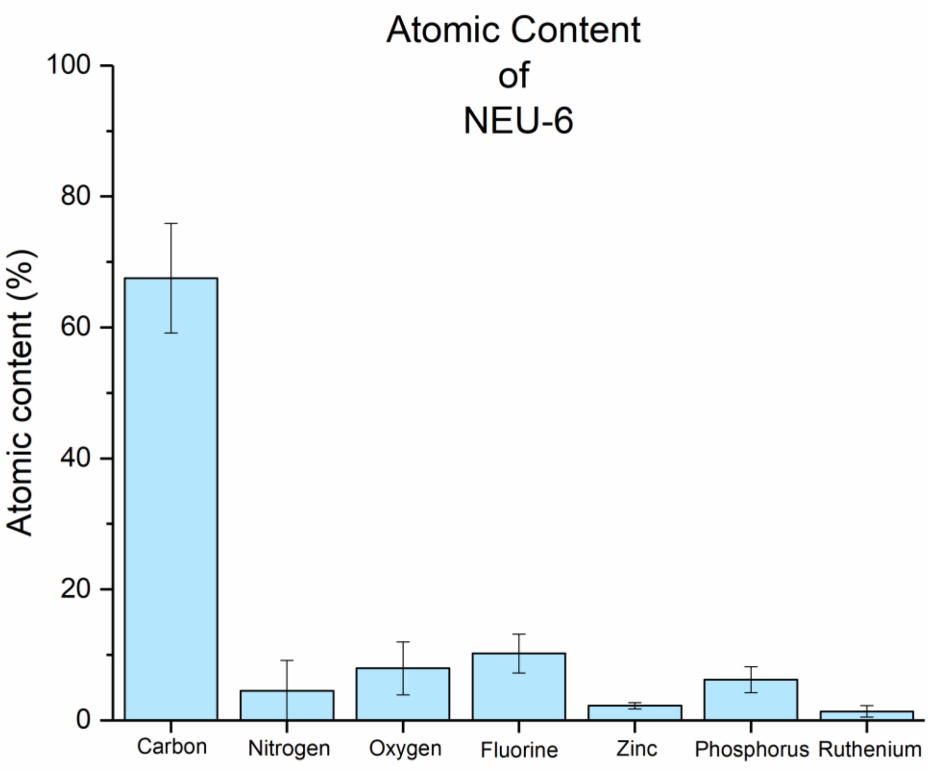

Figure S17. EDX characterization of NEU-7. It shows the presence of iron (~18 %w) and ruthenium (~2 %w) within the sample, as well as that of carbon (~28 %w), nitrogen (~3 %w), oxygen (~32 %w), fluorine (~7 %w), and phosphorus (~10 %w). Weight content was determined in different zones and the average was calculated.

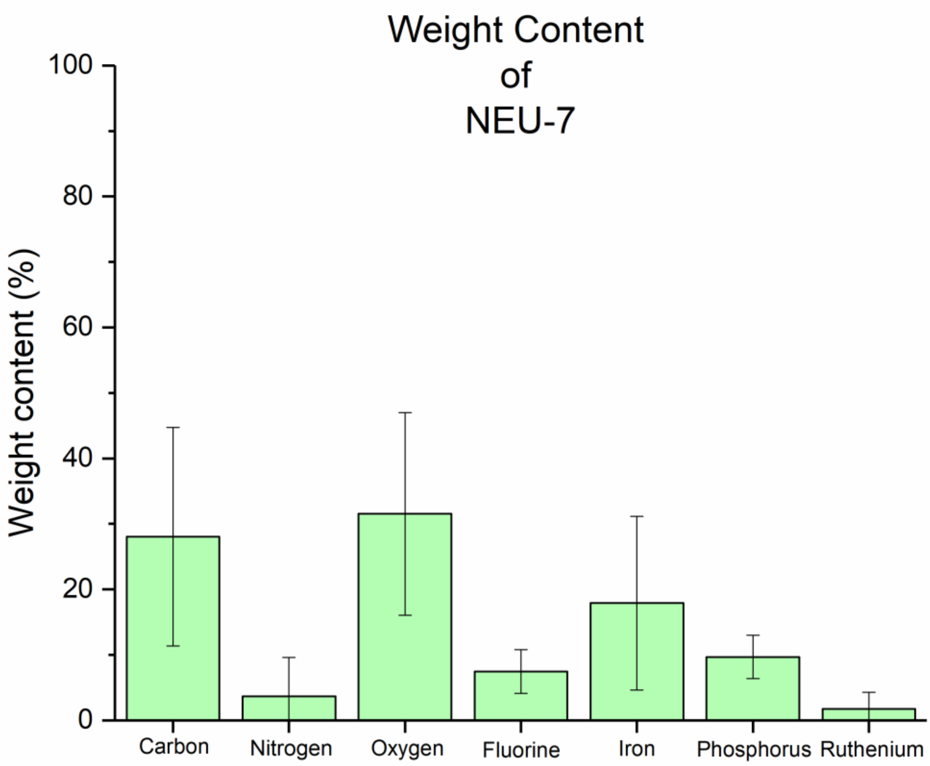

Figure S18. EDX characterization of NEU-7. It shows the presence of iron (~7 %m) and ruthenium (~1 %m) within the sample, as well as that of carbon (~40 %m), nitrogen (~4 %m), oxygen (~35 %m), fluorine (~7 %m), and phosphorus (~6 %m). Atomic content was determined in different zones and the average was calculated.

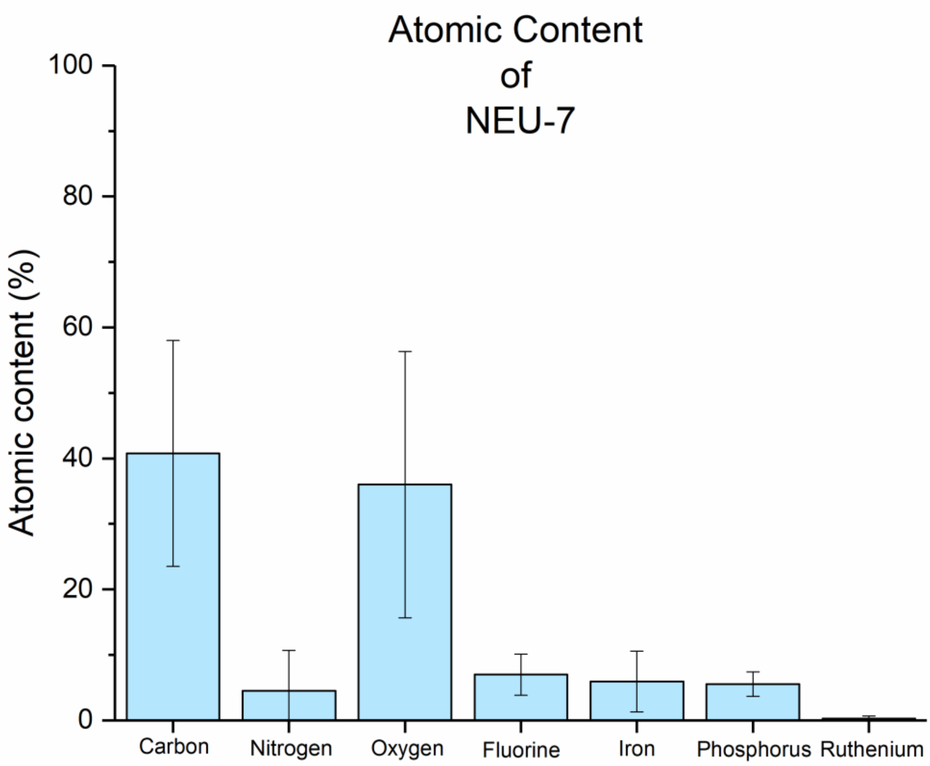

Figure S19. EDX characterization of NEU-8. It shows the presence of titanium (~7 %w) and ruthenium (~9 %w) within the sample, as well as that of carbon (~45 %w), nitrogen (~5 %w), oxygen (~11 %w), fluorine (~12 %w), and phosphorus (~11 %w). Weight content was determined in different zones and the average was calculated.

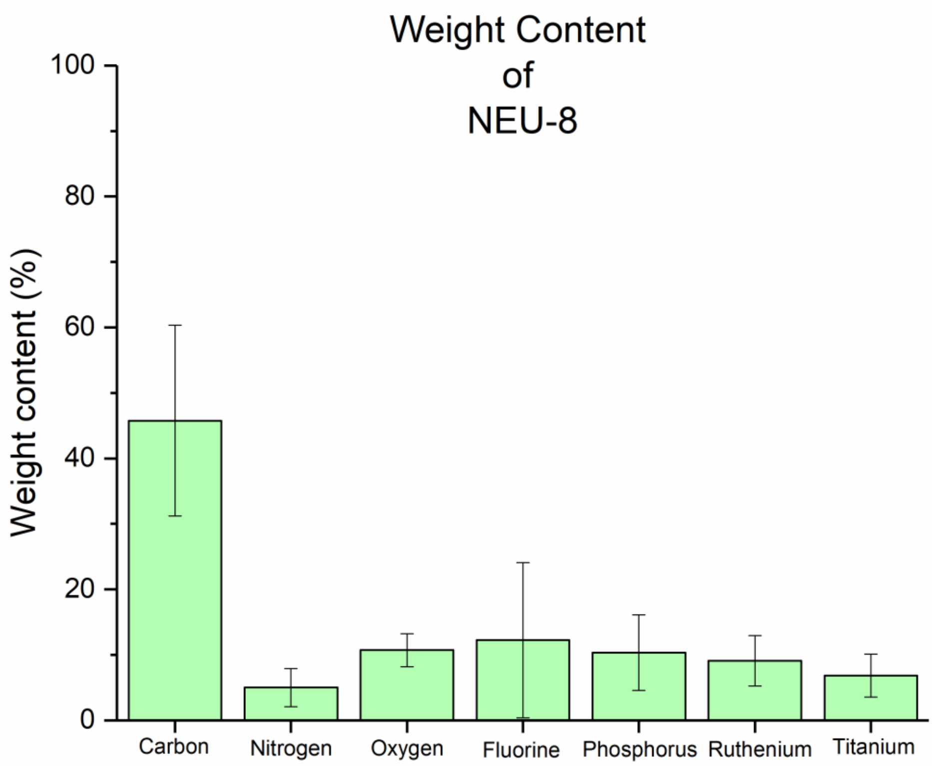

Figure S20. EDX characterization of NEU-8. It shows the presence of titanium (~3 %m) and ruthenium (~2 %m) within the sample, as well as that of carbon (~62 %m), nitrogen (~5 %m), oxygen (~11 %m), fluorine (~11 %m), and phosphorus (~6 %m). Atomic content was determined in different zones and the average was calculated.

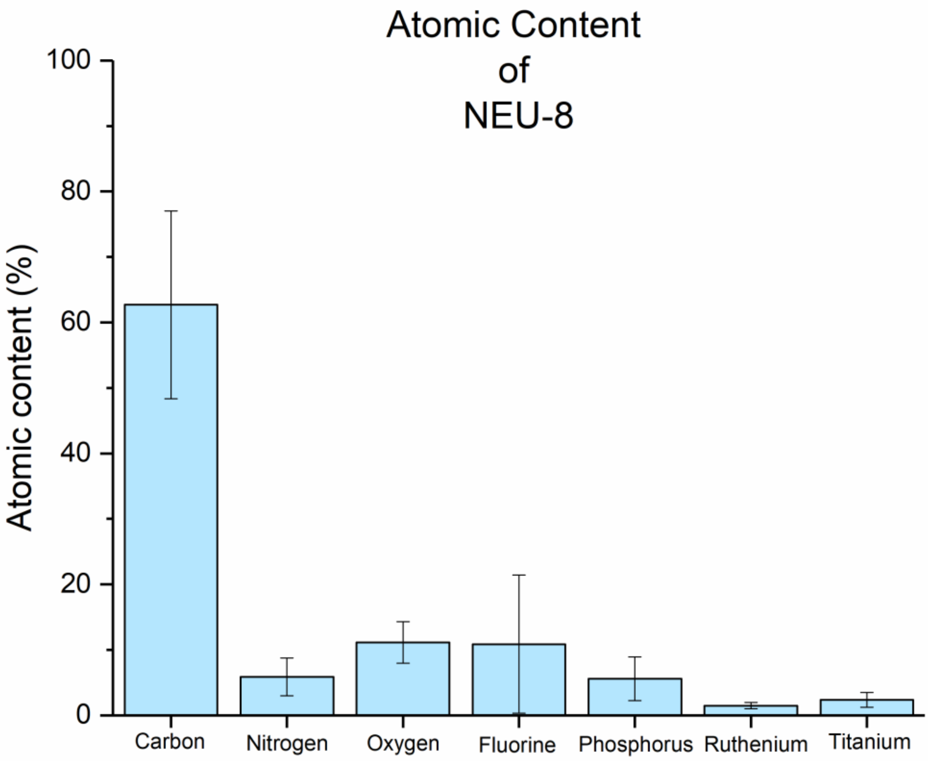

Figure S21. TGA of NEU-5 from room temperature to 1000 °C at a rate of 5 °C min^{-1} under a nitrogen flow. NEU-5 showed a total mass loss of ~49.42 wt% on heating up to 1000 °C. The mass loss occurred in three steps: (1) mass loss of ~4.42 wt% at ~250 °C due to the desorption of trapped moisture, (2) mass loss of ~30.85 wt% on heating up to ~475 °C due to the decomposition of ligated pyridine in axial position, (3) mass loss of ~14.18 wt% on heating up to 800 °C due to the decomposition of the remaining nitrogen-carbon-hydrogen structure.

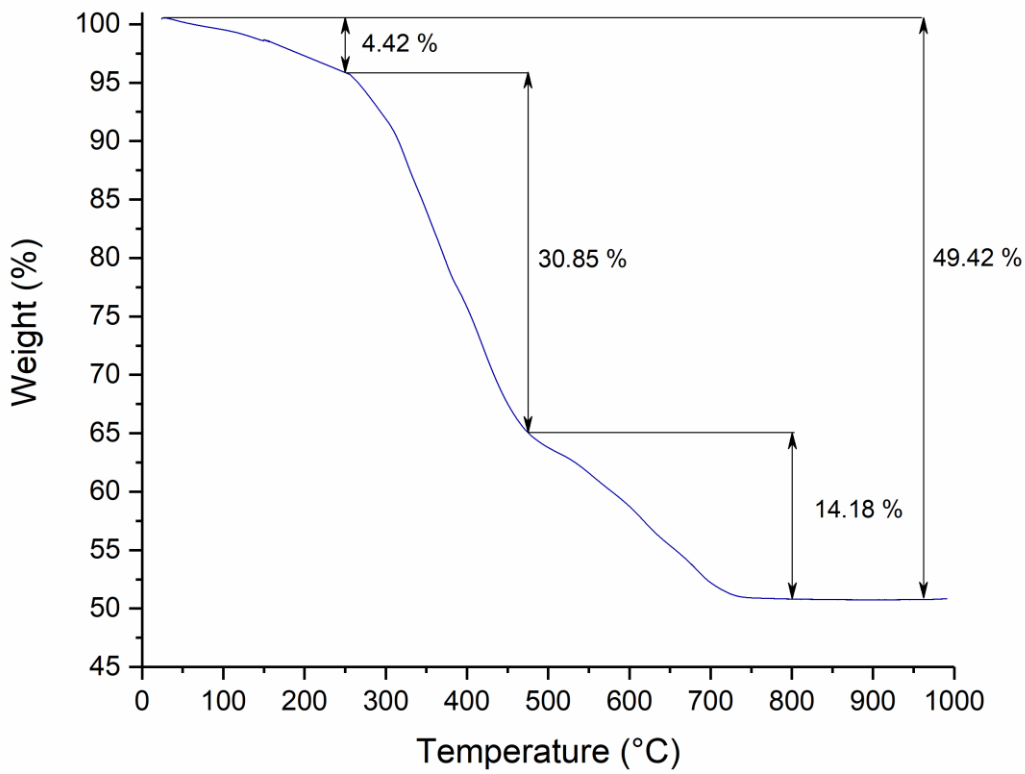

Figure S22. TGA of NEU-6 from room temperature to 1000 °C at a rate of 5 °C min^{-1} under a nitrogen flow. NEU-6 showed a total mass loss of ~54.76 wt% on heating up to 1000 °C. The mass loss occurred in three steps: (1) mass loss of ~3.12 wt% at ~150 °C due to the desorption of trapped moisture, (2) mass loss of ~17.07 wt% on heating up to ~350 °C due to the decomposition of ligated pyridine in axial position, (3) mass loss of ~34.15 wt% on heating up to 600 °C due to the decomposition of the remaining nitrogen-carbon-hydrogen structure.

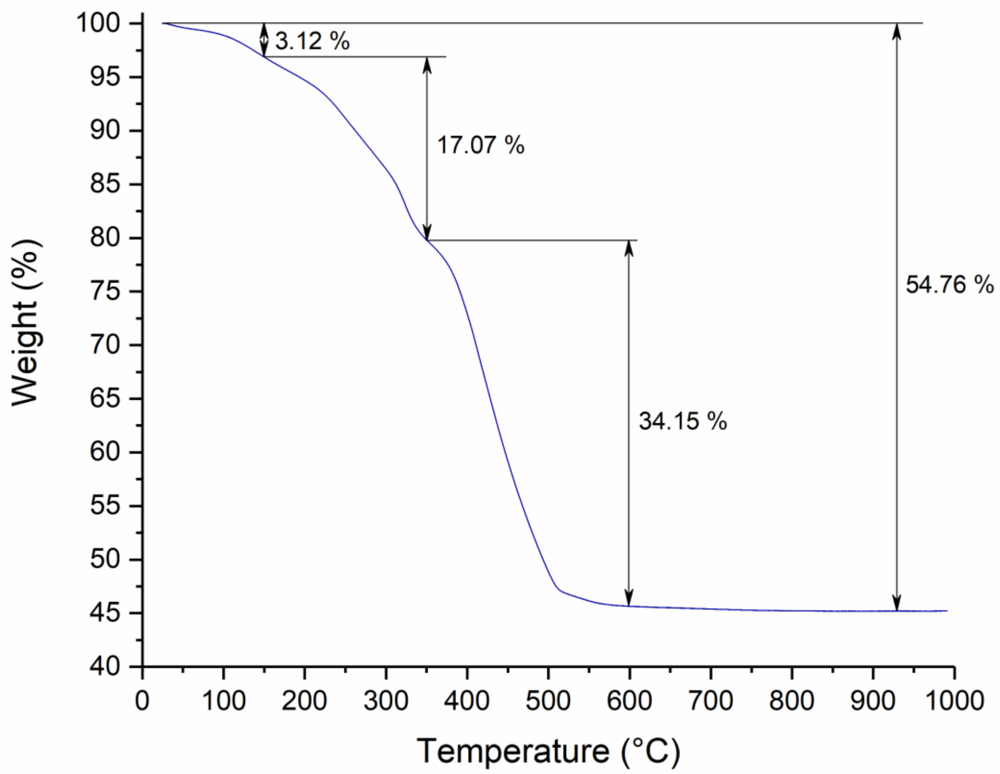

Figure S23. TGA of NEU-7 from room temperature to 1000 °C at a rate of 5 °C min^{-1} under a nitrogen flow. NEU-7 showed a total mass loss of ~29.57 wt% on heating up to 1000 °C. The mass loss occurred in three steps: (1) mass loss of ~2.06 wt% at ~150 °C due to the desorption of trapped moisture, (2) mass loss of ~5.64 wt% on heating up to ~275 °C due to the decomposition of ligated pyridine in axial position, (3) mass loss of ~21.34 wt% on heating up to 600 °C due to the decomposition of the remaining nitrogen-carbon-hydrogen structure.

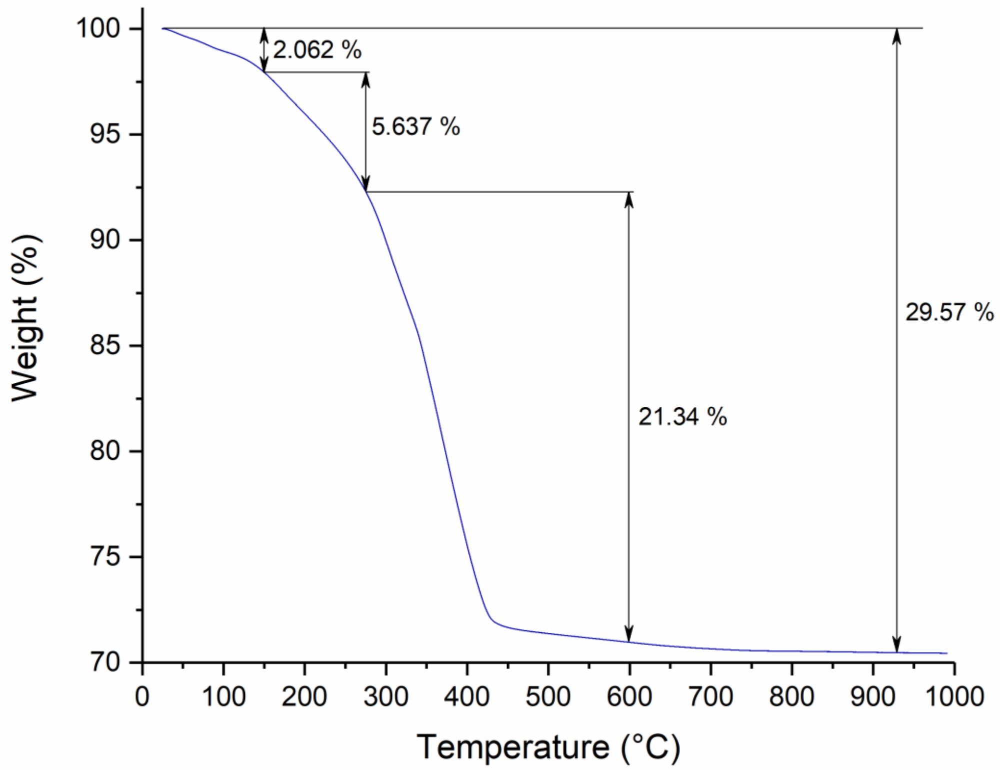

Figure S24. TGA of NEU-8 from room temperature to 1000 °C at a rate of 5 °C min^{-1} under a nitrogen flow. NEU-8 showed a total mass loss of ~65.20 wt% on heating up to 1000 °C. The mass loss occurred in three steps: (1) mass loss of ~6.70 wt% at ~150 °C due to the desorption of trapped moisture, (2) mass loss of ~9.15 wt% on heating up to ~300 °C due to the decomposition of ligated pyridine in axial position, (3) mass loss of ~48.83 wt% on heating up to 600 °C due to the decomposition of the remaining nitrogen-carbon-hydrogen structure.

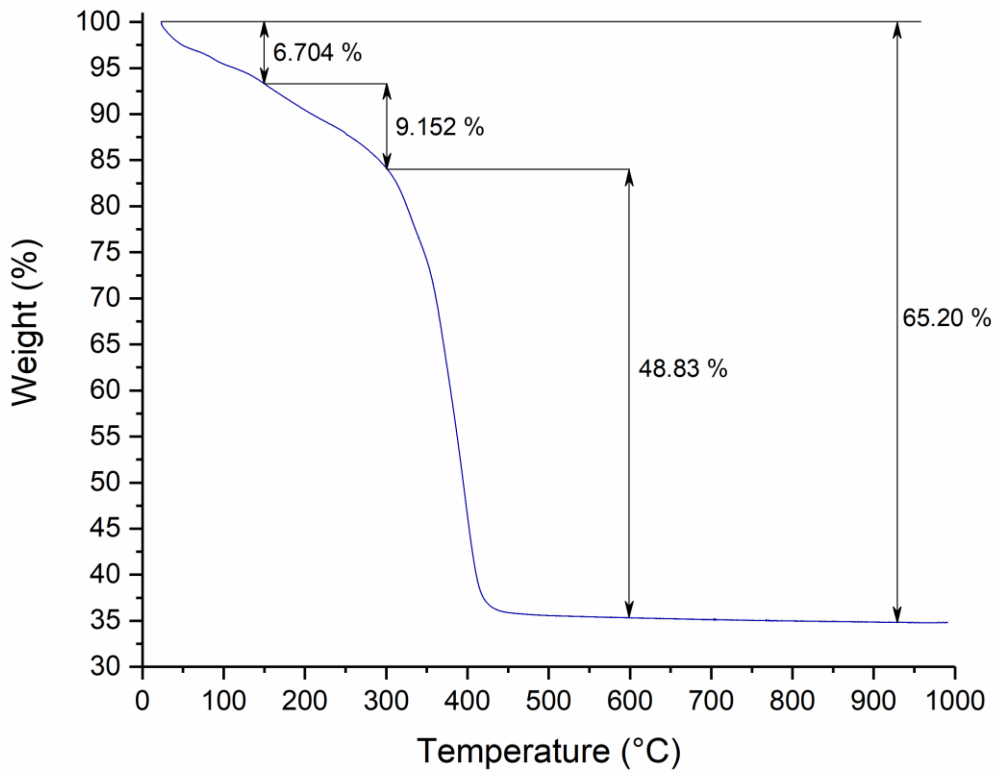

Figure S25. Nitrogen adsorption/desorption isotherms of pristine NEU-5 and Fe_2P@PNDCN.

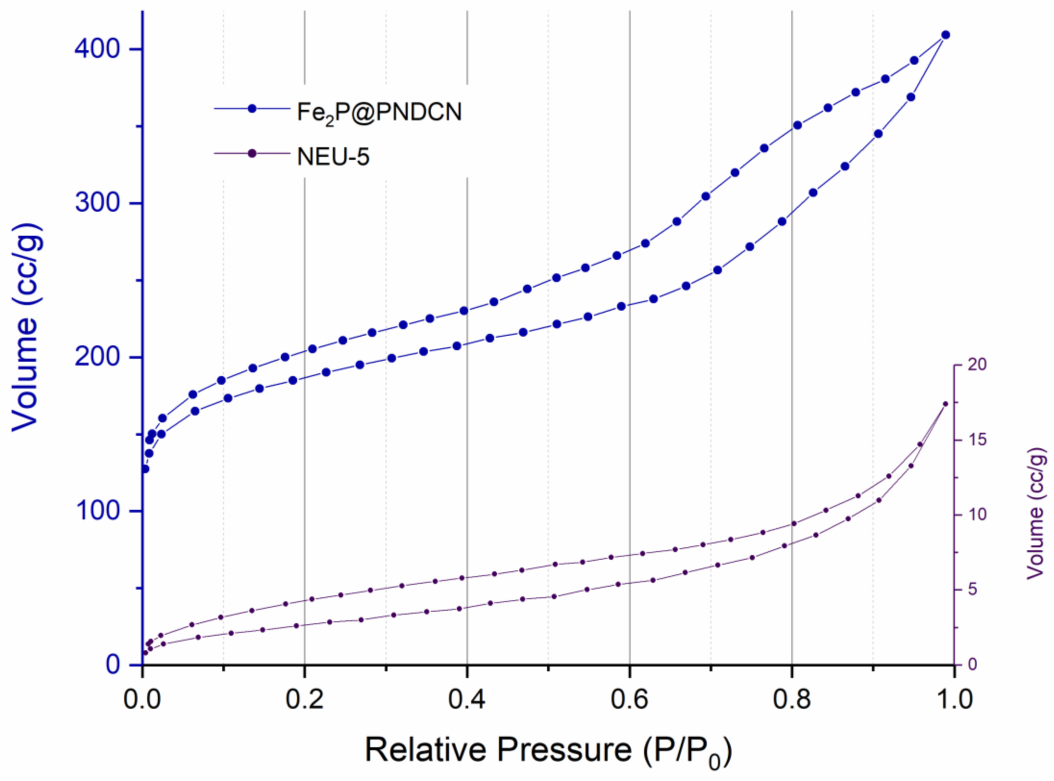

Figure S26. Nitrogen adsorption/desorption isotherms of pristine NEU-6 and RuP@PNDCN.

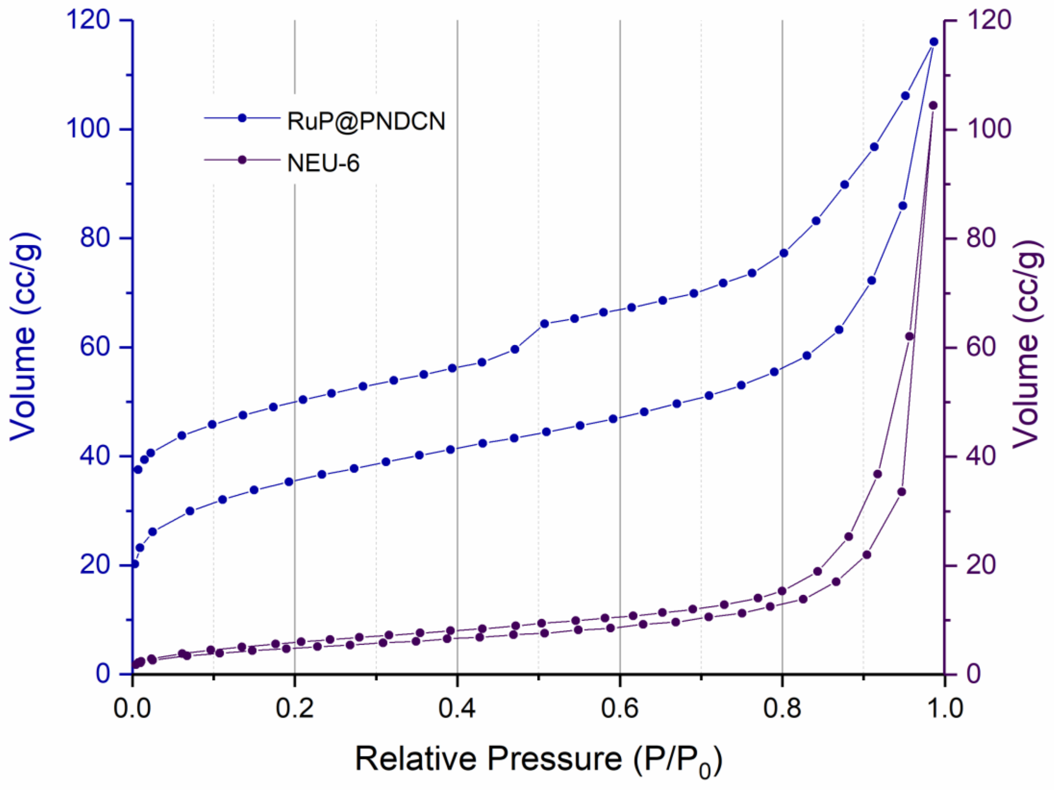

Figure S27. Nitrogen adsorption/desorption isotherms of pristine NEU-7 and Fe_3O_4/RuO_2@NEU-7.

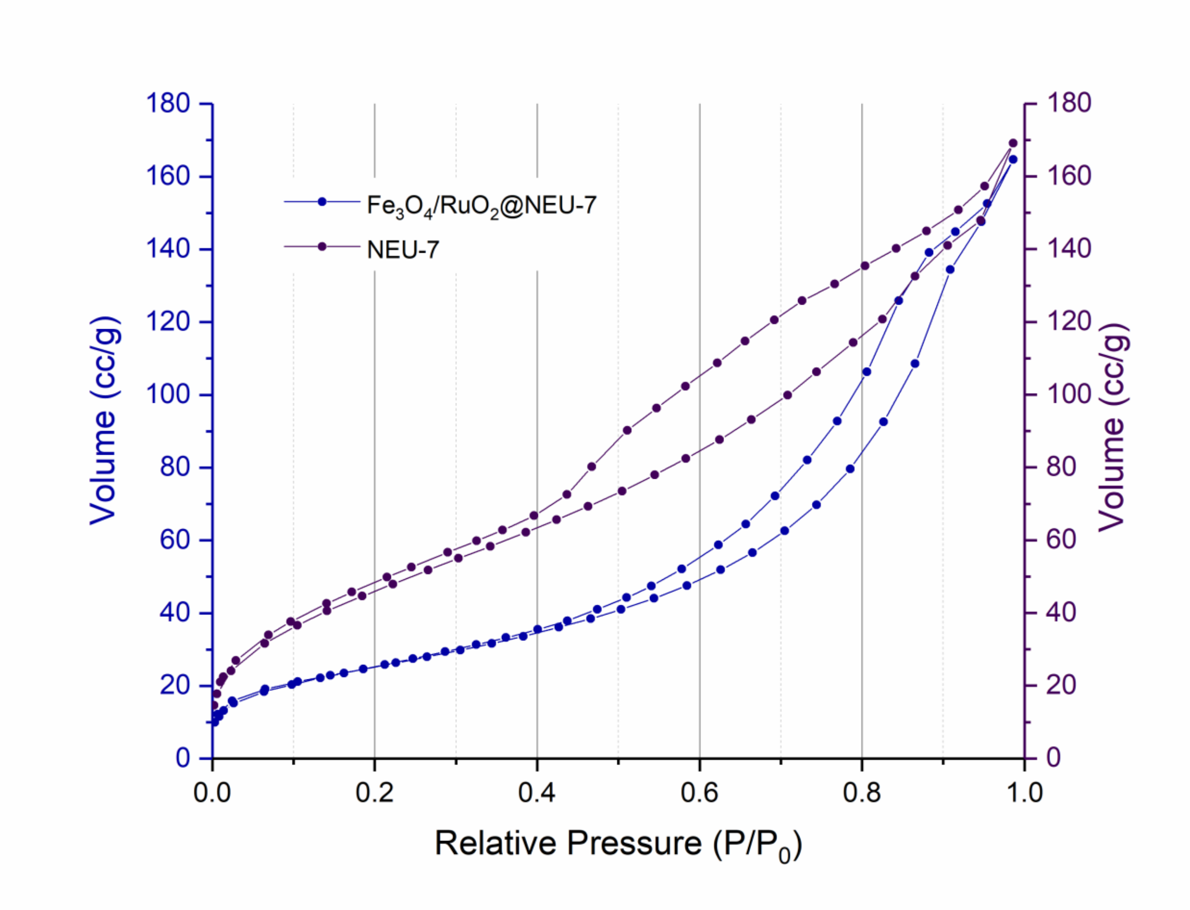

Figure S28. Nitrogen adsorption/desorption isotherms of pristine NEU-8 and $Ru_2O/TiN/TiO_2$@NEU-8.

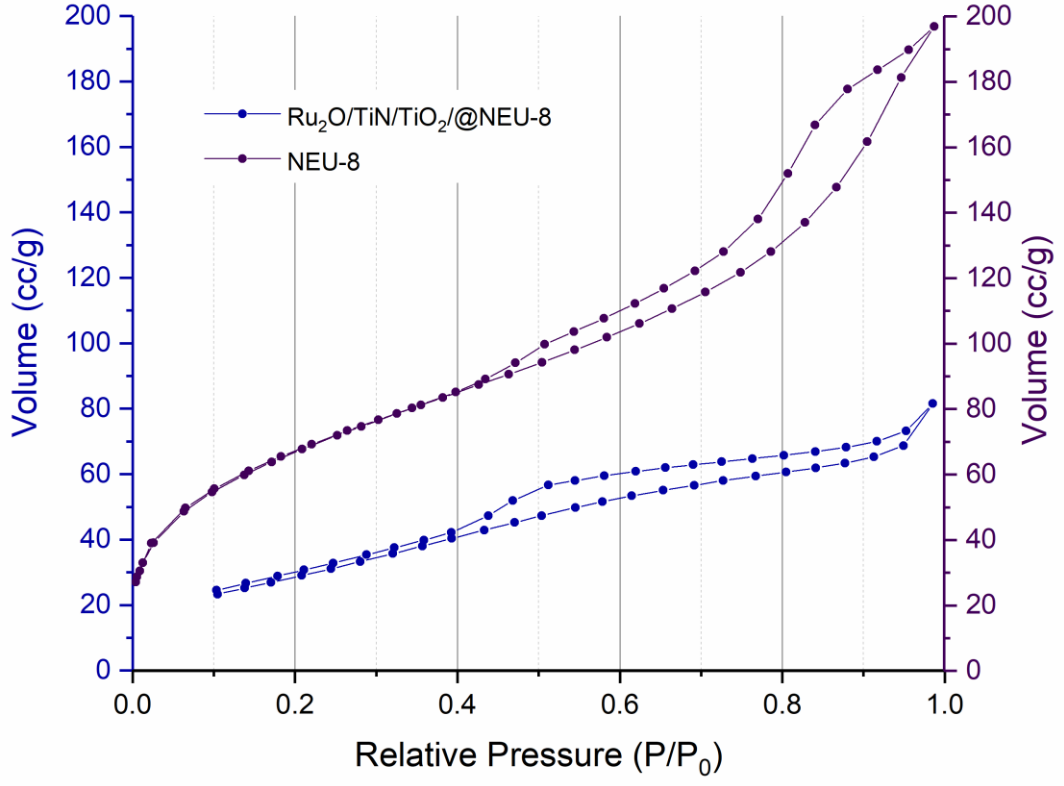

Figure S29. DFT pore analysis of pristine NEU-5 and Fe_2P@PNDCN.

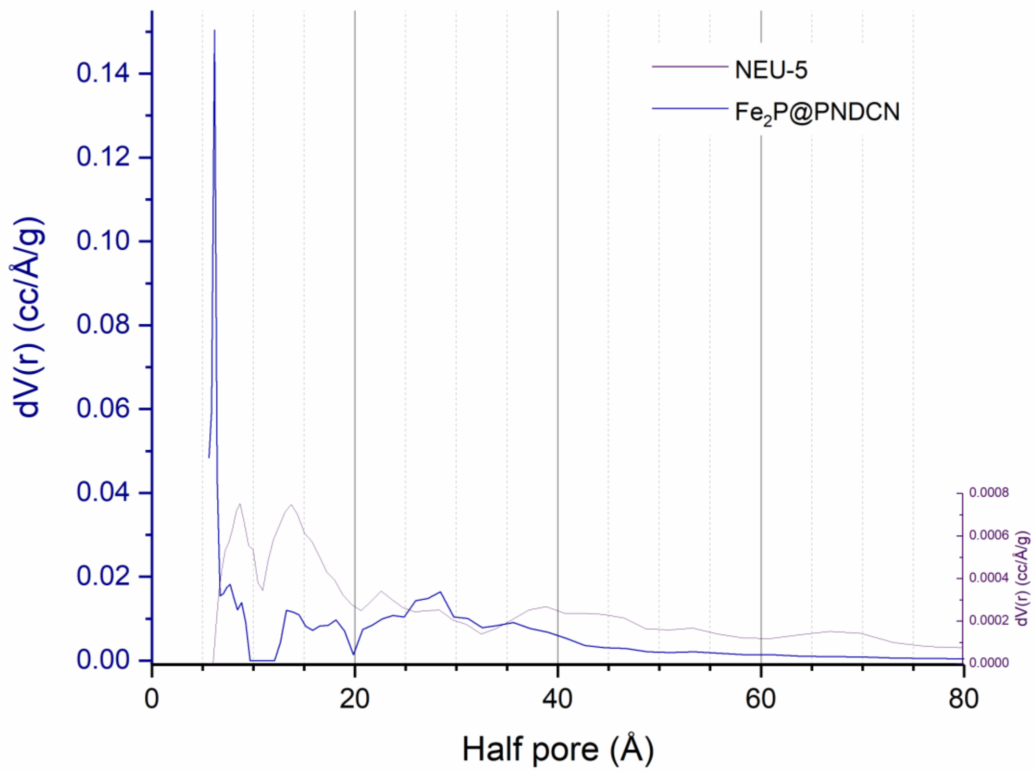

Figure S30. DFT pore analysis of pristine NEU-6 and RuP@PNDCN.

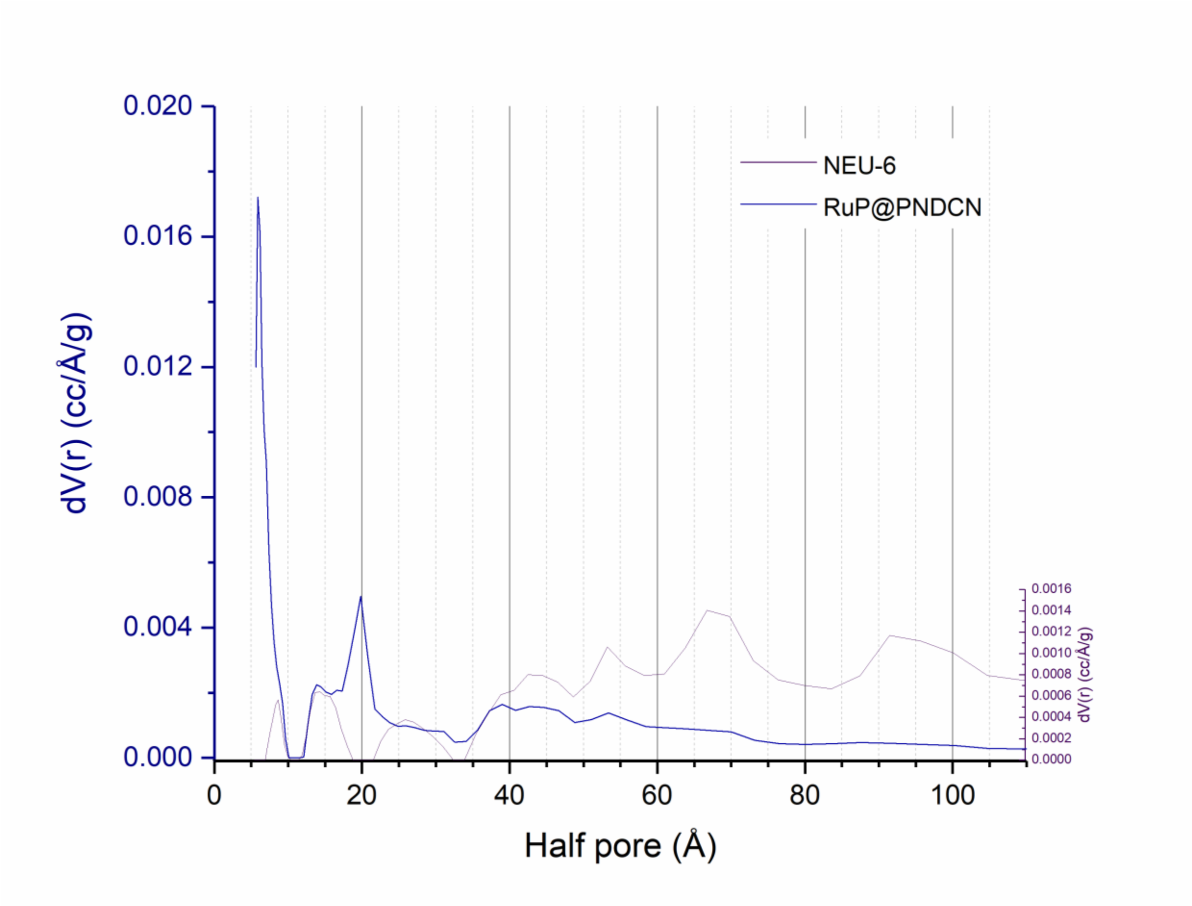

Figure S31. DFT pore analysis of pristine NEU-7 and Fe_3O_4/RuO_2@NEU-7.

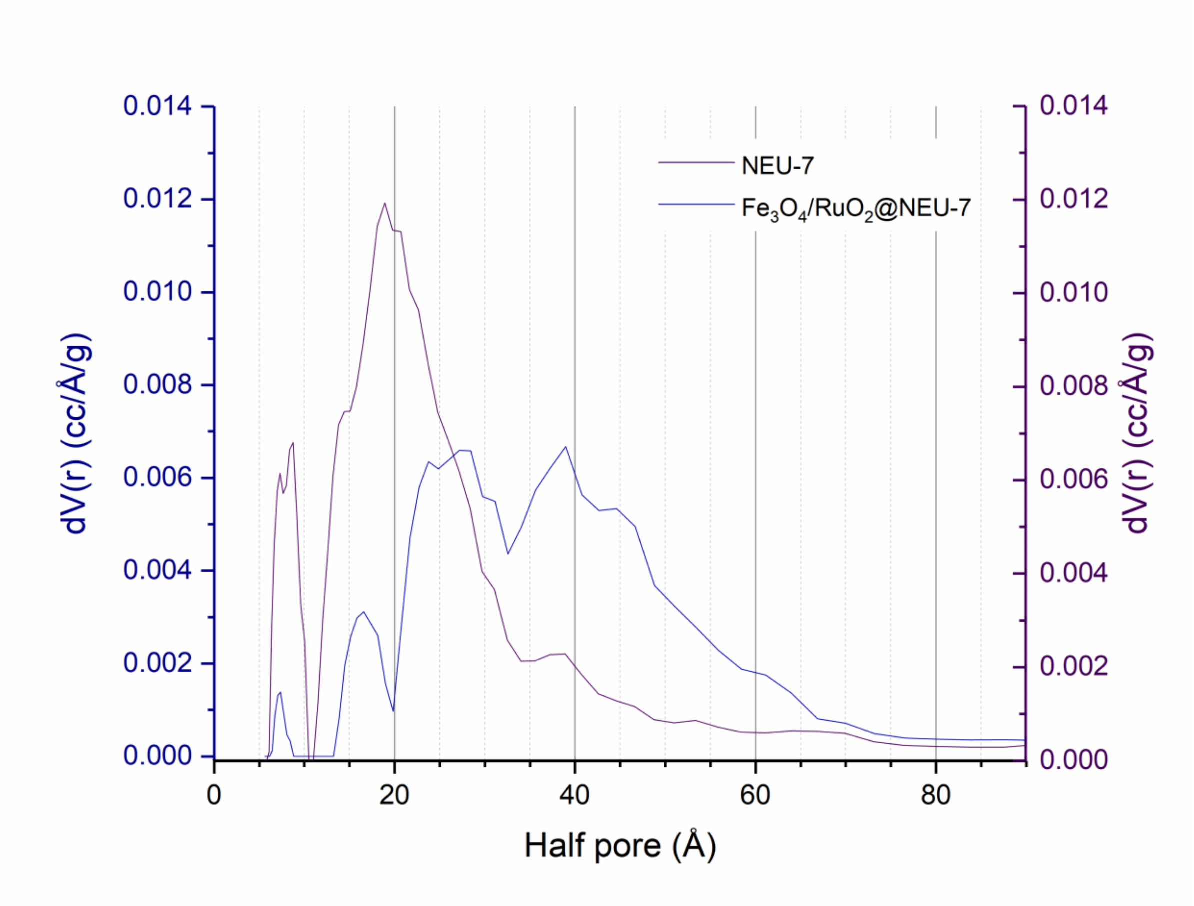

Figure S32. DFT pore analysis of pristine NEU-8 and $Ru_2O/TiN/TiO_2$@NEU-8.

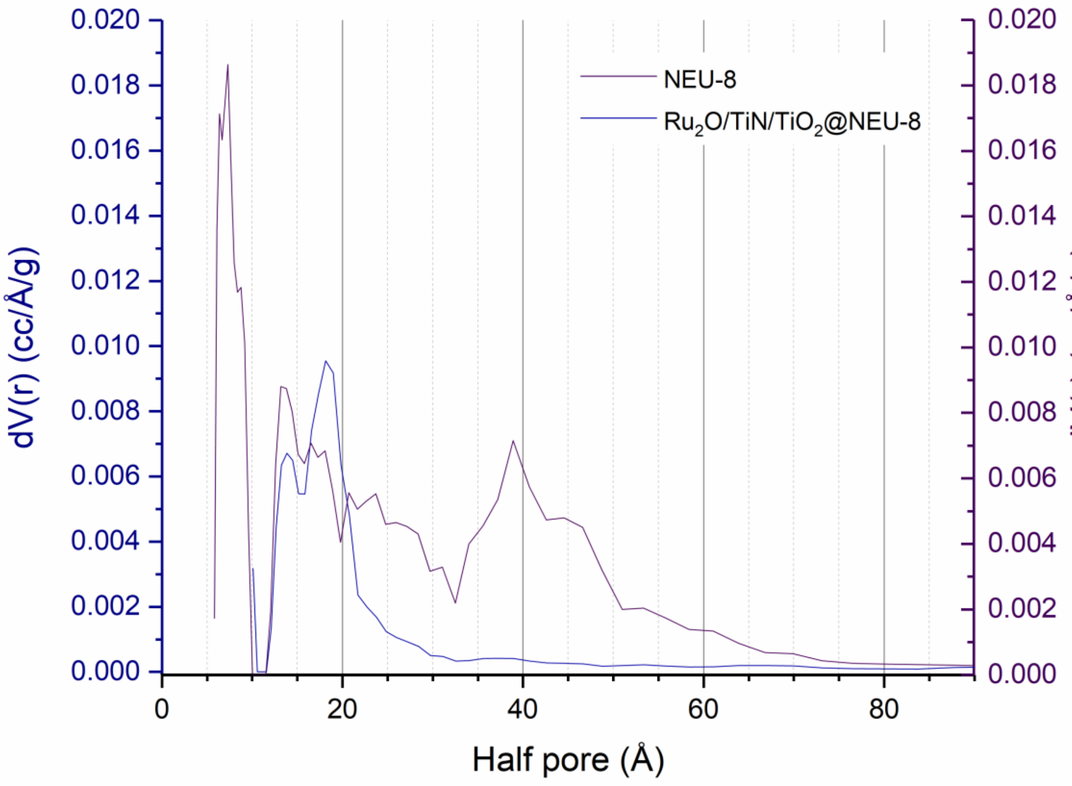

Figure S33. EDX characterization of Fe_2P@PNDCN. It shows the presence of iron (~15 %w) as well as that of carbon (~78 %w), nitrogen (~3 %w), and phosphorus (~5 %w). Weight content was determined in different zones and the average was calculated.

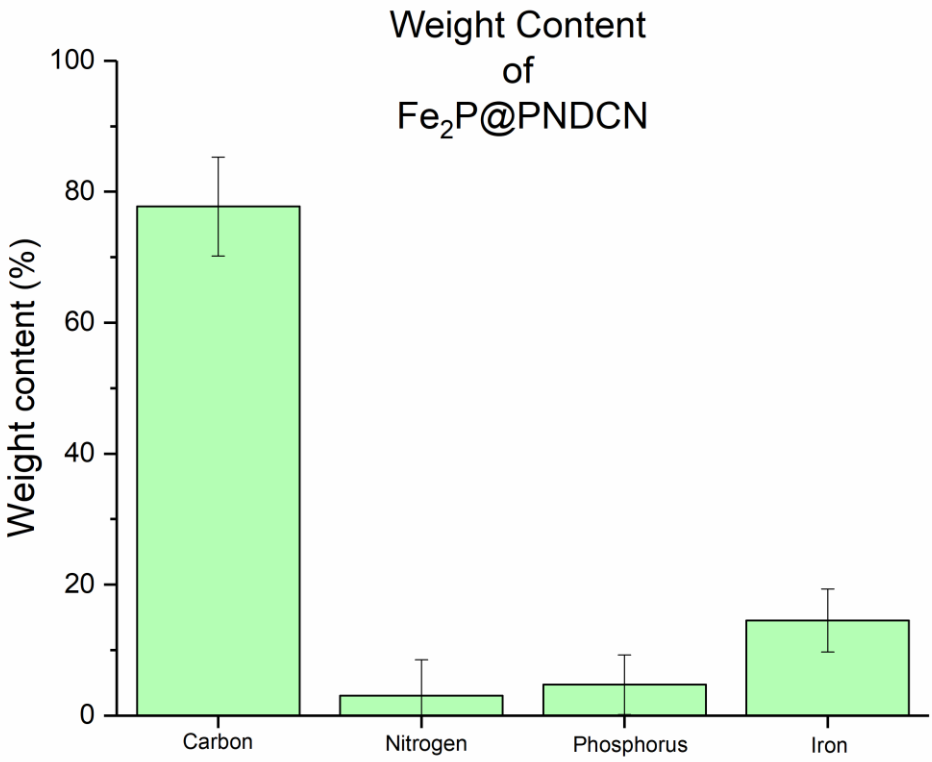

Figure S34. EDX characterization of Fe_2P@PNDCN. It shows the presence of iron (~4 %m) as well as that of carbon (~91 %m), nitrogen (~3 %m), and phosphorus (~2 %m). Atomic content was determined in different zones and the average was calculated.

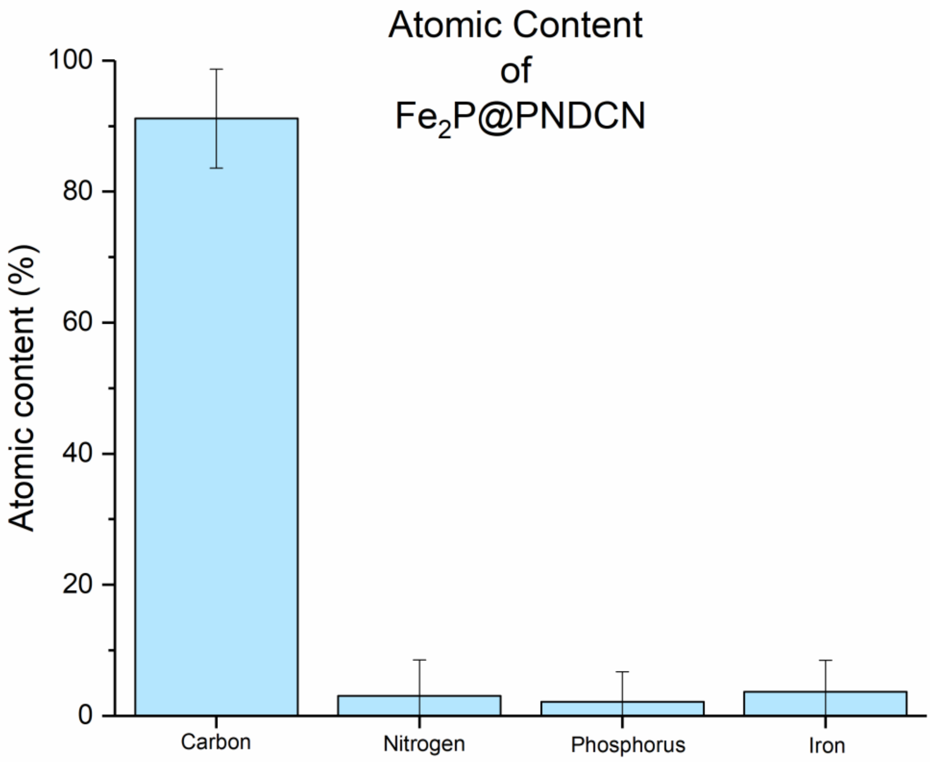

Figure S35. EDX characterization of RuP@PNDCN. It shows the presence of ruthenium (~34 %w) as well as that of carbon (~49 %w), nitrogen (~1 %w), and phosphorus (~16 %w). Weight content was determined in different zones and the average was calculated.

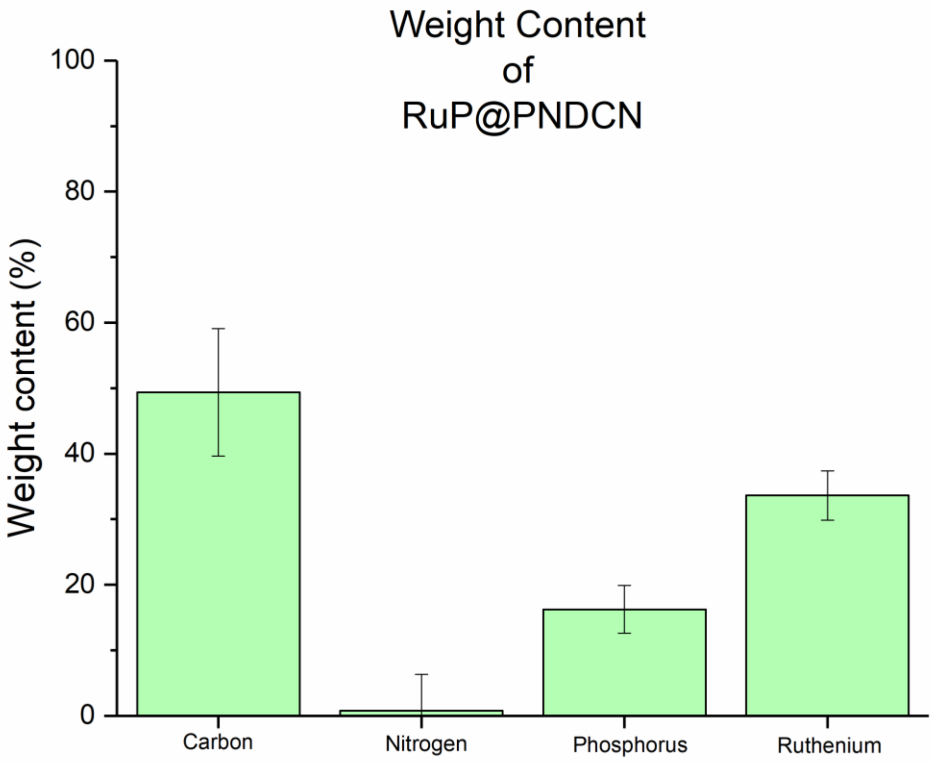

Figure S36. EDX characterization of RuP@PNDCN. It shows the presence of ruthenium (~8 %m) as well as that of carbon (~80 %m), nitrogen (~1 %m), and phosphorus (~12 %m). Atomic content was determined in different zones and the average was calculated.

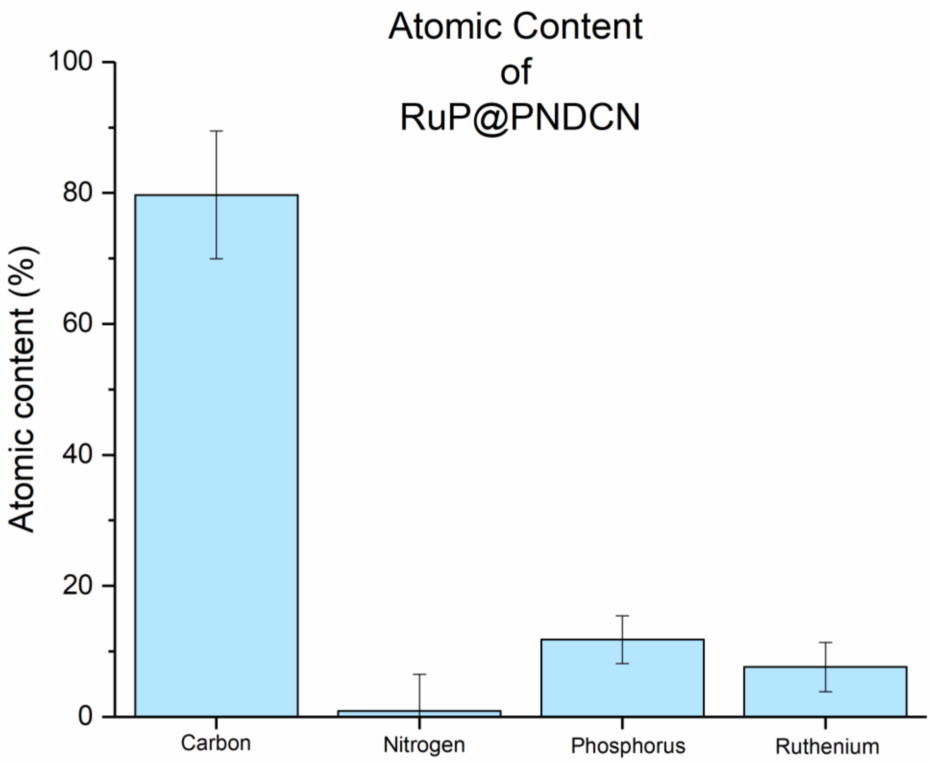

Figure S37. EDX characterization of Fe_3O_4/RuO_2@NEU-7. It shows the presence of ruthenium (~1 %w) and iron (~44 %w), as well as that of carbon (~8 %w), nitrogen (~5 %w), oxygen (~39 %w), and phosphorus (~3 %w). Weight content was determined in different zones and the average was calculated.

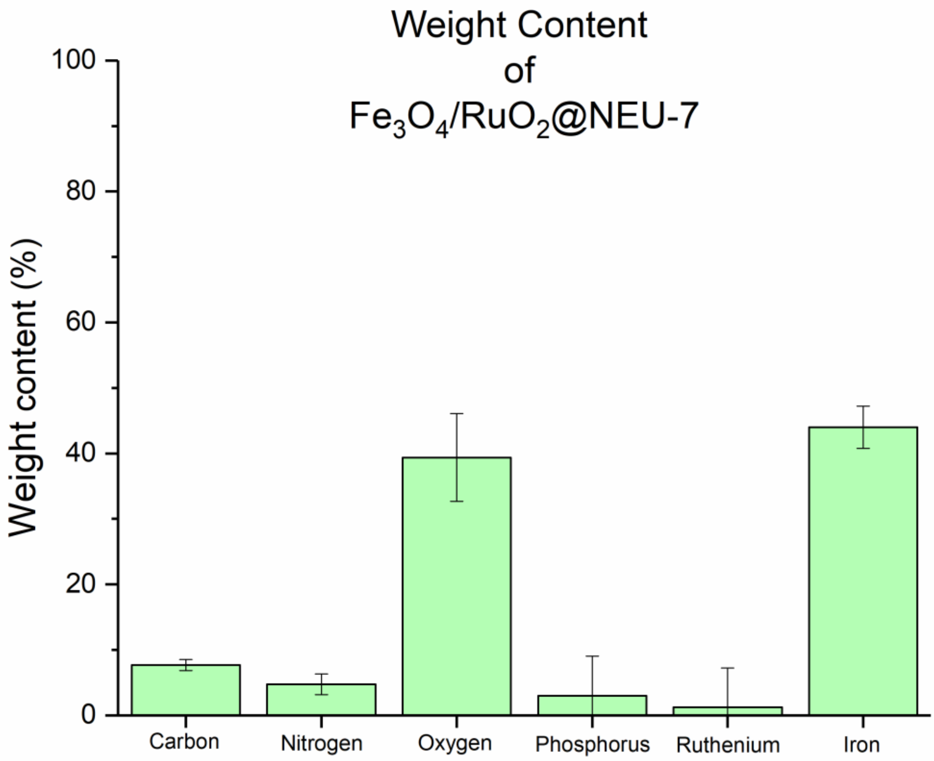

Figure S38. EDX characterization of Fe_3O_4/RuO_2@NEU-7. It shows the presence of ruthenium (~1 %m) and iron (~22 %m), as well as that of carbon (~18 %m), nitrogen (~9 %m), oxygen (~48 %m), and phosphorus (~3 %m). Atomic content was determined in different zones and the average was calculated.

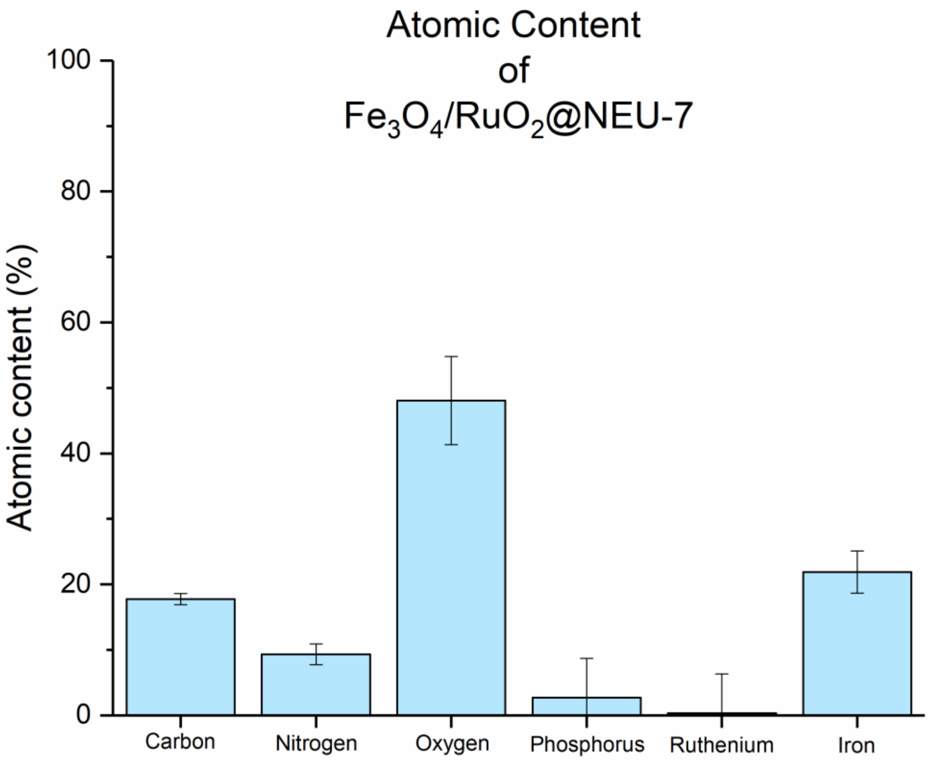

Figure S39. EDX characterization of $Ru_2O/TiO/TiO_2$@NEU-8. It shows the presence of ruthenium (~9 %w) and titanium (~3 %w), as well as that of carbon (~70 %w), nitrogen (~3 %w), oxygen (~11 %w), and phosphorus (~4 %w). Weight content was determined in different zones and the average was calculated.

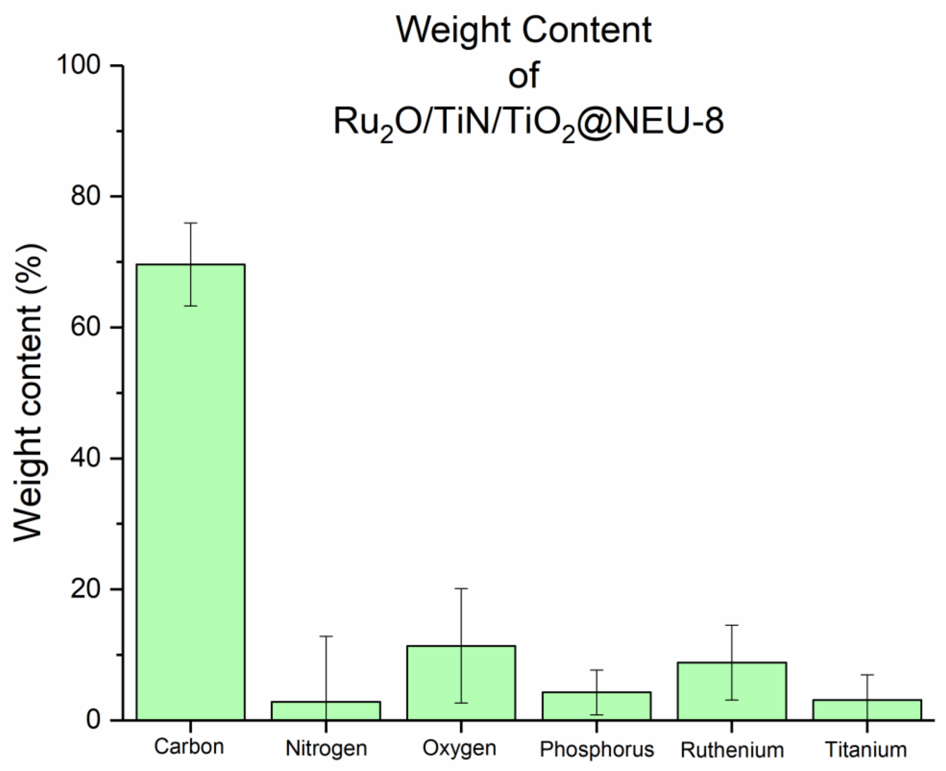

Figure S40. EDX characterization of $Ru_2O/TiO/TiO_2$@NEU-8. It shows the presence of ruthenium (~1 %m) and titanium (~1 %m), as well as that of carbon (~83 %m), nitrogen (~3 %m), oxygen (~10 %m), and phosphorus (~2 %m). Atomic content was determined in different zones and the average was calculated.

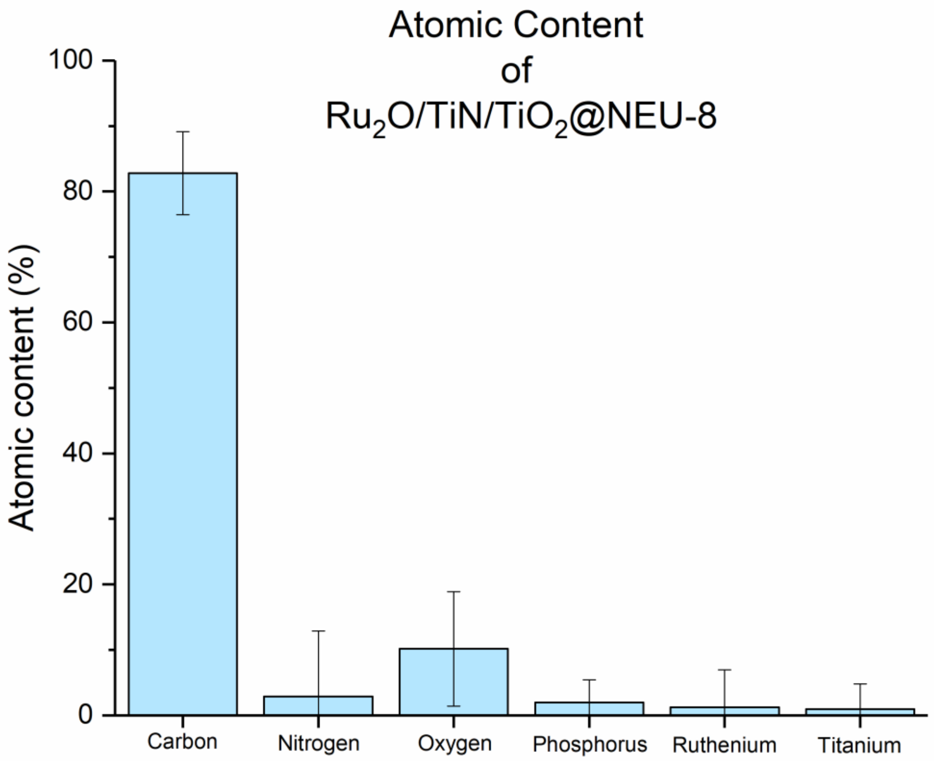

Figure S41. Particle size distribution of Fe_2P in Fe_2P@PNDCN (obtained by counting more than 100 particles).

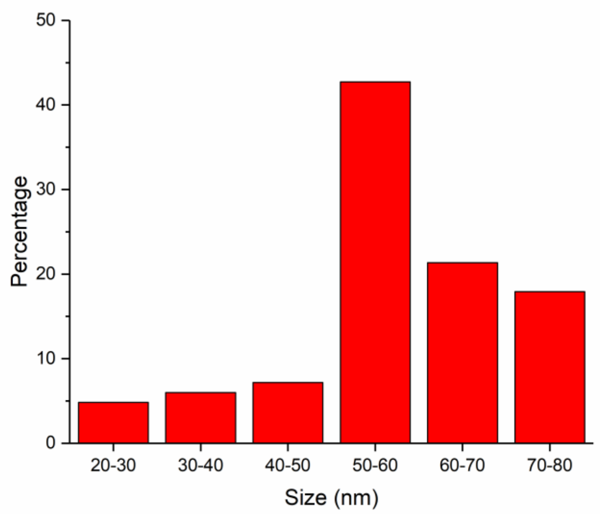

Figure S42. Particle size distribution of RuP in RuP@PNDCN (obtained by counting more than 100 particles).

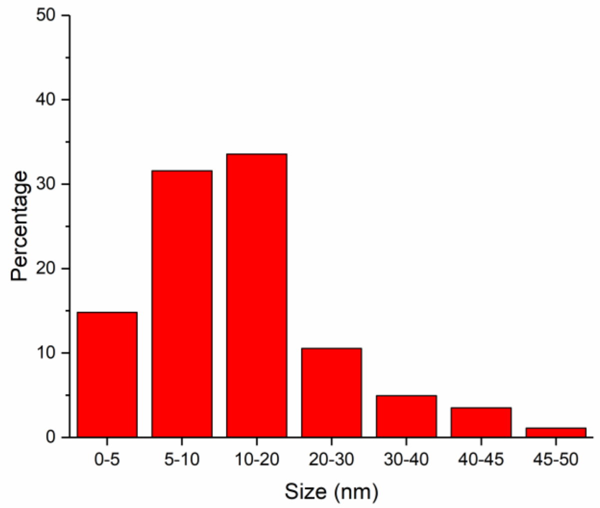

Figure S43. Particle size distribution of Fe_3O_4 and RuO_2 in Fe_3O_4/RuO_2@NEU-7 (obtained by counting more than 100 particles).

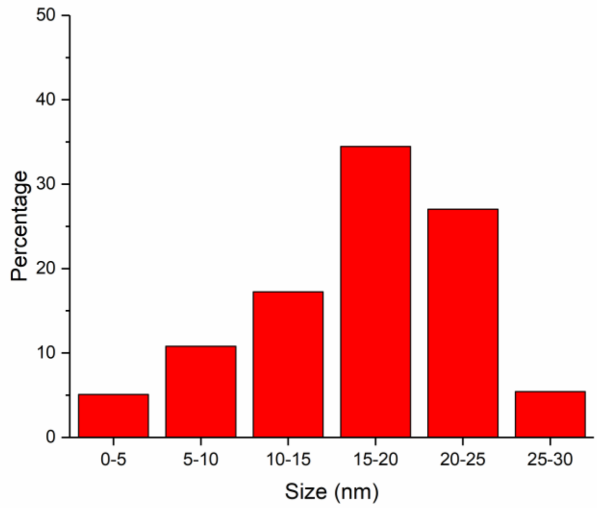

Figure S44. Particle size distribution of Ru_2O, TiN and TiO_2 in $Ru_2O/TiN/TiO_2$@NEU-8 (obtained by counting more than 100 particles).

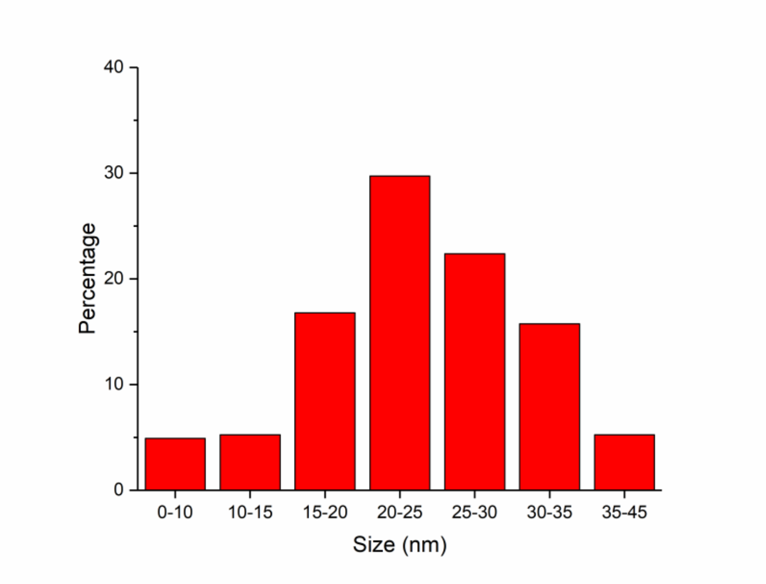

Figure S45. CVs of Fe_2P@PNDCN catalyst recorded in O_2- and Ar-saturated 0.5 M H_2SO_4 electrolyte, measured at the scan rate of 10 mV s^{-1}.

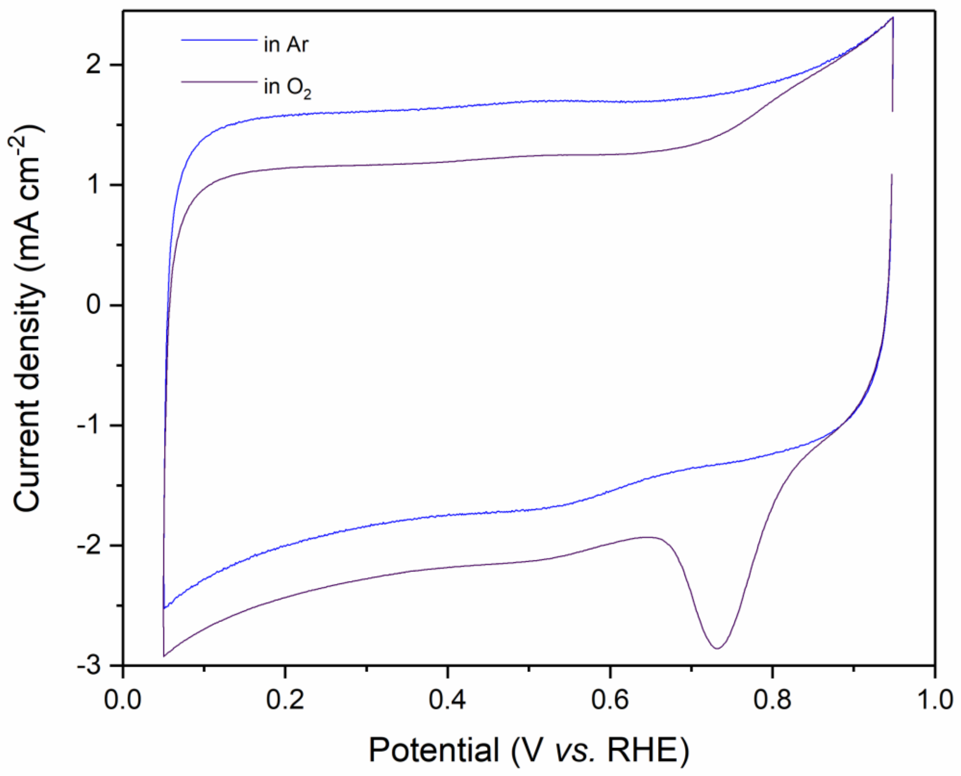

Figure S46. Polarization curves of Fe_2P@PNDCN initially and after 5000 cyclic voltammetry sweeps. Recorded in O_2-saturated 0.5 M H_2SO_4 electrolyte, measured at a scan rate of 50 mV s^{-1}. Catalyst loading: 0.8 mg cm^{-2} (with iR compensation).

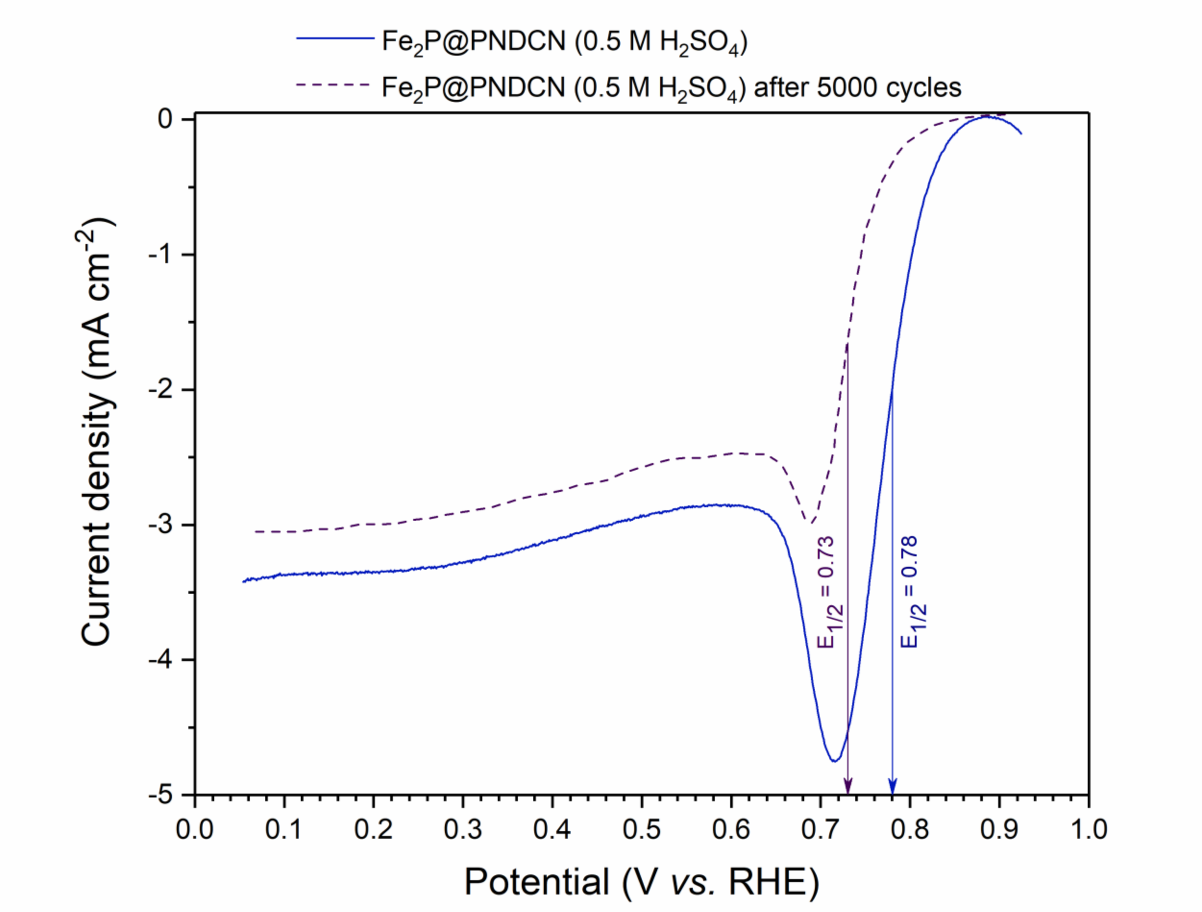

Figure S47. (a) XRD, (b) SEM and (c) TEM of Fe_2P@PNDCN after the stability test in O_2-saturated 0.5 M H_2SO_4 electrolyte.

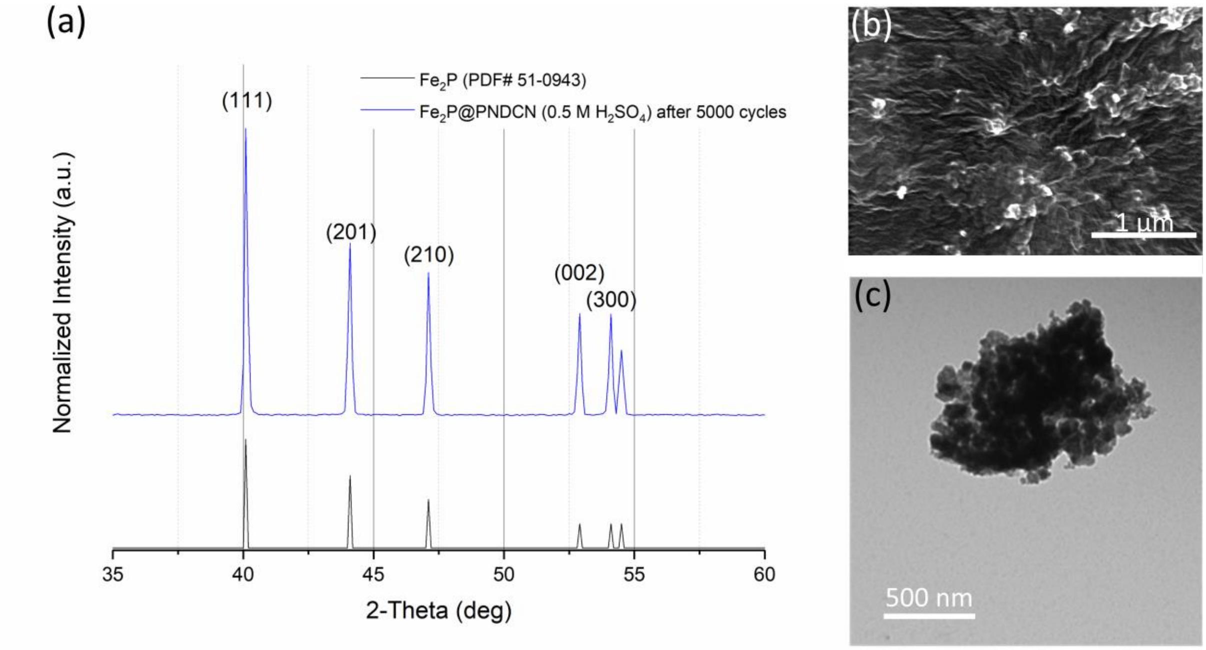

Figure S48. Polarization curves of Fe_2P@PNDCN initially and after 5000 cyclic voltammetry sweeps. Recorded in O_2-saturated 0.1 M $HClO_4$ electrolyte, measured at a scan rate of 50 mV s^{-1}. Catalyst loading: 0.8 mg cm^{-2} (with iR compensation).

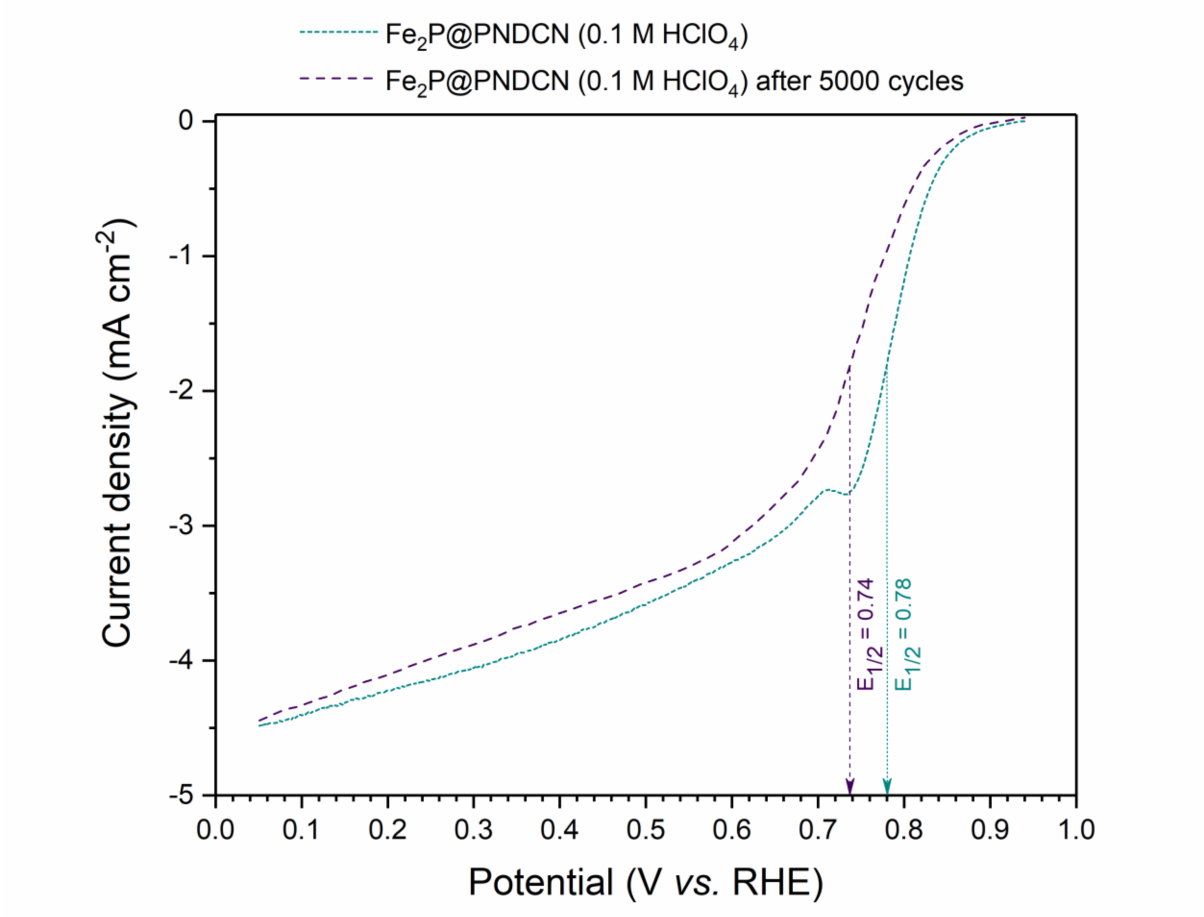

Figure S49. (a) XRD, (b) SEM and (c) TEM of Fe_2P@PNDCN after the stability test in O_2-saturated 0.1 M $HClO_4$ electrolyte.

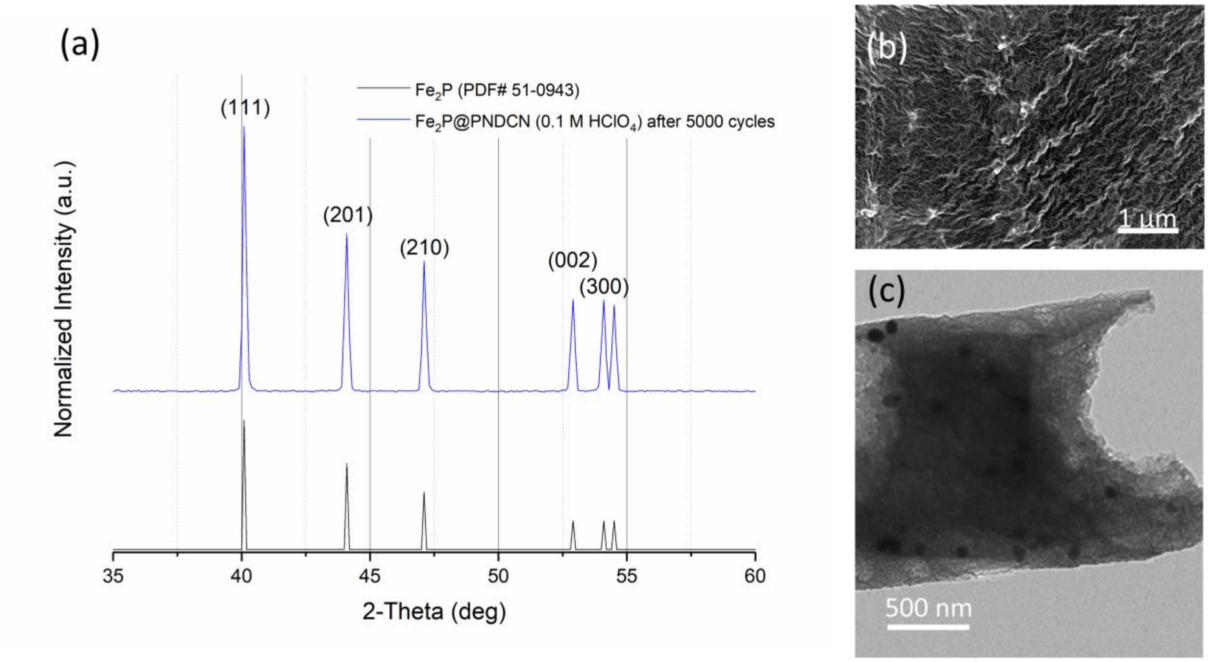

Figure S50. Polarization curves of Fe_2P@PNDCN initially and after 5000 cyclic voltammetry sweeps. Recorded in O_2-saturated 1 M KOH electrolyte, measured at a scan rate of 50 mV s^{-1}. Catalyst loading: 0.8 mg cm^{-2} (with iR compensation).

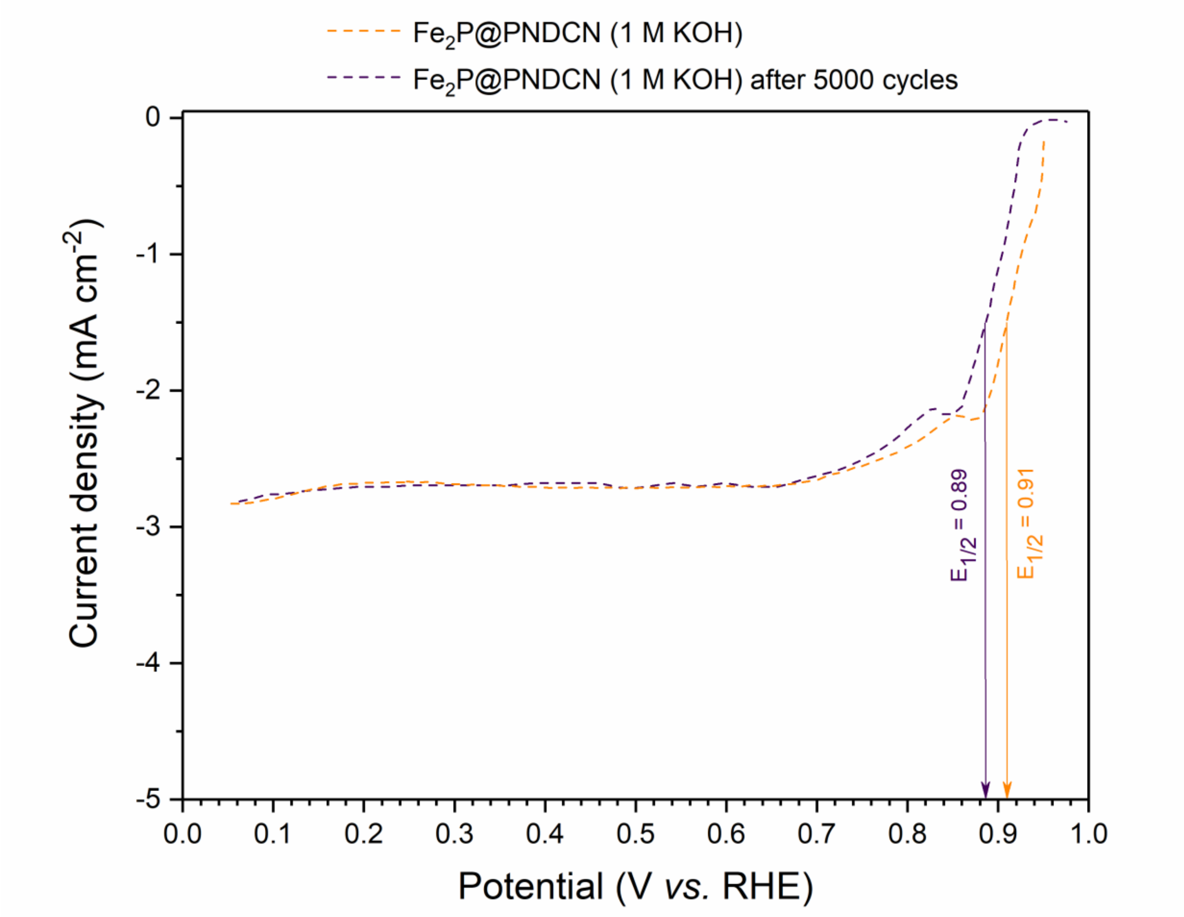

Figure S51. (a) XRD, (b) SEM and (c) TEM of Fe_2P@PNDCN after the stability test in O_2-saturated 1 M KOH electrolyte.

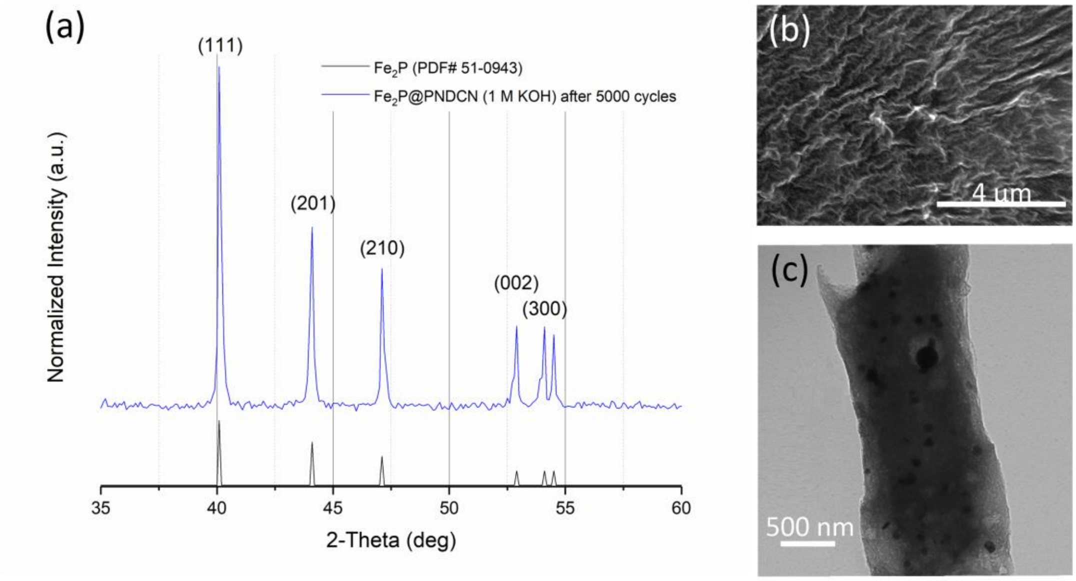

Figure S52. Polarization curves of RuP@PNDCN initially and after 5000 cyclic voltammetry sweeps. Recorded in H_2-saturated 0.5 M H_2SO_4 electrolyte, measured at a scan rate of 50 mV s^{-1}. Catalyst loading: 0.285 mg cm^{-2} (with iR compensation).

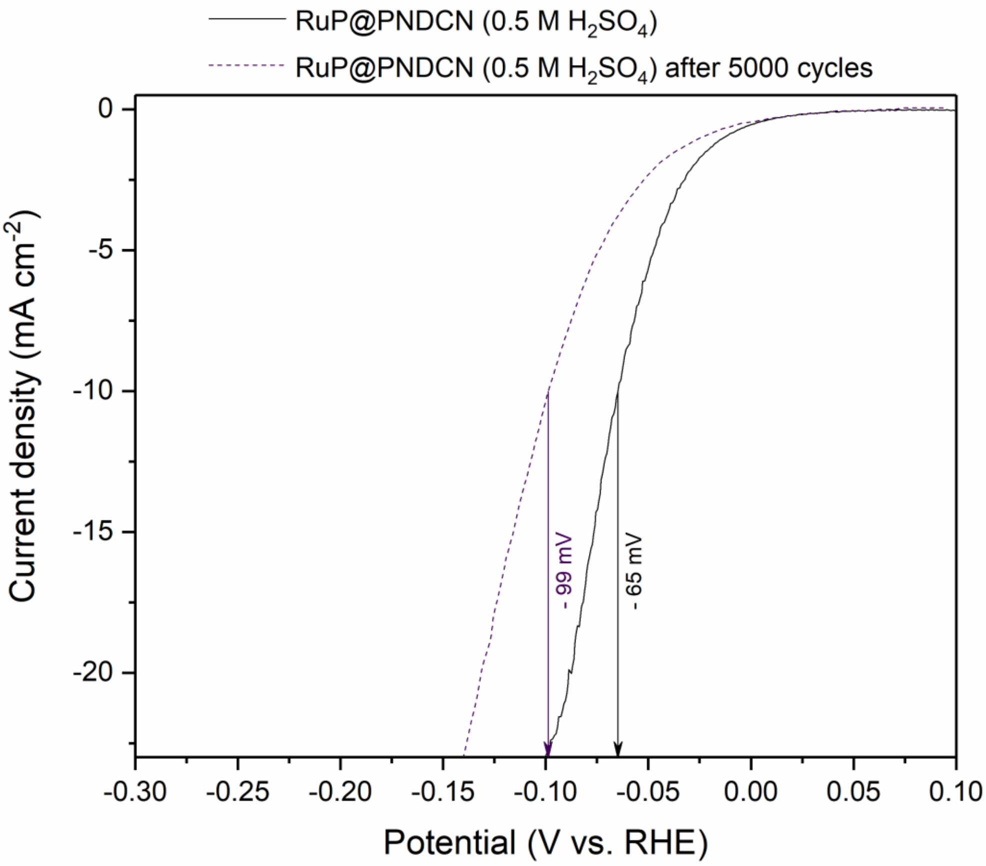

Figure S53. (a) XRD, (b) SEM and (c) TEM of RuP@PNDCN after the stability test in H_2-saturated 0.5 M H_2SO_4 electrolyte.

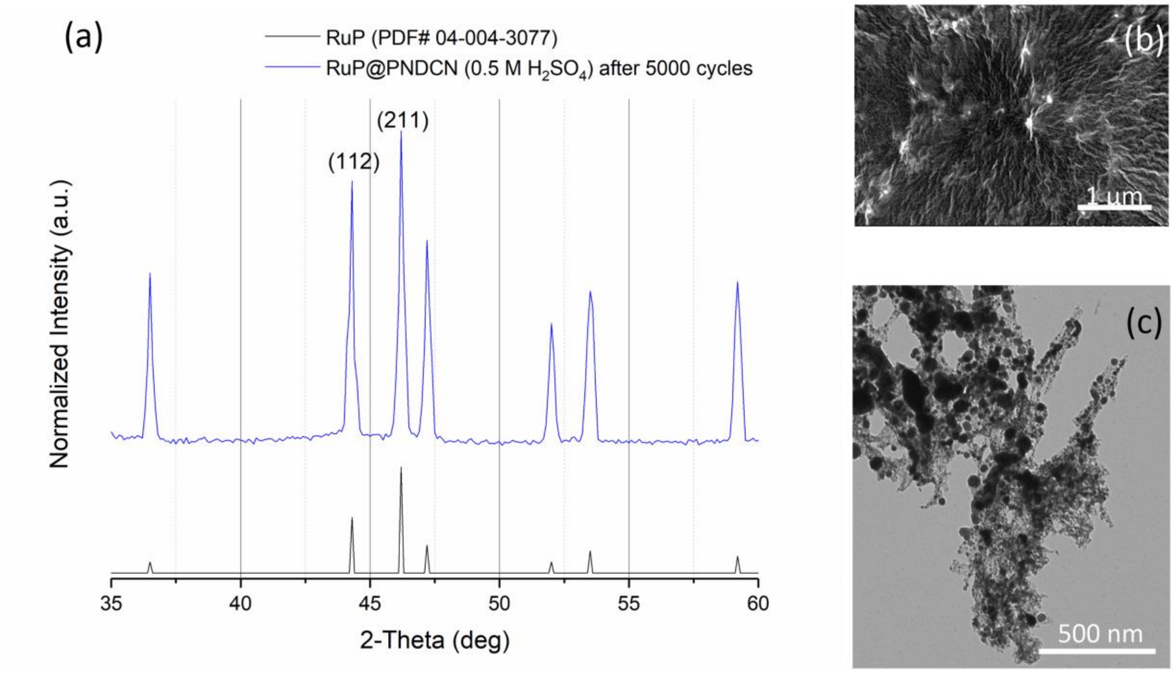

Figure S54. Polarization curves of RuP@PNDCN initially and after 5000 cyclic voltammetry sweeps. Recorded in H_2-saturated 1 M KOH electrolyte, measured at a scan rate of 50 mV s^{-1}. Catalyst loading: 0.285 mg cm^{-2} (with iR compensation).

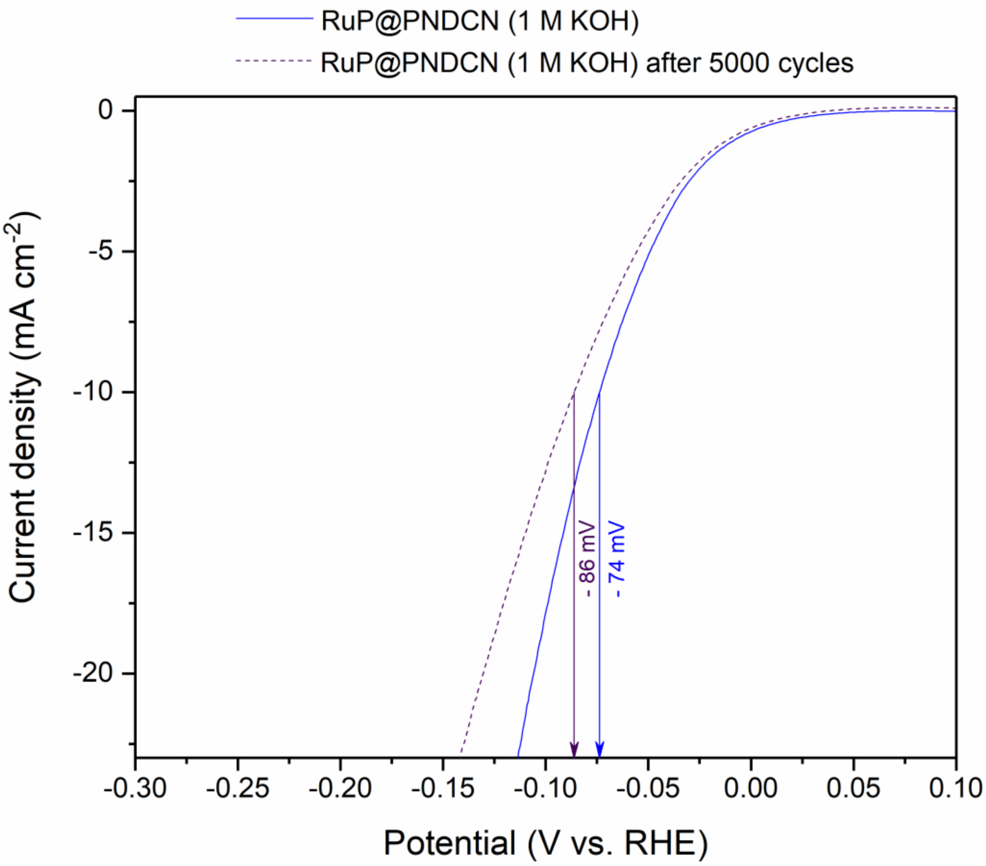

Figure S55. (a) XRD, (b) SEM and (c) TEM of RuP@PNDCN after the stability test in H_2-saturated 1 M KOH electrolyte.

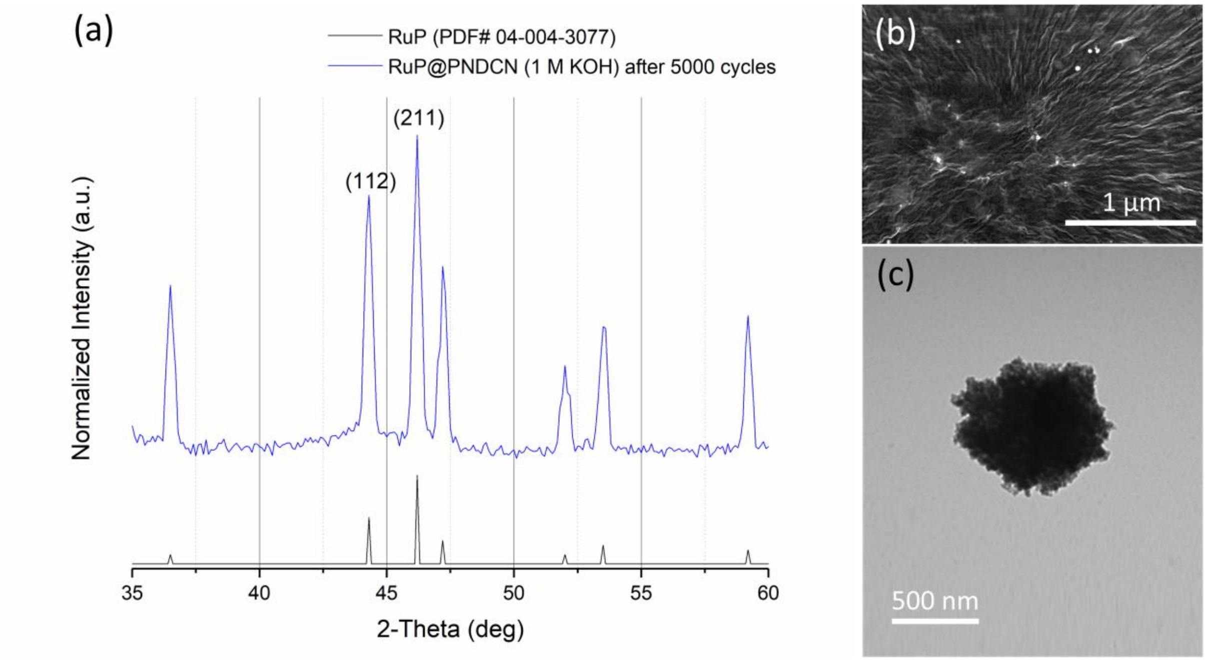

Figure S56. LSVs of the Fe_3O_4/RuO_2@NEU-7 catalyst, showing significant current density loss even after one LSV cycle.

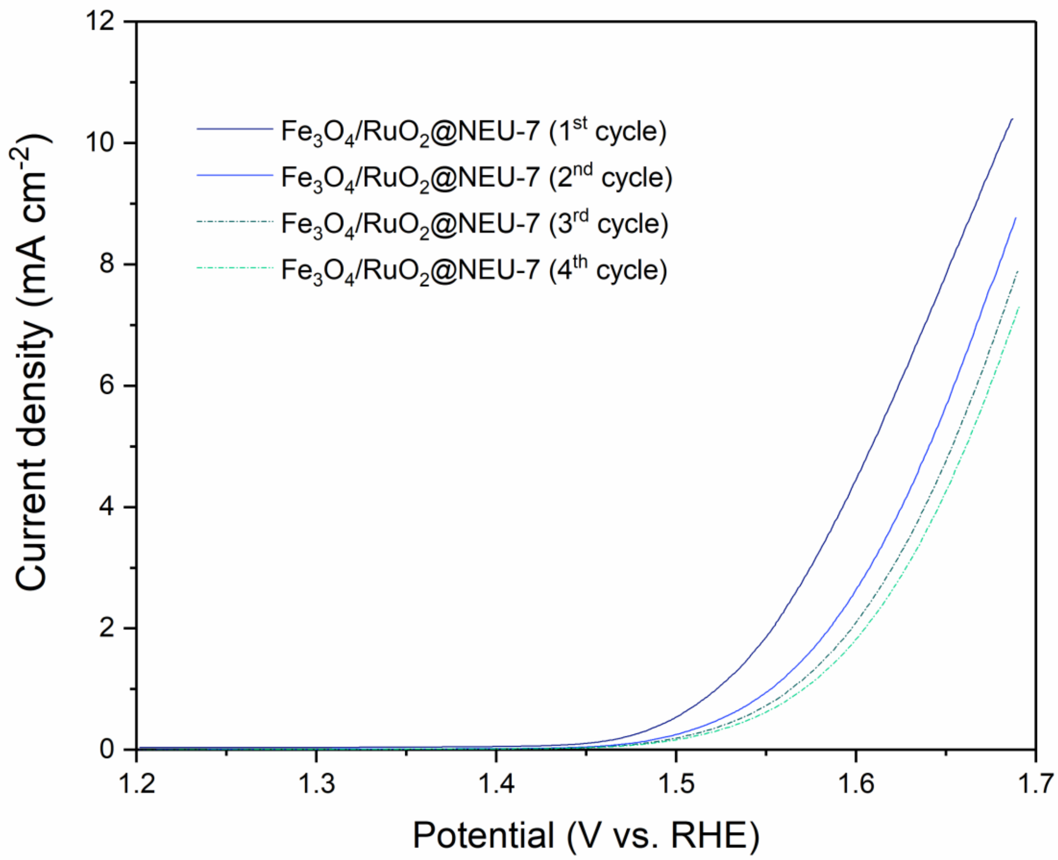

Figure S57. Polarization curves of Fe_3O_4/RuO_2@NEU-7 initially and after 5000 cyclic voltammetry sweeps. Recorded in O_2-saturated 1 M KOH electrolyte, measured at a scan rate of 50 mV s^{-1}. Catalyst loading: 0.255 mg cm^{-2} (with iR compensation).

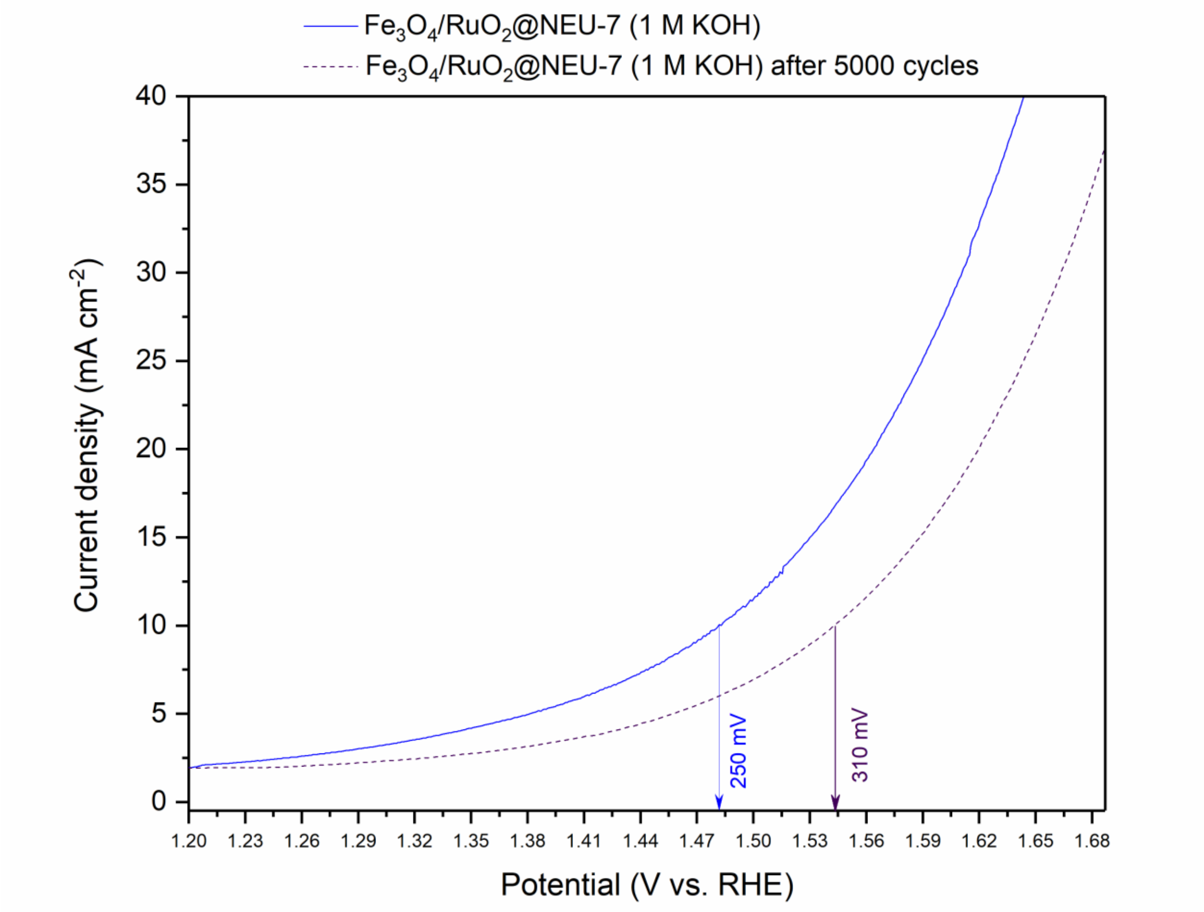

Figure S58. (a) XRD, (b) SEM and (c) TEM of Fe_3O_4/RuO_2@NEU-7 after the stability test in O_2-saturated 1 M KOH electrolyte.

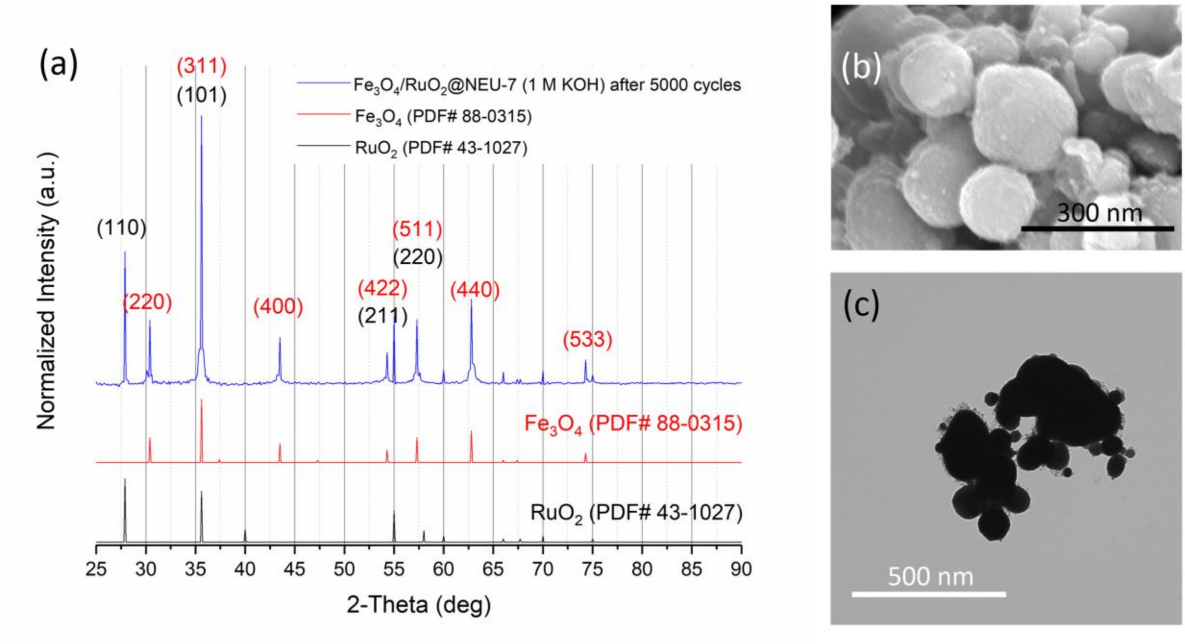

Figure S59. Polarization curves of $Ru_2O/TiN/TiO_2$@NEU-8 initially and after 5000 cyclic voltammetry sweeps in dark. Recorded in H_2-saturated 0.5 M H_2SO_4 electrolyte, measured at a scan rate of 50 mV s^{-1}. Catalyst loading: 0.285 mg cm^{-2} (with iR compensation).

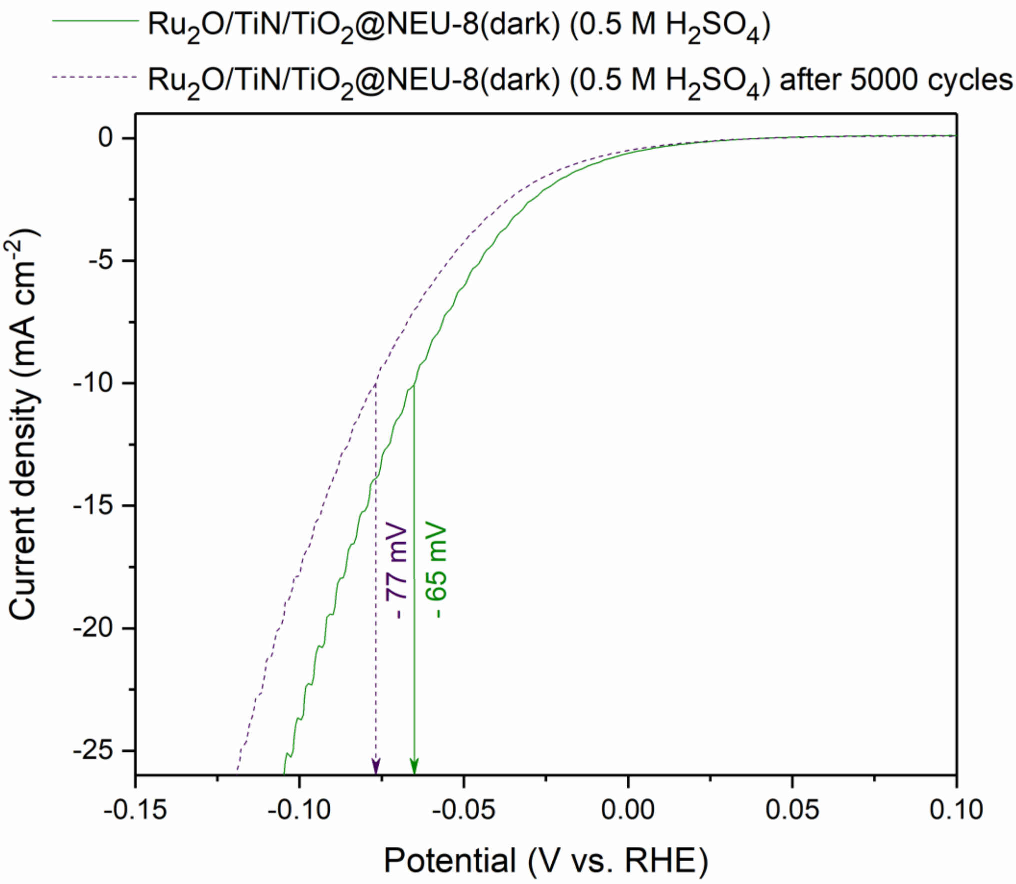

Figure S60. (a) XRD, (b) SEM and (c) TEM of $Ru_2O/TiN/TiO_2$@NEU-8 after the stability test in dark in H_2-saturated 0.5 M H_2SO_4 electrolyte.

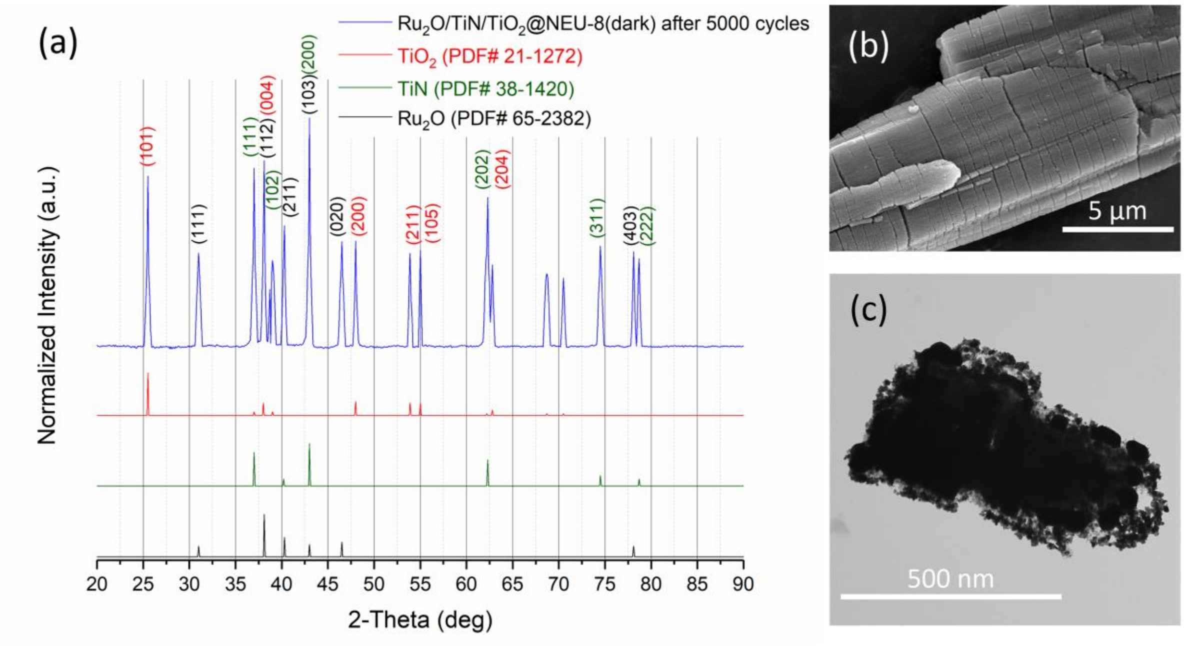

Figure S61. Polarization curves of $Ru_2O/TiN/TiO_2$@NEU-8 initially and after 5000 cyclic voltammetry sweeps in light. Recorded in H_2-saturated 0.5 M H_2SO_4 electrolyte, measured at a scan rate of 50 mV s^{-1}. Catalyst loading: 0.285 mg cm^{-2} (with iR compensation).

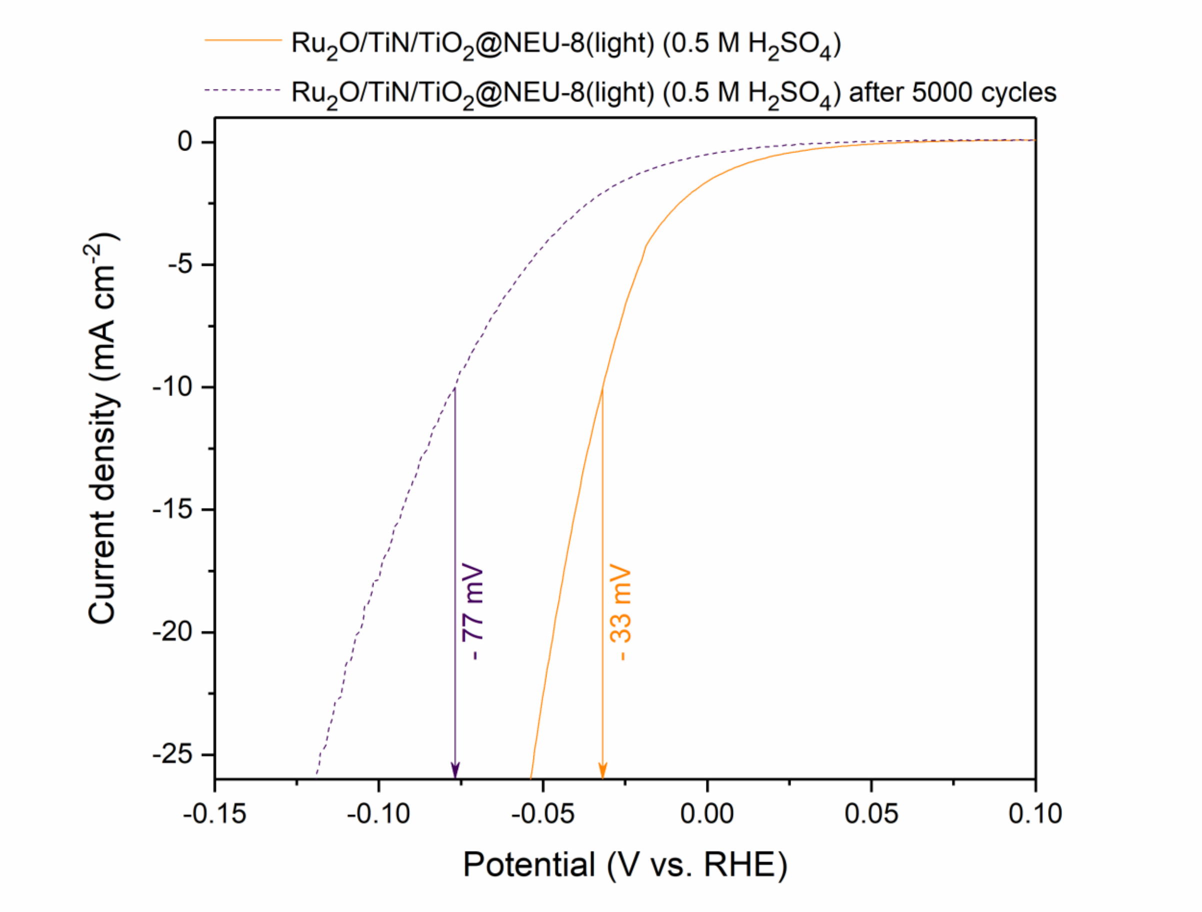

Figure S62. (a) XRD, (b) SEM and (c) TEM of $Ru_2O/TiN/TiO_2$@NEU-8 after the stability test in light in H_2-saturated 0.5 M H_2SO_4 electrolyte.

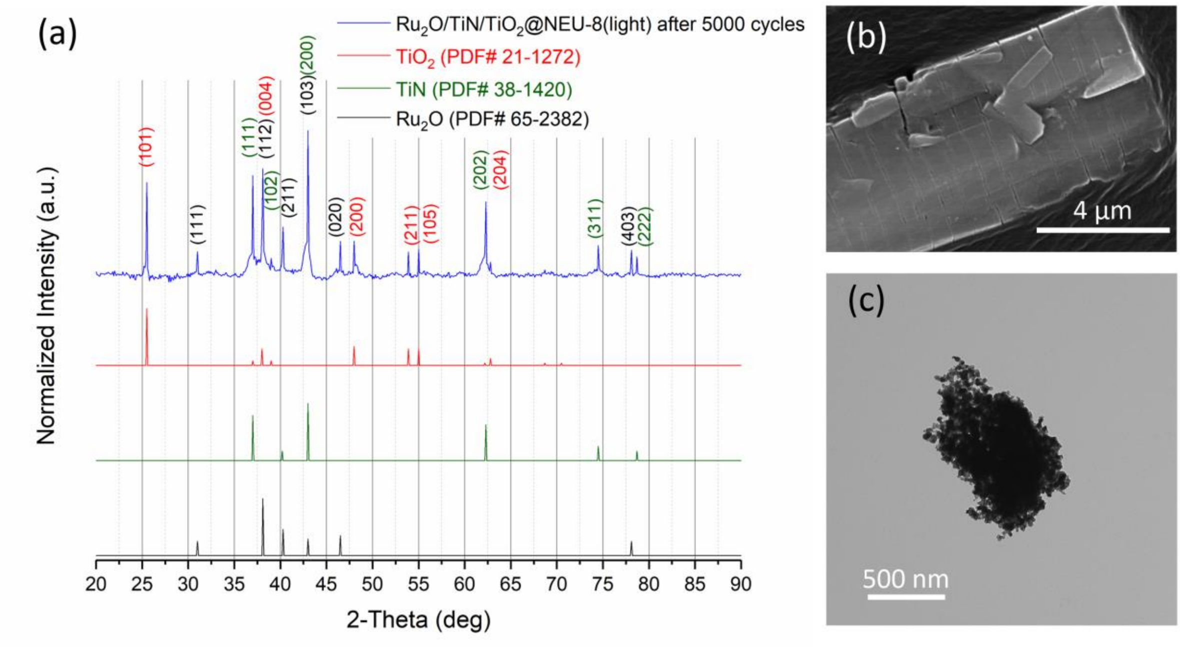

Figure S63. UV/Vis spectrum of NEU-8 and $Ru_2O/TiN/TiO_2$@NEU-8 recorded in DI water.

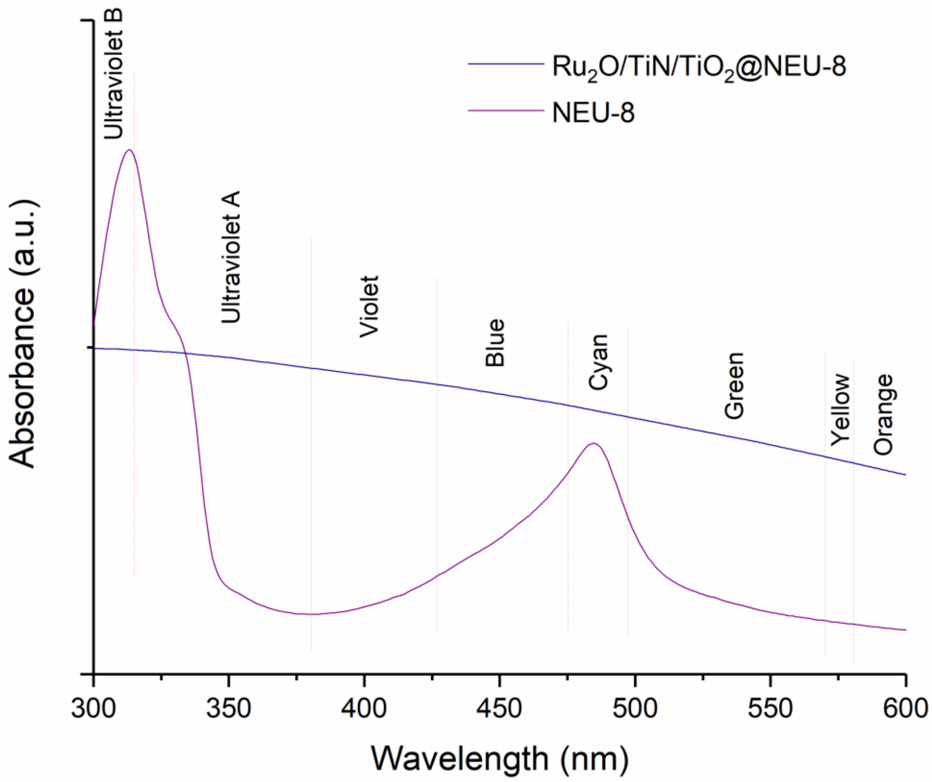

Figure S64. Comparison between trends in activities for the ORR, expressed as half-wave potential in acidic electrolyte.

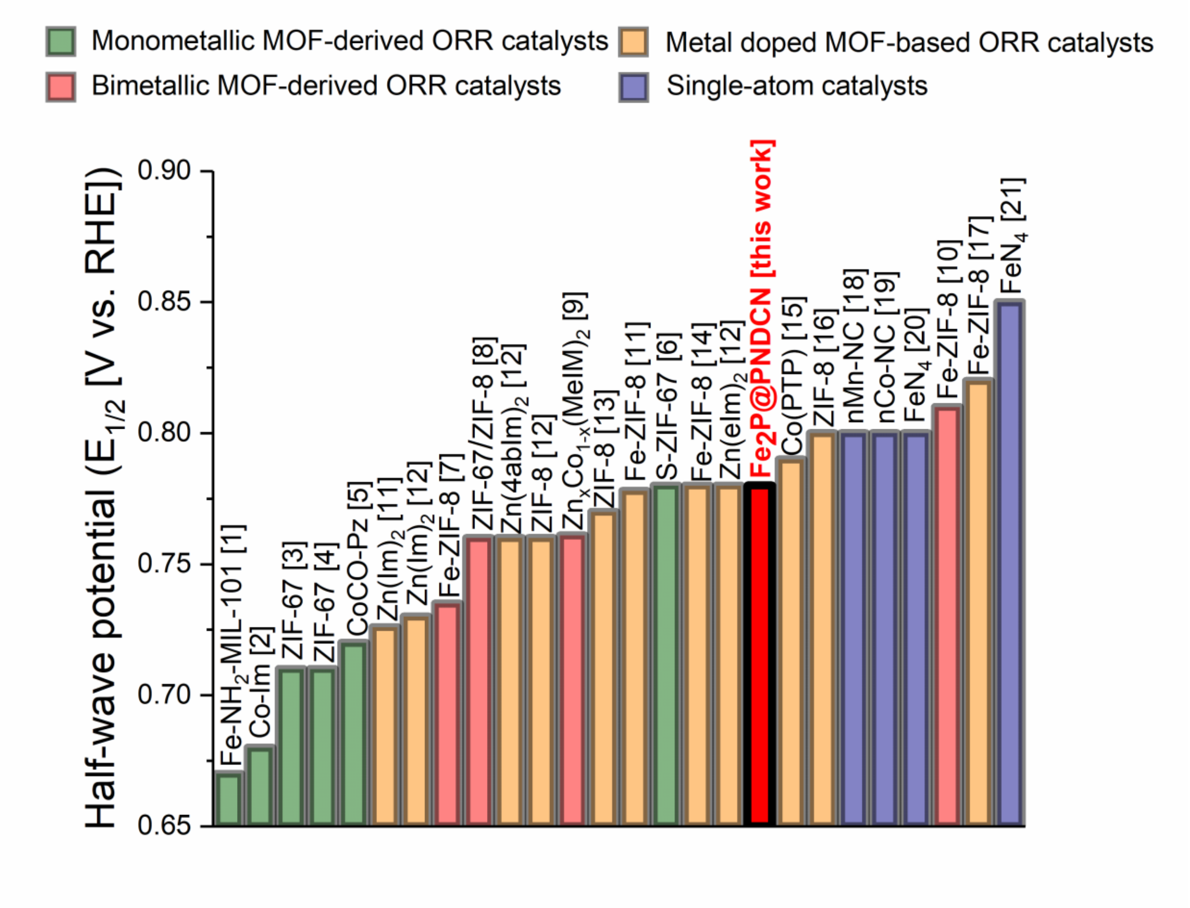

Figure S65. Comparison between trends in activities for the ORR, expressed as half-wave potential in basic electrolyte.

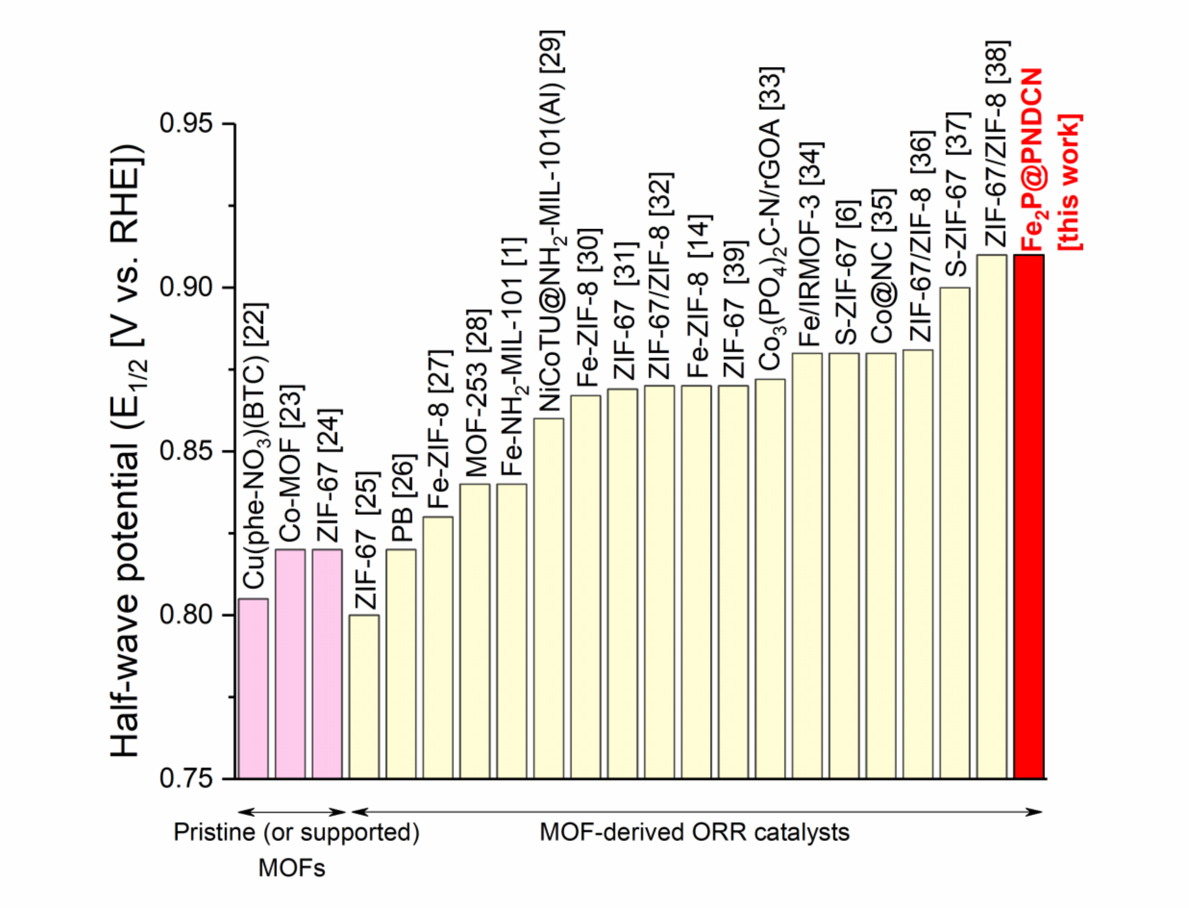

Figure S66. Comparison between trends in activities for the HER in acidic electrolyte.

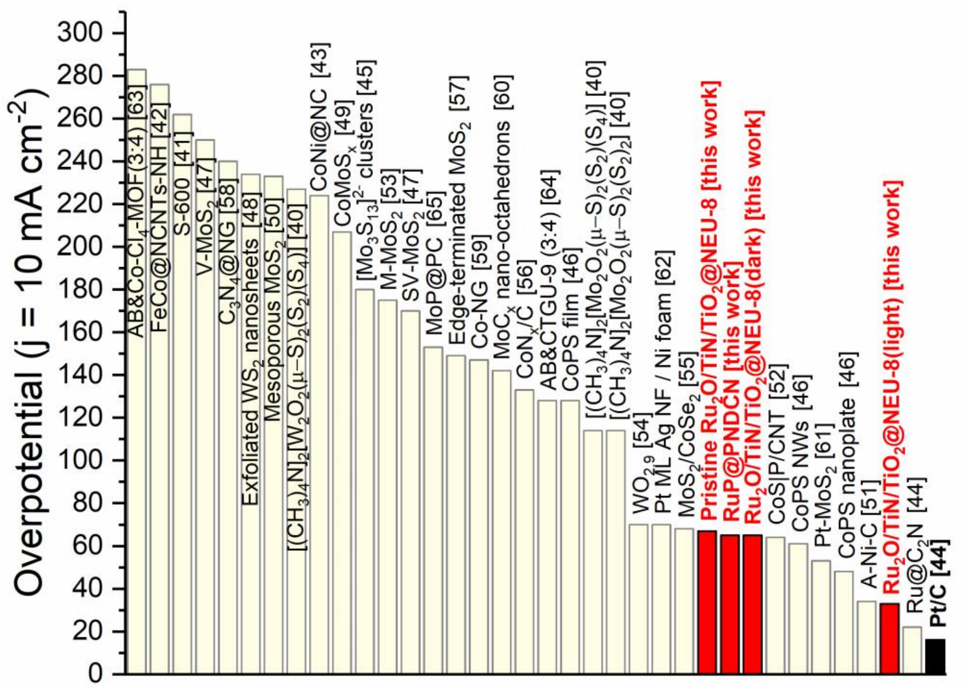

Figure S67. Comparison between trends in activities for the HER in basic electrolyte.

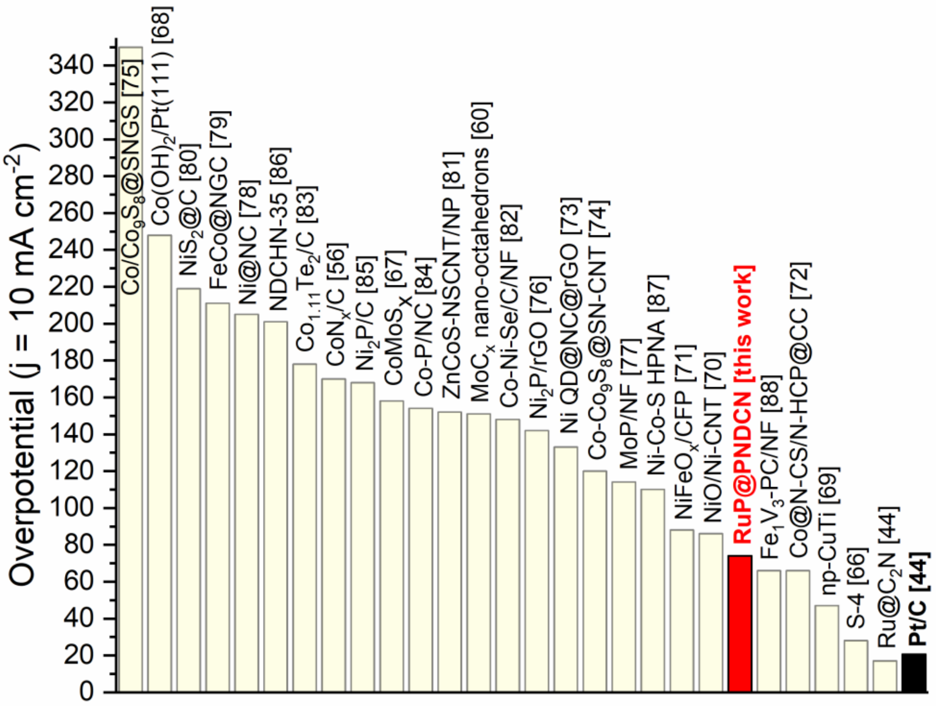

Figure S68. Comparison between trends in activities for the OER in acidic electrolyte.

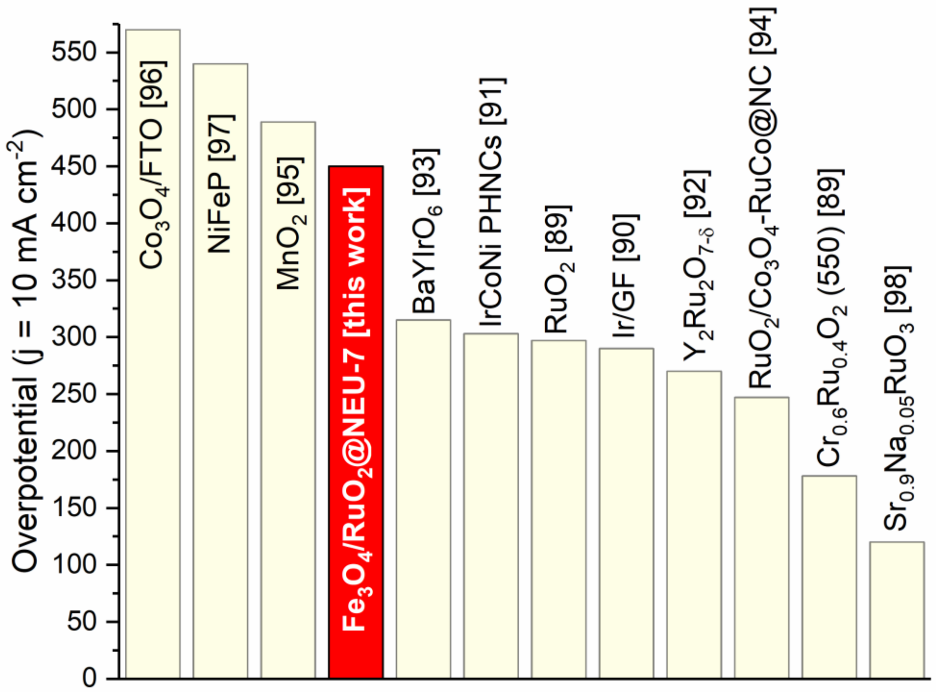

Figure S69. Comparison between trends in activities for the OER in basic electrolyte.

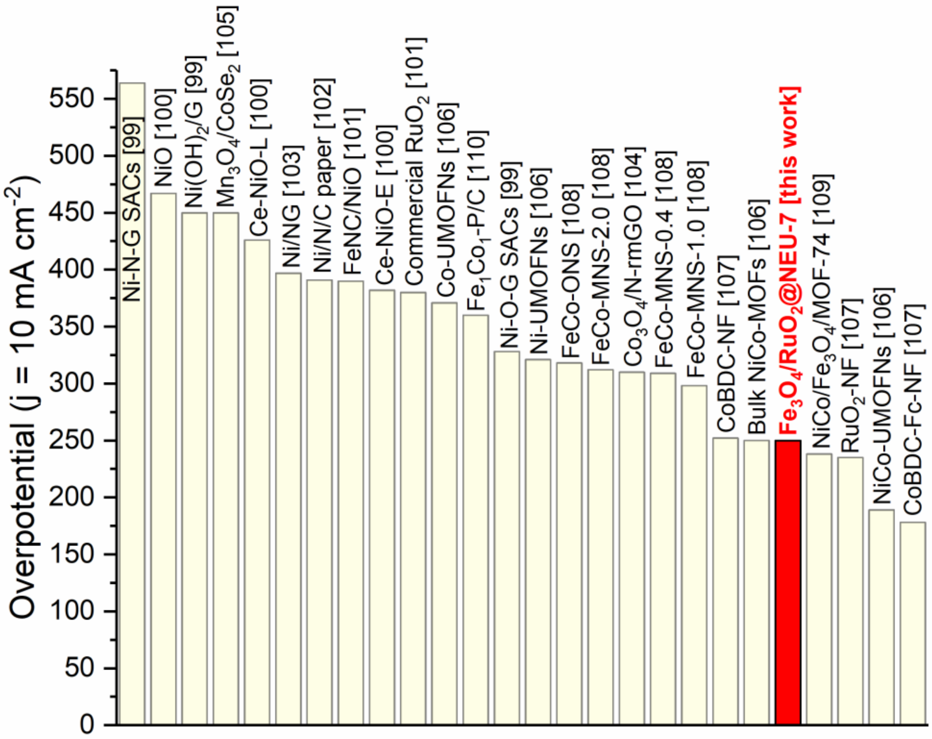

2. Supplementary Tables

Table S1. Summaries of the EXAFS fitting results of the NEU-5 to determine the local molecular structure of zinc within the MOF.

Scattering	R (Å)	N	σ^2 (Å^2)
Zn-O_{43}	1.81920 ± 0.15908	2	0.00911
Zn-O_{21}	1.85390 ± 0.18984	1	0.00911
Zn-N_1	1.91010 ± 0.05204	2	0.00911
Zn-O_{30}	1.90480 ± 0.08131	1	0.00911
Zn-C_{20}	2.03870 ± 0.09627	2	0.00911
Zn-C_{16}	2.82960 ± 0.04593	1	0.00911
Zn- C_{14}	2.86810 ± 0.25040	2	0.02092
Zn-H_{52}	2.87280 ± 0.49990	2	0.02092
Zn-N_{15}-C_{16}	3.05880 ± 0.05165	6	0.01003
Zn-C_1	3.51750 ± 0.00389	2	0.01003
Zn-C_{20}-C_1	3.51880 ± 0.01113	4	0.02629
Zn-C_{20}-C_1-C_{20}	3.52000 ± 0.10376	2	0.00382
Zn-O_{43}	3.63840 ± 0.08736	2	0.00902
Zn-O_{43}-C_{20}	3.76460 ± 0.15603	4	0.00200
Zn-O_{21}	3.75870 ± 0.07232	2	0.02156
Zn-O_{21}-C_{45}	3.80350 ± 0.07232	4	0.00208

Fits were done at the Zn K-edge in R-space, $k^{1,2,3}$ weighting. 1.0 < R < 3.5 Å and Δk = 3.000 – 12.896 Å^{-1} were used for fitting. The fitting result of the E_0 and S_0^2 are 1.59962215 ± 0.45005218 eV and 0.93216328 ± 0.05304799, respectively. The goodness of the fit is reflected by χ_v^2 = 1250.11 and R-factor = 0.0045642.

Table S2. Summaries of the EXAFS fitting results of the NEU-5 to determine the local molecular structure of iron within the MOF.

Scattering	R (Å)	N	σ^2 (Å^2)
Fe-N_4	1.85220 ± 0.05722	2	0.00116
Fe-N_{29}	1.93410 ± 0.05722	4	0.00459
Fe-C_{36}	2.77770 ± 0.05722	8	0.00575
Fe-C_{24}	2.92430 ± 0.05722	4	0.02344
Fe-N_4-C_5	2.98290 ± 0.05722	8	0.01927
Fe-H_{52}	3.02150 ± 0.05722	4	0.01927
Fe-N_{29}-C_{28}	3.03950 ± 0.05722	8	0.01927
Fe-N_{15}-C_{16}	3.09540 ± 0.05722	8	0.01927
Fe-N_4-N_{15}	3.13040 ± 0.05722	8	0.01927
Fe-N_4-C_5-N_4	3.19820 ± 0.05722	4	0.01927
Fe-N_{15}-C_{16}-N_{15}	3.26660 ± 0.05722	4	0.01927
Fe-N_{15}-C_{14}-N_{15}	3.29130 ± 0.05722	4	0.01927
Fe-N_{29}-N_{11}	3.31630 ± 0.05722	8	0.01927
Fe-N_4-N_{32}	3.32670 ± 0.05722	8	0.01927
Fe-N_4-C_{14}	3.47380 ± 0.05722	8	0.01927
Fe-C_{36}-C_{28}	3.50010 ± 0.05722	8	0.01927
Fe-N_{29}-C_{36}	3.52120 ± 0.05722	8	0.01927
Fe-N_4-N_{25}	3.70440 ± 0.05722	2	0.01927
Fe-N_4	3.70440 ± 0.05722	2	0.01927
Fe-N_{15}-N_{11}	3.84740 ± 0.05722	4	0.01927
Fe-N_{29}	3.86830 ± 0.05722	4	0.01927
Fe-N_{15}	3.86830 ± 0.05722	4	0.01927
Fe-N_4-C_{31}	3.93010 ± 0.05722	8	0.01927
Fe-C_{14}-C_{16}	4.01640 ± 0.05722	8	0.01927
Fe-C_{37}	4.06710 ± 0.05722	4	0.01927
Fe-C_{36}-C_{37}	4.10750 ± 0.05722	8	0.01927
Fe-C_5-N_4-C_5	4.11370 ± 0.05722	4	0.01927
Fe-C_{27}	4.11490 ± 0.05722	4	0.01927
Fe-N_{32}-C_{14}	4.12380 ± 0.05722	18	0.01927
Fe-N_{35}-C_{37}	4.14090 ± 0.05722	8	0.01927
Fe-N_{11}-C_{36}	4.14190 ± 0.05722	14	0.01927
Fe-C_{28}-C_{27}	4.14180 ± 0.05722	8	0.01927
Fe-C_5-N_4-C_5	4.14480 ± 0.05722	4	0.01927
Fe-C_{36}-C_{37}-C_{36}	4.14790 ± 0.05722	4	0.01927
Fe-N_{29}-C_{10}	4.15510 ± 0.05722	16	0.01927
Fe-C_{28}-C_{27}-C_{28}	4.16860 ± 0.05722	4	0.01927
Fe-C_{25}	4.20990 ± 0.05722	4	0.01927
Fe-N_{35}-C_{37}-N_{35}	4.21460 ± 0.05722	4	0.01927
Fe-N_{29}-C_{27}	4.21800 ± 0.05722	8	0.01927
Fe-N_{15}-C_3	4.25400 ± 0.05722	8	0.01927
Fe-C_{24}-C_{25}	4.25700 ± 0.05722	8	0.01927
Fe-C_{16}-N_{15}-C_{16}	4.25680 ± 0.05722	4	0.01927
Fe-N_{29}-C_{25}	4.25780 ± 0.05722	8	0.01927

Fe-N_4-C_{16}	4.28920 ± 0.05722	8	0.01927
Fe-C_{16}-C_{17}-C_{16}	4.30410 ± 0.05722	4	0.01927
Fe-N_{29}-C_{25}-N_{29}	4.30560 ± 0.05722	4	0.01927
Fe-N_{29}-C_{27}-N_{29}	4.32120 ± 0.05722	4	0.01927
Fe-N_4-C_{15}-N_4	3.02150 ± 0.05722	4	0.01927

Fits were done at the Fe K-edge in R-space, $k^{1,2,3}$ weighting. $1.0 < R < 3.8$ Å and $\Delta k = 3.000 – 12.821$ Å^{-1} were used for fitting. The fitting result of the E_0 and S_0^2 are -3.17785465 ± 1.38773601 eV and 0.66889769 ± 0.08181721, respectively. The goodness of the fit is reflected by $\chi_\nu^2 = 245.67$ and R-factor = 0.0182571.

Table S3. BET surface area and total pore volume of NEU-5, NEU-6, NEU-7 and NEU-8, as well as Fe_2P@PNDCN, RuP@PNDCN, Fe_3O_4/RuO_2@NEU-7 and $Ru_2O/TiN/TiO_2$@NEU-8.

Sample	**BET** $m^2\ g^{-1}$	**Total pore volume** $cm^3\ g^{-1}$
NEU-5	10.2	0.027
NEU-6	18.2	0.162
NEU-7	174.2	0.262
NEU-8	244.2	0.305
Fe_2P@PNDCN	681.4	0.633
RuP@PNDCN	126.5	0.180
Fe_3O_4/RuO_2@NEU-7	92.0	0.255
$Ru_2O/TiN/TiO_2$@NEU-8	112.1	0.126

Table S4. Reported catalysts for ORR in acidic electrolyte.

Monometallic MOF-derived ORR catalysts

Name/Other precursors	**Heat treatment temperature (°C)**	**Electrolyte**	**E_{onset}**	**$E_{1/2}$**	**Reference**
Fe-NH_2-MIL-101	700	0.5 M H_2SO_4	0.92 V vs. RHE	0.67 V vs. RHE	[1]
Co-Im = Co-Imidazolate	750	0.1 M $HClO_4$	0.83 V vs. RHE	0.68 V vs. RHE	[2]
ZIF-67 = Co-mIm	750	0.1 M $HClO_4$	0.86 V vs. RHE	0.71 V vs. RHE	[3]
ZIF-67 = Co-mIm	900	0.5 M H_2SO_4	0.85 V vs. RHE	0.71 V vs. RHE	[4]
CoCO-Pz = Co-pyrazinedicarboxylate	700	0.5 M H_2SO_4	0.97 V vs. RHE	0.72 V vs. RHE	[5]
S-ZIF-67 = Co-mIm-S	700	0.1 M $HClO_4$	0.90 V vs. RHE	0.78 V vs. RHE	[6]

Bimetallic MOF-derived ORR catalysts

Fe-ZIF-8 = Fe-Zn-mIm	900	0.5 M H_2SO_4	0.861 V vs. RHE	0.735 V vs. RHE	[7]
ZIF-67/ZIF-8	1. 1000 (Ar) 2. 950 (NH_3)	0.1 M $HClO_4$	0.93 V vs. RHE	0.76 V vs. RHE	[8]
$Zn_xCo_{1-x}(MeIM)_2$	900	0.1 M $HClO_4$	---	0.761 V vs. RHE	[9]
Fe_2P@PNDCN	**1050**	**0.5 M H_2SO_4**	**0.88 V vs. RHE**	**0.78 V vs. RHE**	**This work**
Fe_2P@PNDCN	**1050**	**0.1 M $HClO_4$**	**0.89 V vs. RHE**	**0.78 V vs. RHE**	**This work**
Fe-ZIF-8 = Fe-Zn-mIm	950	0.1 M $HClO_4$	0.95 V vs. RHE	0.81 V vs. RHE	[10]

Metal doped MOFs-based ORR catalysts

$Zn(Im)_2$/Tris-1,10-phenanthroline and iron (II) perchlorate	1050	0.1 M $HClO_4$	0.88 V vs. RHE	0.726 V vs. RHE	[11]
Fe-ZIF-8 = Fe-Zn-mIm/Tris-1,10-phenanthroline and iron (II) perchlorate	1. 1050 (Ar) 2. 1050 (NH_3)	0.1 M $HClO_4$	0.91 V vs. RHE	0.778 V vs. RHE	[11]
$Zn(Im)_2$/Tris-1,10-phenanthroline and iron (II) perchlorate	1. 1050 (Ar) 2. 950 (NH_3)	0.1 M $HClO_4$	0.881 V vs. RHE	0.73 V vs. RHE	[12]
$Zn(4abIm)_2$/Tris-1,10-phenanthroline and iron (II) perchlorate	1. 1050 (Ar) 2. 950 (NH_3)	0.1 M $HClO_4$	0.904 V vs. RHE	0.76 V vs. RHE	[12]
ZIF-8/Tris-1,10-phenanthroline and iron (II) perchlorate	1. 1050 (Ar) 2. 950 (NH_3)	0.1 M $HClO_4$	0.902 V vs. RHE	0.76 V vs. RHE	[12]
$Zn(eIm)_2$/Tris-1,10-phenanthroline and iron (II) perchlorate	1. 1050 (Ar) 2. 950 (NH_3)	0.1 M $HClO_4$	0.914 V vs. RHE	0.78 V vs. RHE	[12]
ZIF-8/1,10-phenanthroline and iron (II) acetate	1. 1050 (Ar) 2. 1050 (NH_3)	0.1 M $HClO_4$	0.93 V vs. RHE	0.77 V vs. RHE	[13]
Fe-ZIF-8 = Fe-Zn-mIm/1,10-phenanthroline and iron (II) acetate	1. 1050 (Ar) 2. 1050 (NH_3)	0.1 M $HClO_4$	0.98 V vs. RHE	0.78 V vs. RHE	[14]
Co(PTP)/ Dicyandiamide and Iron acetate (II)	1000	0.5 M H_2SO_4	0.95 V vs. RHE	0.79 V vs. RHE	[15]
ZIF-8/Tris-1,10-phenanthroline and iron (II) perchlorate	1. 1000 (Ar) 2. 900 (NH_3)	0.5 M H_2SO_4	0.93 V vs. RHE	0.80 V vs. RHE	[16]
Fe-ZIF-8	1000 (Ar)	0.1 M HClO4	0.95 V vs. RHE	0.82 V vs. RHE	[17]

Metal doped MOFs-based ORR catalysts

nMn-NC/Mn-doped ZIF-8	1100	0.5 M H_2SO_4	---	0.80 V vs. RHE	[18]
nCo-NC/nCo-ZIF-8	1100	0.5 M H_2SO_4	---	0.80 V vs. RHE	[19]

FeN_4 embedded into the carbon planes/ Cyanamide, $FeCl_3$, Carbon (Black Pearls 2000), PANI	900 (N_2)	0.5 M H_2SO_4	---	0.80 V vs. RHE	[20]
FeN_4 embedded into the carbon planes/ Fe-ZIF	1100	0.5 M H_2SO_4	---	0.85 V vs. RHE	[21]

Table S5. Reported catalysts for ORR in alkaline electrolyte.

Supported or pristine MOF ORR catalysts

Name	**Support**	**Electrolyte**	**E_{onset}**	**$E_{1/2}$**	**Reference**
Cu(phen-NO_3)(BTC) = Cu(nitrophenanthroline)(BTC)	CNTs@TiO_2	0.1 M KOH	0.988 V vs. RHE	0.805 V vs. RHE	[22]
Co-MOF = Co-benzimidazolate	CNTs	0.1 M KOH	0.91 V vs. RHE	0.82 V vs. RHE	[23]
ZIF-67 = Co-methyl-imidazolate	pomelo-peel-derived carbon	0.1 M KOH	---	0.82 V vs. RHE	[24]

MOF-derived ORR catalysts

Name	**Heat treatment temperature (°C)**	**Electrolyte**	**E_{onset}**	**$E_{1/2}$**	**Reference**
ZIF-67 = Co-mIm	700	0.1 M KOH	0.97 V vs. RHE	0.87 V vs. RHE	[39]
Fe-NH_2-MIL-101	700	0.1 M KOH	0.99 V vs. RHE	0.84 V vs. RHE	[1]
S-ZIF-67 = Co-mIm-S	700	0.1 M KOH	0.98 V vs. RHE	0.88 V vs. RHE	[6]
Fe-ZIF-8 = Fe-Zn-mIm	1. 1050 (Ar) 2. 1050 (NH3)	0.1 M KOH	1.05 V vs. RHE	0.87 Vvs. RHE	[14]
ZIF-67 = Co-mIm	900	0.1 M KOH	0.94 V vs. RHE	0.8 V vs. RHE	[25]
PB = Prussian blue	800	0.1 M KOH	0.95 V vs. RHE	0.82 V vs. RHE	[26]
Fe-ZIF-8 = Fe-pyrrole-Zn-mIm	800	0.1 M KOH	0.96 V vs. RHE	0.83 V vs. RHE	[27]
MOF-253 = Fe-Al(OH)(bpydc)	900	0.1 M KOH	0.98 V vs. RHE	0.84 V vs. RHE	[28]
NiCoTU@NH_2-MIL-101(Al) = NiCo-thiourea-NH_2-MIL-101(Al)	900	0.1 M KOH	0.94 V vs. RHE	0.86 V vs. RHE	[29]
Fe-ZIF-8 = Fe-Zn-mIm	950	0.1 M KOH	0.975 V vs. RHE	0.867 V vs. RHE	[30]
ZIF-67 = Co-mIm	800	0.1 M KOH	0.938 V vs. RHE	0.869 V vs. RHE	[31]
ZIF-67/ZIF-8 = Co-mIm/Zn-mIm	950	0.1 M KOH	1.0 V vs. RHE	0.87 V vs. RHE	[32]
$Co_3(PO_4)_2$C-N/rGOA = $Co_3(O_3PCH_2$–NC_4H_7–$CO_2)_2$	800	0.1 M KOH	0.968 V vs. RHE	0.872 V vs. RHE	[33]
Fe/IRMOF-3 = Fe(Zn-NH_2-BDC)	900	0.1 M KOH	1.02 V vs. RHE	0.88 V vs. RHE	[34]
Co@NC	900	0.1 M KOH	0.97 V vs. RHE	0.88 V vs. RHE	[35]
ZIF-67/ZIF-8 = Co-mIm/Zn-mIm	900	0.1 M KOH	0.982 V vs. RHE	0.881 V vs. RHE	[36]
S-ZIF-67 = Co-mIm-S	700	0.1 M KOH	0.97 V vs. RHE	0.9 V vs. RHE	[37]
ZIF-67/ZIF-8 = Co-mIm/Zn-mIm	850	0.1 M KOH	0.992 V vs. RHE	0.91 V vs. RHE	[38]
Fe_2P@PNDCN	**1050**	**1 M KOH**	**0.95 V vs. RHE**	**0.91 V vs. RHE**	**This work**

Table S6. Reported catalysts for HER in acidic electrolyte.

Name	Electrolyte	Catalyst Loading	Overpotential (j = 10 mA cm^{-2}) (mV)	Tafel slope (mV dec^{-1})	Overpotential (j = 10 mA cm^{-2}) after certain cycles	Reference
$[(CH_3)_4N]_2[Mo_2O_2(\mu\text{-}S)_2(S_2)_2]$	1 M H_2SO_4	2.85 μmol/cm^2	114 ± 3	52	132, 1000th	[40]
$[(CH_3)_4N]_2[Mo_2O_2(\mu\text{-}S)_2(S_2)(S_4)]$	1 M H_2SO_4	2.85 μmol/cm^2	114 ± 2	55	About 140, 1000th	[40]
$[(CH_3)_4N]_2[W_2O_2(\mu\text{-}S)_2(S_2)(S_4)]$	1 M H_2SO_4	2.85 μmol/cm^2	227 ± 2	100	About 235, 1000th	[40]
S-600	0.1 M H_2SO_4	0.285 mg/cm^2	262	74	276, 2000th; 286,10000th	[41]
FeCo@NCNTs-NH	0.1 M H_2SO_4	0.32 mg/cm^2	276	96	About 350, 10 000th	[42]
CoNi@NC (475 °C)	0.1 M H_2SO_4	0.32 mg/cm^2	224	104	About 260, 1000th	[43]
Ru@C_2N	0.5 M H_2SO_4	0.285 mg/cm^2	22	30	13.5, 10000th	[44]
Pt/C	0.5 M H_2SO_4	0.285 mg/cm^2	16	27	About 55, 10000th	[44]
$[Mo_3S_{13}]^{2-}$ clusters	0.5 M H_2SO_4	0.100 mg/cm^2	180	40	About 195, 1000th	[45]
CoPS nanoplate	0.5 M H_2SO_4	---	48	56	---	[46]
CoPS NWs	0.5 M H_2SO_4	---	61	48	---	[46]
CoPS film	0.5 M H_2SO_4	---	128	57	---	[46]
SV-MoS_2	0.5 M H_2SO_4	---	170	60	---	[47]
V-MoS_2	0.5 M H_2SO_4	---	250	82	---	[47]
Exfoliated WS_2 nanosheets	0.5 M H_2SO_4	6.5 μg/cm^2	About 234	55	---	[48]
$CoMoS_x$	0.1 M $HClO_4$	50 μg/cm^2	About 207	---	---	[49]
Mesoporous MoS_2	0.5 M H_2SO_4	60 μg/cm^2	About 233	50	---	[50]
A-Ni–C	0.5 M H_2SO_4	0.283 mg/cm^2	34	41	About 45, 8000th	[51]
CoS|P/CNT	0.5 M H_2SO_4	1.6 mg/cm^2	64	55	About 80, 2000th	[52]
M-MoS_2	0.5 M H_2SO_4	43 μg/cm^2	175	41	About 180, 1000th	[53]
$WO_{2.9}$	0.5 M H_2SO_4	0.285 mg/cm^2	70	50	About 70, 1000th	[54]
$MoS_2/CoSe_2$	0.5 M H_2SO_4	0.285 mg/cm^2	68	36	---	[55]
CoN_x/C	0.5 M H_2SO_4	2 mg/cm^2	133	57	144, 5000th	[56]
Edge-terminated MoS_2	0.5 M H_2SO_4	0.28 mg/cm^2	149	49	About 155, 3000th	[57]
C_3N_4@NG	0.5 M H_2SO_4	0.1 mg/cm^2	240	51.5	About 250, 1000th	[58]
Co-NG	0.5 M H_2SO_4	0.285 mg/cm^2	147	82	About 155, 1000th	[59]
MoC_x nano-octahedrons	0.5 M H_2SO_4	0.8 mg/cm^2	142	53	About 167, 1000th	[60]
Pt-MoS_2	0.5 M H_2SO_4	75 μg/cm^2	53	40	---	[61]
Pt MLAg NF/Ni foam	0.5 M H_2SO_4	---	About 70	53	---	[62]
AB&Co–Cl_4-MOF(3:4)	0.5 M H_2SO_4	---	283	86	About 285, 1000th	[63]
AB&CTGU-9 (3:4)	0.5 M H_2SO_4	About 0.0706 mg/cm^2	128	87	About 128, 21h	[64]
MoP@PC	0.5 M H_2SO_4	0.41 mg/cm^2	153	66	About 155, 2000th	[65]
RuP@PNDCN	**0.5 M H_2SO_4**	**0.285 mg/cm^2**	**65**	**50**	**---**	**This work**
Pristine $Ru_2O/TiN/TiO_2$@PNDCN	**0.5 M H_2SO_4**	**0.285 mg/cm^2**	**67**	**51**	**---**	**This work**
$Ru_2O/TiN/TiO_2$@PNDCN(dark)	**0.5 M H_2SO_4**	**0.285 mg/cm^2**	**65**	**50**	**---**	**This work**
$Ru_2O/TiN/TiO_2$@PNDCN(light)	**0.5 M H_2SO_4**	**0.285 mg/cm^2**	**33**	**34**	**---**	**This work**

Table S7. Reported catalysts for HER in alkaline electrolyte.

Name	Electrolyte	Catalyst Loading	Overpotential (j = 10 mA cm^{-2}) (mV)	Tafel slope (mV dec^{-1})	Overpotential (j = 10 mA cm^{-2}) after certain cycles	Reference
Ru@C_2N	1.0 M KOH	0.285 mg/cm^2	17	38	about 45, 10000th	[44]
Pt/C	1.0 M KOH	0.285 mg/cm^2	20.7	43	---	[44]
CoN_x/C	0.1 M KOH	2 mg/cm^2	170	75	---	[56]
MoCx nano-octahedrons	1.0 M KOH	0.8 mg/cm^2	151	59	About 195, 3000th	[60]
S-4	1.0 M KOH	0.275 mg/cm^2	28	31	32, 10000th	[66]
$CoMoS_x$	0.1 M KOH	50 μg cm–2	About 158 (j = 5 mA cm^{-2})	---	---	[67]
$Co(OH)_2$/Pt(111)	0.1 M KOH	---	About 248	---	---	[68]
np-CuTi	0.1 M KOH	---	About 47	110	About 50, 5000th	[69]
NiO/Ni-CNT	1.0 M KOH	0.28 mg/cm^2	About 86	82	---	[70]
$NiFeO_x$/CFP	1.0 M KOH	1.6 mg/cm^2	88	150	---	[71]
Co@N-CS/N-HCP@CC	1.0 M KOH	About 3.2 mg/cm^2	66	65	About 66, 30 h	[72]
Ni QD@NC@rGO	1.0 M KOH	0.71 mg/cm^2	133	64	About 133, 30 h	[73]
Co-Co_9S_8@SN-CNT	0.1 M KOH	0.4 mg/cm^2	120	92	139, 5000th	[74]
Co/Co_9S_8@SNGS	0.1 M KOH	0.305 mg/cm^2	350	96.1	---	[75]
Ni_2P/rGO	1.0 M KOH	0.25 mg/cm^2	142	58	About 145, 2000th	[76]
MoP/NF	1.0 M KOH	0.3 mg/cm^2	114	54.6	About 115, 1000th	[77]
Ni@NC	1.0 M KOH	About 0.31 mg/cm^2	205	160	About 205, 1000th	[78]
FeCo@NGC	1.0 M KOH	0.32 mg/cm^2	211	77	211, 10000th	[79]
NiS_2@C	1.0 M KOH	0.21 mg/cm^2	219	157	About 300, 10 h	[80]
ZnCoS-NSCNT/NP	1.0 M KOH	About 0.21 mg/cm^2	152	103	About 155, 1000th	[81]
Co-Ni-Se/C/NF	1.0 M KOH	1.5 mg/cm^2	148	81	---	[82]
$Co_{1.11}Te_2$/C	1.0 M KOH	---	178	77.3	About 200, 20 h	[83]
Co-P/NC	1.0 M KOH	0.283 mg/cm^2	154	51	157, 1000th	[84]
Ni_2P/C	1.0 M KOH	About 0.34 mg/cm^2	168	63	About 175, 1000th	[85]
NDCHN-35	1.0 M KOH	0.5 mg/cm^2	201	133.2	---	[86]
Ni-Co-S HPNA	1.0 M KOH	---	110	56	About 110, 5000th	[87]
Fe_1V_3-PC/NF	1.0 M KOH	---	66	37	About 66, 5000th	[88]
RuP@PNDCN	**1.0 M KOH**	**0.285 mg/cm^2**	**74**	**59**	**---**	**This work**

Table S8. Reported catalysts for OER in acidic electrolyte.

Name	Electrolyte	Working electrode	Catalyst Loading	Overpotential (j = 10 mA cm^{-2}) (mV)	Tafel slope (mV dec^{-1})	Reference
$Cr_{0.6}Ru_{0.4}O_2$ (550)	0.5 M H_2SO_4	glassy carbon	0.283 mg/cm^2	178	58	[89]
RuO_2	0.5 M H_2SO_4	glassy carbon	0.283 mg/cm^2	297	64	[89]
Ir/GF	0.5 M H_2SO_4	graphite foam	0.82 mg/cm^2	290	46	[90]
IrCoNi PHNCs	0.1 M $HClO_4$	glassy carbon	10 μg$_{Ir}$/cm^2	303	60.1	[91]
$Y_2Ru_2O_{7-\delta}$	0.1 M $HClO_4$	glassy carbon	---	270	55	[92]
$BaYIrO_6$	0.1 M $HClO_4$	Pt ring–Au disk	15 μg$_{oxide}$/cm$_{disk}^2$	~315	219	[93]
RuO2/Co_3O_4−RuCo@NC	0.5 M H_2SO_4	glassy carbon	0.35 mg/cm^2	247	89	[94]
MnO_2	1 M H_2SO_4	---	---	489	80	[95]
Co_3O_4/FTO	0.5 M H_2SO_4	---	---	570	80	[96]
NiFeP	0.05 M H_2SO_4	glassy carbon	---	540	---	[97]
$Sr_{0.9}Na_{0.05}RuO_3$	0.1 M $HClO_4$	glassy carbon	0.51 mg/cm^2	120	~40	[98]
Fe_3O_4/RuO_2@NEU-7	**0.5 M H_2SO_4**	**glassy carbon**	**0.255 mg/cm^2**	**450**	**305**	**This work**

Table S9. Reported catalysts for OER in alkaline electrolyte.

Name	Electrolyte	Working electrode	Catalyst Loading	Overpotential (j = 10 mA cm^{-2}) (mV)	Tafel slope (mV dec^{-1})	Reference
Ni-O-G SACs	1.0 M KOH	Carbon cloth	0.5 mg/cm^2	328	84	[99]
Ni-N-G SACs	1.0 M KOH	Carbon cloth	0.5 mg/cm^2	564	364	[99]
$Ni(OH)_2$/G	1.0 M KOH	Carbon cloth	0.5 mg/cm^2	450	142	[99]
Ce-NiO-E	1.0 M KOH	carbon paper	~0.56 mg/cm^2	382	118.7	[100]
Ce-NiO-L	1.0 M KOH	carbon paper	~0.56 mg/cm^2	426	131.6	[100]
NiO	1.0 M KOH	carbon paper	~0.56 mg/cm^2	467	140.7	[100]
FeNC/NiO	0.1 M KOH	glassy carbon	~0.24 mg/cm^2	390	76	[101]
Commercial RuO_2	0.1 M KOH	glassy carbon	~0.24 mg/cm^2	380	~91	[101]
Ni/N/C paper	0.1 M KOH	glassy carbon	0.4 mg/cm^2	391	40	[102]
Ni/NG	0.1 M KOH	---	1.74 mg/cm^2	397	188.6	[103]
Co_3O_4/N-rmGO	1 M KOH	glassy carbon	0.1 mg/cm^2	310	67	[104]
Mn_3O_4/$CoSe_2$	0.1 M KOH	glassy carbon	~0.2 mg/cm^2	450	49	[105]
NiCo-UMOFNs	1.0 M KOH	glassy carbon	0.2 mg/cm^2	189	42	[106]
Ni-UMOFNs	1.0 M KOH	glassy carbon	0.2 mg/cm^2	321	65	[106]
Co-UMOFNs	1.0 M KOH	glassy carbon	0.2 mg/cm^2	371	103	[106]
Bulk NiCo-MOFs	1.0 M KOH	glassy carbon	0.2 mg/cm^2	250	61	[106]
CoBDC-NF	1.0 M KOH	glassy carbon	0.35 mg/cm^2	252	63	[107]
CoBDC-Fc-NF	1.0 M KOH	glassy carbon	0.35 mg/cm^2	178	51	[107]
RuO_2-NF	1.0 M KOH	glassy carbon	0.35 mg/cm^2	235	88	[107]
FeCo-ONS	0.1 M KOH	glassy carbon	0.36 mg/cm^2	318	38.3	[108]
FeCo-MNS-0.4	0.1 M KOH	glassy carbon	0.36 mg/cm^2	309	24.5	[108]
FeCo-MNS-1.0	0.1 M KOH	glassy carbon	0.36 mg/cm^2	298	21.6	[108]
FeCo-MNS-2.0	0.1 M KOH	glassy carbon	0.36 mg/cm^2	312	23.7	[108]
NiCo/Fe_3O_4/MOF-74	1.0 M KOH	glassy carbon	---	238	29	[109]
Fe_1Co_1-P/C	1.0 M KOH	---	---	360	58.4	[110]
Fe_3O_4/RuO_2@NEU-7	**1 M KOH**	**glassy carbon**	**0.255 mg/cm^2**	**250**	**266**	**This work**

3. References

[1] W. Gu, L. Hu, J. Li, E. Wang, ACS Appl. Mater. Interfaces, 8 (2016) 35281-35288.

[2] S. Ma, G. A. Goenaga, A. V. Call, D.-J. Liu, Chem. Eur. J., 17 (2011) 2063-2067.

[3] W. Xia, J. Zhu, W. Guo, L. An, D. Xia, R. Zou, J. Mater. Chem. A, 2 (2014) 11606-11613.

[4] X. Wang, J. Zhou, H. Fu, W. Li, X. Fan, G. Xin, J. Zheng, X. Li, J. Mater. Chem. A, 2 (2014) 14064-14070.

[5] A. K. Diaz-Duran, F. Roncaroli, Electrochimica Acta, 251 (2017) 638-650.

[6] C. Zhang, B. An, L. Yang, B. Wu, W. Shi, Y.-C. Wang, L.-S. Long, C. Wang, W. Lin, J. Mater. Chem. A, 4 (2016) 4457-4463.

[7] Q. Lai, L. Zheng, Y. Liang, J. He, J. Zhao, J. Chen, ACS Catal., 7 (2017) 1655-1663.

[8] L. Chong, G. A. Goenaga, K. Williams, H. M. Barkholtz, L., R. Grabstanowicz, J. A. Brooksbank, A. B. Papandrew, R. Elzein, R. Schlaf, T. A. Zawodzinski, J. Zou, S. Ma, D.-J. Liu, ChemElectroChem, 3 (2016) 1541-1545.

[9] B. You, N. Jiang, M. Sheng, W. S. Drisdell, J. Yano, J. Sun, ACS Catal., 5 (2015) 7068-7076.

[10] C. Zhang, Y.-C. Wang, B. An, R. Huang, C. Wang, Z. Zhou, W. Lin, Adv. Mater., 29 (2017) 1-7.

[11] H. M. Barkholtz, L. Chong, Z. B. Kaiser, D. J. Liu, FUEL CELLS, 16 (2016) 428-433.

[12] D. Zhao, J.-L. Shui, L. R. Grabstanowicz, C. Chen, S. M. Commet, T. Xu, J. Lu, D.-J. Liu, Adv. Mater., 26 (2014) 1093-1097.

[13] K. Strickland, E. Miner, Q. Jia, U. Tylus, N. Ramaswamy, W. Liang, M.-T. Sougrati, F. Jaouen, S. Mukerjee, Nature Communications, 6 (2015) 1-8.

[14] J. Li, Q. Jia, S. Ghoshal, W. Liang, S. Mukerjee, Langmuir, 33 (2017) 9246-9253.

[15] Q. Li, P. Xu, W. Gao, S. Ma, G. Zhang, R. Cao, J. Cho, H.-L. Wang, G. Wu, Adv. Mater., 26 (2014) 1378-1386.

[16] J. Shui, C. Chen, L. Grabstanowicz, D. Zhao, D.-L. Liu, PNAS, 112 (2015) 10629-10634.

[17] X. Wang, H. Zhang, H. Lin, S. Gupta, C. Wang, Z. Tao, H. Fu, T. Wang, J. Zheng, G. Wu, X. Li, Nano Energy, 25 (2016) 110-119.

[18] J. Li, M. Chen, D. A. Cullen, S. Hwang, M. Wang, B. Li, K. Liu, S. Karakalos, M. Lucero, H. Zhang, C. Lei, H. Xu, G. E. Sterbinsky, Z. Feng, D. Su, K. L. More, G. Wang, Z. Wang, G. Wu, Nature Catalysis, 1 (2018) 935-945.

[19] X. X. Wang, D. A. Cullen, Y.-T. Pan, S. Hwang, M. Wang, Z. Feng, J. Wang, M. H. Engelhard, H. Zhang, Y. He, Y. Shao, D. Su, K. L. More, J. S. Spendelow, G. Wu, Adv. Mater., 30 (2018) 1-11.

[20] H. T. Chung, D. A. Cullen, D. Higgins, B. T. Sneed, E. F. Holby, K. L. More, P. Zelenay, Science, 357 (2017) 479-484.

[21] H. Zhang, S. Hwang, M. Wang, Z. Feng, S. Karakalos, L. Luo, Z. Qiao, X. Xie, C. Wang, D. Su, Y. Shao, G. Wu, J. Am. Chem. Soc., 139 (2017) 14143-14149.

[22] F.-F. Wang, P.-J. Wei, G.-Q. Yu, J.-G. Liu, Chem. Eur. J., 22 (2016) 382-389.

[23] Y. Fang, X. Li, F. Li, X. Lin, M. Tian, X. Long, X. An, Y. Fu, J. Jin, J. Ma, Journal of Power Sources, 326 (2016) 50-59.

[24] H. Wang, F.-X. Yin, B.-H. Chen, X.-B. He, P.-L. Lv, C.-Y. Ye, D.-J. Liu, Applied Catalysis B: Environmental, 205 (2017) 55-67.

[25] C. Lin, S. S. Shinde, Z. Jiang, X. Song, Y. Sun, L. Guo, H. Zhang, J.-Y. Jung, X. Li, J.-H. Lee, J. Mater. Chem. A, 5 (2017) 13994-14002.

[26] Y. Liu, H. Wang, D. Lin, J. Zhao, C. Liu, J. Xie, Y. Cui, Nano Research, 10 (2017) 1213-1222.

[27] A. Aijaz, J. Masa, C. Rösler, H. Antoni, R. A. Fischer, W. Schuhmann, M. Muhler, Chem. Eur. J., 23 (2017) 12125-12130.

[28] Y. Wang, X. Chen, Q. Lin, A. Kong, Q.-G. Zhai, S. Xie, P. Feng, Nanoscale, 9 (2017) 862-868.

[29] J. Wang, H. Lu, Q. Hong, Y. Cao, X. Li, J. Bai, Chemical Engineering, 330 (2017) 1342-1350.

[30] S. H. Ahn, X. Yu, A. Manthiram, Adv. Mater., 29 (2017) 1-10.

[31] L. Huang, X. Zhang, Y. Han, Q. Wang, Y. Fang, S. Dong, J. Mater. Chem. A., 5 (2017) 18610-18617.

[32] S. H. Ahn, M. J. Klein, A. Manthiram, Adv. Energy Mater., 7 (2017) 1-9.

[33] T. Zhou, Y. Du, S. Yin, X. Tian, H. Yang, X. Wang, B. Liu, H. Zheng, S. Qiao, R. Xu, Energy Environ. Sci., 9 (2016) 2563-2570.

[34] H. Sun, H. Su, X. Ma, P. Zhang, X. Zhang, X. Dai, J. Gao, C. Chen, S.-G. Sun, Electrochimica Acta, 205 (2016) 53-61.

[35] S. G. Peera, J. Balamurugan, N. H. Kim, J. H. Lee, Small, 14 (2018) 1-15.

[36] P. Yin, T. Yao, Y. Wu, L. Zheng, Y. Lin, W. Liu, H. Ju, J. Zhu, X. Hong, Z. Deng, G. Zhou, S. Zhou, Y. Li, Angew. Chem. Int. Ed., 55 (2016) 10800-10805.

[37] J. Xiao, C. Zhao, C. Hu, J. Xi, S. Wang, Journal of Power Sources, 348 (2017) 57-65.

[38] S. S. A. Shah, L. Peng, T. Najam, C. Cheng, G. Wu, Y. Nie, W. Ding, X. Qi, S. Chen, Z. Wei, Electrochimica Acta, 251 (2017) 498-504.

[39] B. Y. Xia, Y. Yan, N. Li, H. B. Wu, X. W. Lou, X. Wang, Nature Energy, 1 (2016) 1-8.

[40] J. McAllister, N. A. G. Bandeira, J. C. McGlynn, A. Y. Ganin, Y.-F. Song, C. Bo, H. N. Miras, Nature Communications, 10 (2019) 1-10.

[41] Y. Yang, Z. Lun, G. Xia, F. Zheng, M. He, Q. Chen, Energy Environ. Sci., 8 (2015) 3563-3571.

[42] J. Deng, P. Ren, D. Deng, L. Yu, F. Yang, X. Bao, Energy Environ. Sci., 7 (2014) 1919-1923.

[43] J. Deng, P. Ren, D. Deng, X. Bao, Angew. Chem. Int. Ed., 54 (2015) 2100-2104.

[44] J. Mahmood, F. Li, S.-M. Jung, M. S. Okyay, I. Ahmad, S.-J. Kim, N. Park, H. Y. Jeong, J.-B. Baek, Nature Nanotechnology, 12 (2017) 441-447.

[45] J. Kibsgaard, T. F. Jaramillo, F. Besenbacher, Nature Chemistry, 6 (2014) 248-253.

[46] M. Cabán-Acevedo, M. L. Stone, J. R. Schmidt, J. G. Thomas, Q. Ding, H.-C. Chang, M.-L. Tsai, J.-H. He, S. Jin, Nature Materials, 14 (2015) 1245-1251.

[47] H. Li, C. Tsai, A. L. Koh, L. Cai, A. W. Contryman, A. H. Fragapane, J. Zhao, H. S. Han, H. C. Manoharan, F. Abild-Pedersen, J. K. Nørskov, X. Zheng, Nature Materials, 15 (2016) 48-53.

[48] D. Voiry, H. Yamaguchi, J. Li, R. Silva, D. C. B. Alves, T. Fujita, M. Chen, T. Asefa, V. B. Shenoy, G. Eda, M. Chhowalla, Nature Materials, 12 (2013) 850-855.

[49] J. Staszak-Jirkovský, C. D. Malliakas, P. P. Lopes, N. Danilovic, S. S. Kota, K.-C. Chang, B. Genorio, D. Strmcnik, V. R. Stamenkovic, M. G. Kanatzidis, M. M. Markovic, Nature Materials, 15 (2016) 197-203.

[50] J. Kibsgaard, Z. Chen, B. N. Reinecke, T. F. Jaramillo, Nature Materials, 11 (2012) 963- 969.

[51] L. Fan, P. F. Liu, X. Yan, L. Gu, Z. Z. Yang, H. G. Yang, S. Qiu, X. Yao, Nature Communications, 7 (2016) 1-7.

[52] W. Liu, E. Hu, H. Jiang, Y. Xiang, Z. Weng, M. Li, Q. Fan, X. Yu, E. I. Altman, H. Wang, Nature Communications, 7 (2016) 1-9.

[53] X. Geng, W. Sun, W. Wu, B. Chen, A. Al-Hilo, M. Benamara, H. Zhu, F. Watanabe, J. Cui, T.-P. Chen, Nature Communications, 7 (2016) 1-7.

[54] Y. H. Li, P. F. Liu, L. F. Pan, H. F. Wang, Z. Z. Yang, L. R. Zheng, P. Hu, H. J. Zhao, L. Gu, H. G. Yang, Nature Communications, 6 (2015) 1-7.

[55] M.-R. Gao, J.-X. Liang, Y.-R. Zheng, Y.-F. Xu, J. Jiang, Q. Gao, J. Li, S.-H. Yu, Nature Communications, 6 (2015) 1-7.

[56] H.-W. Liang, S. Brüller, R. Dong, J. Zhang, X. Feng, K. Müllen, Nature Communications, 6 (2015) 1-8.

[57] M.-R. Gao, M. K. Y. Chan, Y. Sun, Nature Communications, 6 (2015) 1-8.

[58] Y. Zheng, Y. Jiao, Y. Zhu, L. H. Li, Y. Han, Y. Chen, A. Du, M. Jaroniec, S. Z. Qiao, Nature Communications, 5 (2014) 1-8.

[59] H. Fei, J. Dong, M. J. Arellano-Jiménez, G. Ye, N. D. Kim, E. L. G. Samuel, Z. Peng, Z. Zhu, F. Qin, J. Bao, M. J. Yacaman, P. M. Ajayan, D. Chen, J. M. Tour, Nature Communications, 6 (2015) 1-8.

[60] H. B. Wu, B. Y. Xia, L. Yu, X.-Y. Yu, X. W. Lou, Nature Communications, 6 (2015) 1-8.

[61] X. Huang, Z. Zeng, S. Bao, M. Wang, X. Qi, Z. Fan, H. Zhang, Nature Communications, 4 (2013) 1-8.

[62] M. Li, Q. Ma, W. Zi, X. Liu, X. Zhu, S. Liu, Sci. Adv., 1 (2015) 1-7.

[63] Y.-S. Li, J.-W. Yi, J.-H. Wei, Y.-P. Wu, B. Li, S. Liu, C. Jiang, H.-G. Yu, D.-S. Li, Journal of Solid State Chemistry, 281 (2020) 1-7.

[64] W. Zhou, Y.-P. Wu, X. Wang, J.-W. Tian, D.-D. Huang, J. Zhao, Y.-Q. Lan, D.-S. Li, CrystEngComm, 20 (2018) 4804-4809.

[65] J. Yang, F. Zhang, X. Wang, D. He, G. Wu, Q. Yang, X. Hong, Y. Wu, Y. Li, Angew. Chem. Int. Ed., 55 (2016) 12854-12858.

[66] J. Su, Y. Yang, G. Xia, J. Chen, P. Jiang, Q. Chen, Nature Communications, 8 (2017) 1-10.

[67] J. Staszak-Jirkovský, C. D. Malliakas, P. P. Lopes, N. Danilovic, S. S. Kota, K.-C. Chang, B. Genorio, D. Strmcnik, V. R. Stamenkovic, M. G. Kanatzidis, N. M. Markovic, Nature Materials, 15 (2016) 197-203.

[68] R. Subbaraman, D. Tripkovic, K.-C. Chang, D. Strmcnik, A. P. Paulikas, P. Hirunsit, M. Chan, J. Greeley, V. Stamenkovic, N. M. Markovic, Nature Materials, 11 (2012) 550-557.

[69] Q. Lu, G. S. Hutchings, W. Yu, Y. Zhou, R. V. Forest, R. Tao, J. Rosen, B. T. Yonemoto, Z. Cao, H. Zheng, J. Q. Xiao, F. Jiao, J. G. Chen, Nature Communications, 6 (2015) 1-8.

[70] M. Gong, W. Zhou, M.-C. Tsai, J. Zhou, M. Guan, M.-C. Lin, B. Zhang, Y. Hu, D.-Y. Wang, J. Yang, S. J. Pennycook, B.-J. Hwang, H. Dai, Nature Communications, 5 (2014) 1-6.

[71] H. Wang, H.-W. Lee, Y. Deng, Z. Lu, P.-C. Hsu, Y. Liu, D. Lin, Y. Cui, Nature Communications, 6 (2015) 1-8.

[72] Z. Chen, Y. Ha, H. Jia, X. Yan, M. Chen, M. Liu, R. Wu, Adv. Energy Mater., 9 (2019) 1-13.

[73] Z. Chen, H. Xu, Y. Ha, X. Li, M. Liu, R. Wu, Applied Catalysis B: Environmental, 250 (2019) 213-223.

[74] H. Han, Z. Bai, T. Zhang, X. Wang, X. Yang, X. Ma, Y. Zhang, L. Yang, J. Lu, Nano Energy, 56 (2019) 724-732.

[75] X. Zhang, S. Liu, Y. Zang, R. Liu, G. Liu, G. Wang, Y. Zhang, H. Zhang, H. Zhao, Nano Energy, 30 (2016) 93-102.

[76] L. Yan, H. Jiang, Y. Xing, Y. Wang, D. Liu, X. Liu, P. Dai, L. Li, X. Zhao, J. Mater. Chem. A, 6 (2018) 1682-1691.

[77] Y. Jiang, Y. Lu, J. Lin, X. Wang, Z. Shen, Small Methods, 2 (2018) 1-10.

[78] Y. Xu, W. Tu, B. Zhang, S. Yin, Y. Huang, M. Kraft, R. Xu, Adv. Mater., 29 (2017) 1-8.

[79] Y. Yang, Z. Lin, S. Gao, J. Su, Z. Lun, G. Xia, J. Chen, R. Zhang, Q. Chen, ACS Catal., 7 (2017) 469-479.

[80] T. Tian, L. Huang, L. Ai, J. Jiang, J. Mater. Chem. A, 5 (2017) 20985-20992.

[81] Z. Yu, Y. Bai, S. Zhang, Y. Liu, N. Zhang, K. Sun, J. Mater. Chem. A, 6 (2018) 10441-10446.

[82] F. Ming, H. Liang, H. Shi, X. Xu, G. Mei, Z. Wang, J. Mater. Chem. A, 4 (2016) 15148-15155.

[83] H. Wang, Y. Wang, L. Tan, L. Fang, X. Yang, Z. Yang, J. Li, H. Zhang, Y. Wang, Applied Catalysis B: Environmental, 244 (2019) 568-575.

[84] B. You, N. Jiang, M. Sheng, S. Gul, J. Yano, Y. Sun, Chem. Mater., 27 (2015) 7636-7642.

[85] Q. Wang, Z. Liu, H. Zhao, H. Huang, H. Jiao, Y. Du, J. Mater. Chem. A, 6 (2018) 18720-18727.

[86] L. Zhang, J.-S. Hu, X.-H. Huang, J. Song, S.-Y. Lu, Nano Energy, 48 (2018) 489-499.

[87] W. Chen, Y. Zhang, G. Chen, R. Huang, Y. Wu, Y. Zhou, Y. Hu, K. Ostrikov, Journal of Colloid and Interface Science, 560 (2020) 426-435.

[88] N. Suo, X. Han, C. Chen, X. He, Z. Dou, Z. Lin, L. Cui, J. Xiang, Electrochimica Acta, 333 (2020) 1-11.

[89] Y. Lin, Z. Tian, L. Zhang, J. Ma, Z. Jiang, B. J. Deibert, R. Ge, L. Chen, Nature Communications, 10 (2019) 1-13.

[90] J. Zhang, G. Wang, Z. Liao, P. Zhang, F. Wang, X. Zhuang, E. Zschech, X. Feng, Nano Energy, 40 (2017) 27-33.

[91] J. Feng, F. Lv, W. Zhang, P. Li, K. Wang, C. Yang, B. Wang, Y. Yang, J. Zhou, F. Lin, G.-C. Wang, S. Guo, Adv. Mater., 29 (2017) 1-8.

[92] J. Kim, P.-C. Shih, K.-C. Tsao, Y.-T. Pan, X. Yin, C.-J. Sun, H. Yang, J. Am. Chem. Soc., 139 (2017) 12076-12083.

[93] O. Diaz-Morales, S. Raaijman, R. Kortlever, P. J. Kooyman, T. Wezendonk, J. Gascon, W. T. Fu, M. T. M. Koper, Nature Communications, 7 (2016) 1-6.

[94] Z. Fan, J. Jiang, L. Ai, Z. Shao, S. Liu, ACS Appl. Mater. Interfaces, 11 (2019) 47894-47903.

[95] A. Li, H. Ooka, N. Bonnet, T. Hayashi, Y. Sun, Q. Jiang, C. Li, H. Han, R. Nakamura, Angew. Chem. Int. Ed., 58 (2019) 5054-5058.

[96] J. S. Mondschein, J. F. Callejas, C. G. Read, J. Y. C. Chen, C. F. Holder, C. K. Badding, R. E. Schaak, Chem. Mater., 29 (2017) 950-957.

[97] F. Hu, S. Zhu, S. Chen, Y. Li, L. Ma, T. Wu, Y. Zhang, C. Wang, C. Liu, X. Yang, L. Song, X. Yang, Y. Xiong, Adv. Mater., 29 (2017) 1-9.

[98] M. Retuerto, L. Pascual, F. Calle-Vallejo, P. Ferrer, D. Gianolio, A. González Pereira, A. García, J. Torrero, M. T. Fernández-Díaz, P. Bencok, M. A. Peña, J. L. Fierro, S. Rojas, Nature Communications, 10 (2019) 1-9.

[99] Y. Xu, W. Zhang, Y. Li, P. Lu, Z.-S. Wu, Journal of Energy Chemistry, 43 (2020) 52-57.

[100] W. Gao, Z. Xia, F. Cao, J. C. Ho, Z. Jiang, Y. Qu, Adv. Funct. Mater., 28 (2018) 1-8.

[101] J. Wang, K. Li, H.-x. Zhong, D. Xu, Z.-l. Wang, Z. Jiang, Z.-j. Wu, X.-b. Zhang, Angew. Chem. Int. Ed., 54 (2015) 10530-10534.

[102] J. Ren, M. Antonietti, T.-P. Fellinger, Adv. Energy Mater., 5 (2015) 1-6.

[103] S. Chen, J. Duan, J. Ran, M. Jaroniec, Z. Qiao, Energy Environ. Sci., 6 (2013) 3693-3699.

[104] Y. Liang, Y. Li, H. Wang, J. Zhou, J. Wang, T. Regier, H. Dai, Nature Materials, 10 (2011) 780-786.

[105] M.-R. Gao, Y.-F. Xu, J. Jiang, Y.-R. Zheng, S.-H. Yu, J. Am. Chem. Soc., 134 (2012) 2930-2933.

[106] S. Zhao, Y. Wang, J. Dong, C.-T. He, H. Yin, P. An, K. Zhao, X. Zhang, C. Gao, L. Zhang, J. Lv, J. Wang, J. Zhang, A. M. Khattak, N. A. Khan, Z. Wei, J. Zhang, S. Liu, H. Zhao, Z. Tang, Nature Energy, 1 (2016) 1-10.

[107] Z. Xue, K. Liu, Q. Liu, Y. Li, M. Li, C.-Y. Su, N. Ogiwara, H. Kobayashi, H. Kitagawa, M. Liu, G. Li, Nature Communications, 10 (2019) 1-8.

[108] L. Zhuang, L. Ge, H. Liu, Z. Jiang, Y. Jia, Z. Li, D. Yang, R. K. Hocking, M. Li, L. Zhang, X. Wang, X. Yao, Z. Zhu, Angew. Chem. Int. Ed., 58 (2019) 13565-13572.

[109] X. Wang, H. Xiao, A. Li, Z. Li, S. Liu, Q. Zhang, Y. Gong, L. Zheng, Y. Zhu, C. Chen, D. Wang, Q. Peng, L. Gu, X. Han, J. Li, Y. Li, J. Am. Chem. Soc., 140 (2018) 15336-15341.

[110] W. Hong, M. Kitta, Q. Xu, Small Methods, 2 (2018) 1-6.